Synthesis and characterization of dirhodium(II) formamidinyl complexes: Preliminary studies as catalyst precursors for the allylic oxidation of cyclohexene

Anna Casimiro

University of Cape Town

University of Parma

2018

Synthesis and characterization of dirhodium(II) formamidinyl complexes: Preliminary studies as catalyst precursors for the allylic oxidation of cyclohexene

Anna Casimiro

A dissertation submitted in fulfilment of the requirements of the degree

Masters in Chemistry

University of Cape Town,

University of Parma

Department of Chemistry

Supervisor:

Dr S. Ngubane

Co-Supervisor:

Dr G. Maestri

February 2018

Declaration

- I know that plagiarism is wrong. Plagiarism is to use another's work and pretend that it is one's own.
- I have used the required convention for citation and referencing. Each contribution to and quotation in this assignment from the work(s) of other people has been attributed, and has been cited and referenced.
- This assignment is my own work.
- I have not allowed, and will not allow, anyone to copy my work with the intention of passing it off as his or her own work.
- I acknowledge that copying someone else's assignment or essay, or part of it, is wrong, and declare that this is my own work.

21/03/2018

.....

Date

Signed by candidate

Anna Casimiro

Dedication

This dissertation is dedicated to my family, with love.

Acknowledgements

Firstly, I would like to express my gratitude to my supervisor, Dr Siyabonga Ngubane. It has been an honour to work with him for his encouragement, guidance and for making me a better chemist. A special thanks to my co-supervisor, Dr Giovanni Maestri for his support and kindness.

I would express my gratitude to Dr Gregory Smith and the organometallic research group for how they welcomed me as part of the group and gave me help, advices but most of all friendship. In particular Thato, Shepherd, Cody and Dylan spurred me to live up to their standards and gave me the best moments in Cape Town.

I would like to thank Mrs. Deirdre Brooks for her constant help. Without her I would probably not have managed to get to Cape Town.

Many thanks go to Mr. Pete Roberts for recording NMR spectra and to Dr Hong Su for the single-crystal X-ray diffraction studies. I am also grateful to the University of Witwatersrand foot the HR-MS analysis and to the organometallic research laboratory for access to equipment for catalysis.

For research funding, I would like to thank the National Research Foundation-Department of Science and Technology.

Special thanks to my friends in Cape Town, especially to Ana with whom I share a sincere friendship. I would also thank the other “Italians” Marcello, Giacomo, Andrea and Riccardo for having shared with me this adventure.

Lastly, I am grateful to my family for their continuous support in all the aspects of my life and for being Family even through hard times.

Table of contents

Abstract

A series of symmetrical substituted formamidine-type ligands, (**L1**, **L2** and **L3**) were synthesized *via* a solvent-free reaction, in which ethanol is produced as by-product. The ligands were characterized as to their spectroscopic and solid-state properties *via* FT-IR, UV-Vis and NMR spectroscopies showing a prototropic tautomerism for **L2** and **L3**. The acetate precursor complexes $Rh_2(O_2CR)_4$ where R = CH_3 (**C1**) or CF_3 (**C2**) were synthetized and fully characterized. Reaction of **C2** with an excess of formamidine ligand yields the complexes **C3**, **C4**, **C5** and **C6** *via* a solventless reaction. The 2-fluorophenyl complex, [Rh_2(di-2F-pf)$_4$] complex, **C5** was structurally characterized by single crystal X-Ray crystallography revealing a paddle-wheel type complex.

Allylic oxidation reactions using the binuclear Rh complexes showed that these are active for cyclohexene conversion giving a range of products. Solvent coordination could have an effect on the catalytic behaviour of the complexes, with acetonitrile being the best solvent probably due to the solubility properties of complexes. Under these conditions, the allylic oxidation of cyclohexene produced enone as major product. The best result in terms of selectivity were obtained with **C1**, **C4**, **C5** and **C6** which yielded only 2-cyclohexene-1-one.

List of abbreviations

°	Degrees
°C	Degrees Celsius
^{13}C NMR	Carbon-13 nuclear magnetic resonance
^{19}F NMR	Fluorine-19 nuclear magnetic resonance
^{1}H NMR	Proton nuclear magnetic resonance
Å	Angstroms
ACN	Acetonitrile
Ar	Aromatic
ATR-IR	Attenuated total reflectance infrared spectroscopy
ax	Axial
br s	Broad signal
Calcd.	Calculated
cap	Caprolactamate
Cat.	Catalyst
$CDCl_3$	Deuterated chloroform
d	Doublet
DCM	Dichloromethane
di-2F-pf	di-2-Fluoro-phenylformamidine
di-4F-pf	di-4-Fluoro-phenylformamidine
di-p-Tolf	di-para-Tolylformamidine
DMSO	Dimethyl sulfoxide
DMSO-d_6	Deuterated dimethyl sulfoxide
dpf	Diphenylformamidine
EPA	Environmental Protection Agency

eq	Equatorial
eq	Equivalent(s)
EtOH	Ethanol
g	gram
GC	Gas chromatography
h	Hour(s)
HOMO	Highest occupied molecular orbital
HSAB	Hard and soft acids and bases
HSQC	Heteronuclear single quantum correlation
J	Coupling constant
LUMO	Lowest unoccupied molecular orbital
m	Metre
m	Multiplet
M.P.	Melting point
m/z	Mass to charge ratio
MeOH	Methanol
mg	Milligram
MHz	Megahertz
mL	Millilitre
mmol	Millimole(s)
mol	Mole(s)
MS	Mass spectrometry
nm	Nanometres
NMR	Nuclear magnetic resonance
PGM	Platinum group metals

ppm	Parts per million
s	singlet
sh	Shoulder
t	Triplet
TBHP	*Tert*-butyl hydroperoxide
TFA	Trifluoroacetic acid
THF	Tetrahydrofuran
UV-Vis	Ultraviolet-Visible
v/v	Volume percent
δ	Chemical shift
λ	Wavelength
µL	Microliter
ν	Wavenumber

Chapter 1

Review of the design of dirhodium (II) complexes, their properties and applications as catalysts in allylic oxidation

1.1 Background

From the late 1980s, the growing global awareness of the human responsibilities towards environment protection, allowed the emergence of ideas related to sustainable development.[1] In the chemistry field, the concept of green chemistry in particular has been introduced as mandated by the United States Environmental Protection Agency (EPA) in 1990. It can be defined as "*the design of chemical products and processes that reduce or eliminates the use or generation of hazardous substances*".[2] Thanks to the work of Paul Anastas and John Warner, who introduced the 12 principles of green chemistry[3] (*Figure 1.1*), increasing attention has been directed to the role played by catalysis.

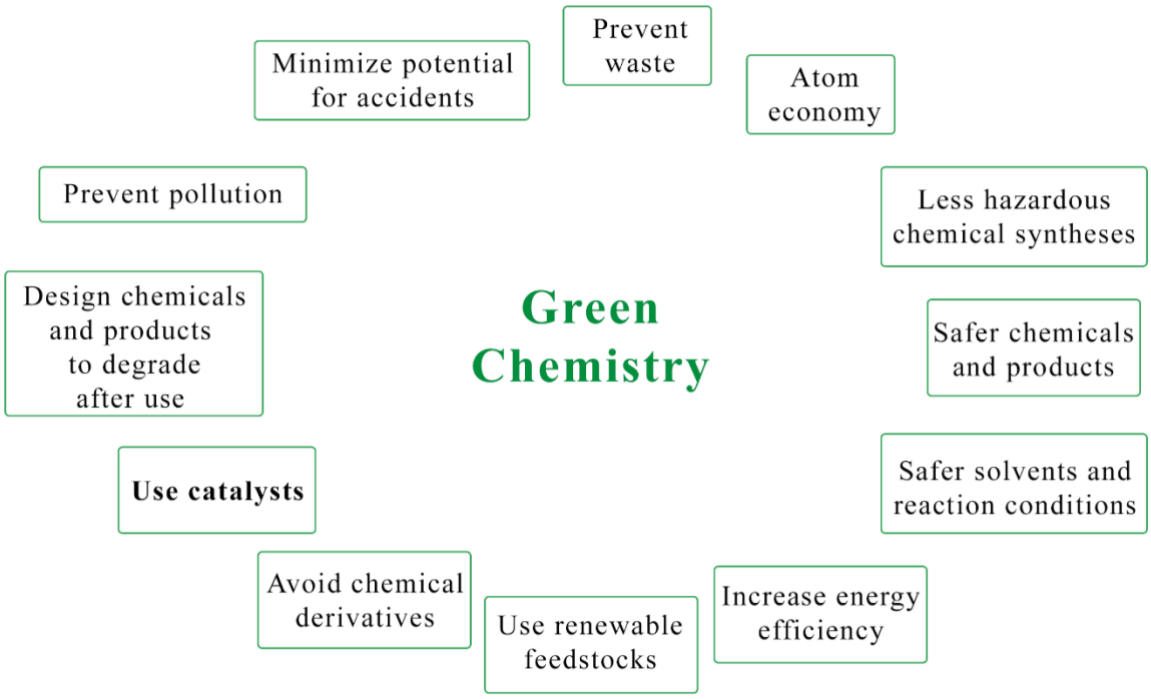

Figure 1. 1: *The 12 principles of green chemistry*

Catalysis, indeed, emerged as one of the key tools to realise all the 12 principles of green chemistry.[4] Through it, is possible to lower energy requirements, increase the selectivity of a process and prevent waste.[5]

It is known that transition metals have become one of the most important ingredients for the development of highly effective catalysts in modern synthetic chemistry. This is explained by their bonding ability in order to form complexes with different type of ligand, their capacity to adopt different oxidation states and the different properties between complexes with different ligands.[6] These catalysts are known to activate many organic substrates towards oxidation, C-H functionalization and formation or cleavage of H-H, C-H or C-C bonds.[7]

South Africa is one of the major suppliers platinum-group metals (PGMs), especially for Rh.[8] This availability of expensive metals needs to be exploited as an important resource for the country. From an economic point of view, the use of Rh catalysts could not be seen as a convenient choice giving the cost of the metal. Its use could be justified if effectiveness, selectivity, minimum amount of catalysts employed, green synthetic method to prepare them and mild reaction conditions are achieved. In this way these catalysts could be considered as a sustainable way to convert raw chemicals into value-added products.

1.2 Allylic oxidation of alkenes

The activation and functionalization of the C-H bond is an essential tool in organic synthesis. Due to the high C-H bond dissociation energy (~101 kcal mol^{-1})[9] generally, the reactions in which its functionalisation occurs require harsh conditions.[10] The activation of the allylic C-H bond has a lower, but still high, bond dissociation energy (~88 kcal mol^{-1}) due to the possible resonance with the C=C double bond. This means that the hydrogens more prone to radical abstraction are the allylic ones.[9] This is the concept that lies at the bottom of all the allylic C-H bond activation.

Allylic oxidation is an important tool in synthetic chemistry. It is the reaction between an olefin, either linear or cyclic, with an oxidizing agent to give a variety of value-added compounds (*Scheme 1.1*).[11]

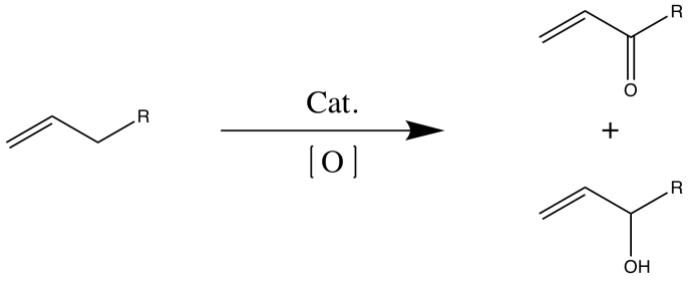

Scheme 1. 1: *Allylic oxidation of linear alkenes*

The products of allylic oxidation can have a wide range of applications: for example, they are useful as synthetic intermediates,[12–15] anticancer products[16–18] or even as flavouring agents.[19–23]

Since 1932[24], most of the strategies that were adopted academically, to carry out this reaction lacked regio- and stereoselectivity or had overoxidation issues. Furthermore, the reagents employed were mainly based on Se[25–27] or Cr[28] oxides in stoichiometric amounts adopted as oxidizing agents.[11]

1.2.1 Allylic oxidation catalyzed by metal complexes

The beforementioned procedures are not adopted nowadays because of the use of stochiometric amounts of poisonous reagents which obviously lead to the production of toxic waste. These methods were therefore incompatible with the industrial requirements. For these reasons, alternatives to these methods have been developed trying to adopt milder reaction conditions, increase the effectiveness of the processes and the compatibility with functional groups. Most of the examples include the use of metal catalysts to activate the C-H bond and the choice of milder and less toxic oxidant to carry out the reaction.[10,11]

To avoid the use of the toxic Se or Cr oxides, milder oxidizing agents, in particular *tert*-butyl hydroperoxide (TBHP), have been introduced as a safe source of oxygen together with catalytic compounds necessary to carry out the reaction. The metal catalyzed methods involve a free radical chain mechanism in which the metal catalyst has the key role to play in a redox capacity.[29] Therefore, in order to generate the radical, metal complexes which are able to undergo a one-electron change ($Fe^{2+} \rightleftarrows Fe^{3+}$, $Cu^{1+} \rightleftarrows Cu^{2+}$, and $Co^{2+} \rightleftarrows Co^{3+}$, etc.) are the most efficient for this catalytic oxidation.[30]

The catalytic use of chromium in association with stochiometric amounts of an oxidant has been extensively studied.[11] It has been showed for example, that the efficiency of the chromium catalysts depends on its structure and on the solvent adopted to carry out the reactions. CrO_3 has been used as catalyst to convert Δ^5-steroids to their corresponding 5-en-7-ones. Despite the good yields obtained for some of the abovementioned specific substrates, a slight variation on their structure lead to lower yields making this catalytic method highly substrate-specific.[31] Furthermore, the removal of the toxic chromium traces from the reaction mixture, even though if used in catalytic amounts, remains a complex problem.

Copper catalysts have been developed to achieve more environmentally friendly methodologies. In some cases, excellent yields and selectivity have been obtained but, it has

been shown in a recent example that the reaction conditions require long times (12 h) and high temperatures (70 °C). Furthermore, the ligand-metal complex is consumed during the course if the reaction preventing the possibility to recycle the catalyst for other catalytic cycles.[32]

Another method adopted for the allylic oxidation of olefins requires the use of Co catalysts. Usually the major products obtained with these catalysts are allyl alcohols or epoxides and just in some of the cases, the selectivity towards the production of carbonyl compounds is higher.[11] One of the best results obtained is the work of Rossi and co-workers, they developed a recyclable cobalt oxide catalyst very active and selective in the allylic oxidation of cyclohexene to the corresponding enone.[33] As for the previous cases, the reaction conditions for the catalysis are optimized at temperatures higher than 75 °C, this could represent a problem when scaling up the reaction for industrial purposes.

Also Ru, Pd and Fe complexes have been used as catalysts for the oxidation of alkenes. In both cases the main drawbacks were the scarce chemoselectivity and the strong influence of the substrates structure on the catalysis outcomes.[11]

The above-mentioned methodologies have many drawbacks that prevent their development as general strategies for the allylic oxidation. One of the main problems is the dependence of the results on the substrate structure and the scarce tolerance of functional groups. Doyle and co-workers developed a Rh(II) catalyst active in the oxidation of a range of substrates.[34] This catalyst results to be promising for both its effectiveness and the mild reaction conditions adopted.

1.3 Dirhodium(II) complexes

Dirhodium(II) complexes have many intriguing properties and their applications embrace photochemistry,[35] design of phototherapeutic reagents but,[36] above all, catalysis. The key in the stabilization of the Rh_2^{4+} units is the formation of the bond between the two metal atoms. This leads to a molecular orbital construction with 14 electrons which are distributed in the σ, π, δ orbitals. The last six electrons occupy the π^* and δ^* orbitals giving a configuration with all paired electrons.[37]

Paddlewheel Rh(II) compounds have the generic structure shown in *Figure 1.2* with ligation at either the equatorial or axial position as indicated. The axial (*ax*) ligands show little influence

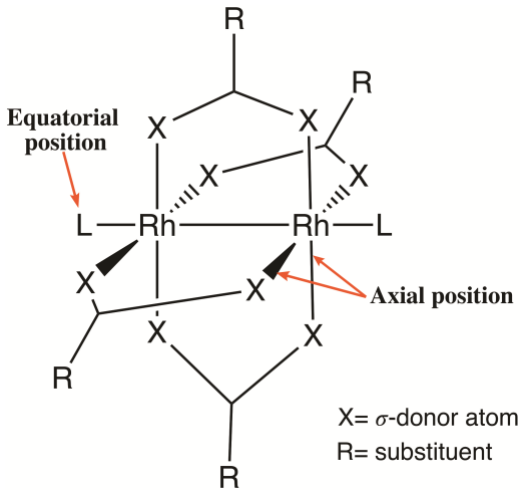

Figure 1. 2: *Structure of the paddlewheel complexes*

on the Rh-Rh bond length while the equatorial ligands (*eq*), are classified based on the nature of the X donor atoms. The distance between the σ-donor atoms is generally comparable to the Rh-Rh bond length.[37]

The reason of the adaptability to catalyze different reactions of the dirhodium(II) complexes lies in the possibility to modify the bridging and axial ligands by changing the nature of the σ-donor atoms and of the bridging ligands substituents.

1.3.1 Dirhodium(II) complexes as catalysts for allylic oxidation

As previously stated, the properties of the dirhodium(II) complexes vary based on the nature of the ligands. It was also highlighted that allylic oxidation is easily catalyzed by metals that can go through one-electron changes, therefore enhancing the electron density within the dimetal core should favor the catalysis.

O,O'-bridging ligands have been used to prepare dirhodium complexes like $Rh_2(O_2CCH_3)_4$ where the equatorial position is occupied by 4 chelating acetates. Kadish and Bear observed that the substitution of the eight oxygen atoms of the acetate ligands with four NH groups, markedly favors the electrochemical access to the Rh_2^{5+} (Rh(II)-Rh(III)) species.[38]

This concept is at the base of the catalyst proposed by Doyle and co-workers.[34] This group showed that using the complex $Rh_2(cap)_4$, most olefins are rapidly oxidized to enones or enediones with mild reaction conditions, low amount of catalyst and great selectivity.[34,39–41]

The proposed mechanism for allylic oxidation of cyclohexene catalyzed by $Rh_2(cap)_4$, as reported by Doyle and co-workers is showed in *Scheme 1.2*.

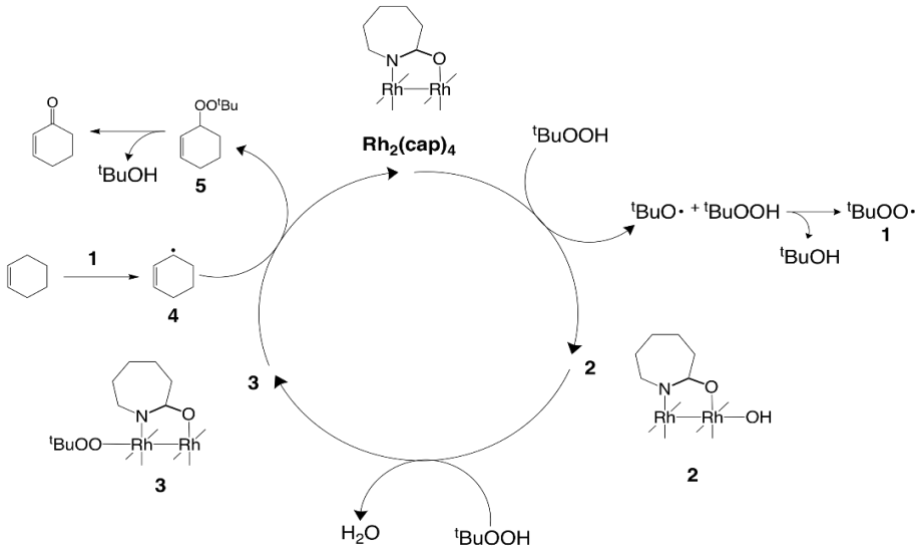

Scheme 1. 2: *Mechanism proposal for the allylic oxidation of cyclohexene catalyzed by* $Rh_2(cap)_4$[34]

The chosen oxidizing agent was TBHP in decane or the cheaper and safer T-Hydro (70% TBHP in water). Its radical chain disproponation mechanism leads to the abstraction of an allyl hydrogen (species **4**) and to the formation of the mixed peroxide species (species **5**). The decomposition of the latter gives, most exclusively, the enone. The key step in this mechanism is the formation of the oxidized species Rh_2^{5+} which coordinates an OH group at the axial position. The complex indeed, serves to initiate the formation of the *tert*-butyl peroxy radical.

The study of the catalytic properties of dirhodium caprolactamate complexes is still ongoing.[40] The optimization of reaction conditions for the allylic oxidation process to be able to obtain a general procedure which can be applied to diverse organic substrates, the request of catalysts recovery methods and the possibility to scale up the reaction are important aims that need to be studied.

1.3.2 Dirhodium(II) complexes with formamidinyl ligands

Dirhodium(II) complexes with *N,N'*-type ligands contain 8 nitrogen atoms which are known to be more σ-donating than oxygen (*Figure 1.3*). This translates to an easier oxidation from the Rh_2^{4+} species to the Rh_2^{5+} species as demonstrated by the work of Kadish and Bear.[42–44]

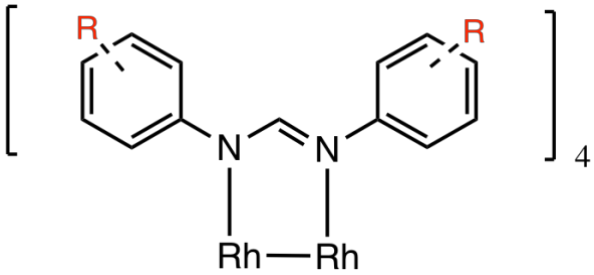

Figure 1. 3: *N,N'-formamidinate type complex*

Formamidinate-type complexes generally have vacant axial sites. This should be ascribed to the steric hindrance of the ligands.[37] Furthermore, the electrochemical aspects of such complexes can be studied through cyclic voltammetry. It has been demonstrated that there is a shift in both the oxidation and the reduction potentials in such a way that electron-donating groups of the ligand, produce easier oxidations and more difficult reductions and electron-withdrawing groups had the opposite effect.[45] This statement is essential to better understand how to tune the electrochemical properties of the complexes by varying the nature of the substituents of the ligands and of the σ-donor atoms. This is also why *N,N'*-type bridging ligands are known to stabilize higher oxidation states of the dirhodium unit.[42]

1.4 Motivation of this study

Giving the electrochemical properties of the *N,N'*-type complexes, the synthesis of ligands with different electron-donating or electron-withdrawing groups and the subsequent preparation of the respective complexes, could lead to the preparation of a series of compounds with different and intriguing properties. The steric hindrance of the ligands is aimed to investigate if it effectively competes with the course of the reaction. The application of the complexes as catalysts in the allylic oxidation of olefins have never been studied and this could give encouraging results in terms of activity of such complexes.

1.5 Aims of this study

The aims of this study are the design, synthesis and characterization of dirhodium(II) complexes, with either acetate or formamidinate bridging ligands, and their evaluation as catalysts in the allylic oxidation of cyclohexene.

1.6 Objectives of this study

- Synthesis and characterization of N,N'-type ligands with different substituents on the aromatic ring
- Synthesis and characterization of dirhodium(II) complexes with acetate bridging ligand and their use as starting material
- Synthesis and characterization of dirhodium(II) complexes with formamidinate ligands
- Evaluation of the sythetized complexes as catalysts in allylic oxidation of cyclohexene.

1.7 References

(1) Brundtland, G. H. *Our common Futur.* **1987**, *42/187*, 8–9.

(2) United States Environmental Protection Agency. Basics of Green Chemistry | Green Chemistry | US EPA http://www2.epa.gov/green-chemistry/basics-green-chemistry#definition.

(3) Anastas, P. T.; Warner, J. C. *Green Chem. Theory Pract. Oxford Univ. Press. New York* **1998**, 30.

(4) Anastas, P. T.; Bartlett, L. B.; Kirchhoff, M. M.; Williamson, T. C. *Catal. Today* **2000**, *55* (1–2), 11–22.

(5) Anastas, P. T.; Kirchhoff, M. M.; Williamson, T. C. *Appl. Catal. A Gen.* **2001**, *221* (1–2), 3–13.

(6) Masters, C. *Homogeneous Transition-metal Catalysis*; Chapman and Hall, 1981.

(7) Zhou, Q. L. *Angew. Chemie - Int. Ed.* **2016**, *55* (18), 5352–5353.

(8) Loferski, P. J. *U.S. Geolocial Surv. Miner. Yearb.* **2012**, No. August.

(9) Blanksby, S. J.; Ellison, G. B. *Acc. Chem. Res.* **2003**, *36* (4), 255–263.

(10) Wencel-Delord, J.; Dröge, T.; Liu, F.; Glorius, F. *Chem. Soc. Rev.* **2011**, *40* (9), 4740.

(11) Weidmann, V.; Maison, W. *Synth.* **2013**, *45* (16), 2201–2221.

(12) Smith III, A. B.; Konopelski, J. P. *J. Org. Chem.* **1984**, *49* (21), 4094–4095.

(13) Fürstner, A.; De Souza, D.; Parra-Rapado, L.; Jensen, J. T. *Angew. Chemie - Int. Ed.* **2003**, *42* (43), 5358–5360.

(14) Kurasaki, H.; Okamoto, I.; Morita, N.; Tamura, O. *Chem. - A Eur. J.* **2009**, *15* (46), 12754–12763.

(15) Robinson, E. E.; Thomson, R. J. *J. Am. Chem. Soc.* **2018**, 1956–1965.

(16) Salvador, J. A. R.; Clark, J. H. *Green Chem.* **2002**, *4* (4), 352–356.

(17) Mahapatra, D.; Bharti, S.; Asati, V. *Eur. J. Med. Chem.* **2015**, *98*, 69–114.

(18) Garg, G.; Forsberg, L. K.; Zhao, H.; Blagg, B. S. J. *Chem. - A Eur. J.* **2017**, *23* (65), 16574–16585.

(19) Hunter, G. L. K.; Brogden, W. B. *J. Food Sci.* **1965**, *30* (5), 876–878.

(20) Saint-Lary, L.; Roy, C.; Paris, J. P.; Tournayre, P.; Berdagué, J. L.; Thomas, O. P.; Fernandez, X. *Chem. Biodivers.* **2014**, *11* (6), 843–860.

(21) Schiefner, A.; Sinz, Q.; Neumaier, I.; Schwab, W.; Skerra, A. *J. Biol. Chem.* **2013**, *288* (23), 16815–16826.

(22) Uehara, K.; Watanabe, J.; Mogi, Y.; Tsukioka, Y. *J. Biosci. Bioeng.* **2017**, *123* (3), 333–341.

(23) Schmidberger, P. C.; Schieberle, P. *J. Agric. Food Chem.* **2017**, *65* (42), 9287–9296.

(24) Riley, H. L.; Morley, J. F.; Friend, N. A. C. *J. Chem. Soc.* **1932**, 1875–1883.

(25) Trachtenberg, E. N.; Nelson, C. H.; Carver, J. R. *J. Org. Chem.* **1970**, *35* (5), 1653–1658.

(26) Umbreit, M. A.; Sharpless, K. B. *J. Am. Chem. Soc.* **1977**, *99* (16), 5526–5528.

(27) Sharpless, K. B.; Lauer, R. F. *J. Am. Chem. Soc.* **1972**, *94* (20), 7154–7155.

(28) Salmond, W. G.; Barta, M. A.; Havens, J. L. *J. Org. Chem.* **1978**, *43* (10), 2057–2059.

(29) Kochi, J. K. *Free radicals*, Vol. 1.; Wiley: New York, 1973.

(30) Srinivasan, K.; Perrier, S.; Kochi, J. K. *J. Mol. Catal.* **1986**, *36* (3), 297–317.

(31) Fousteris, M. A.; Koutsourea, A. I.; Nikolaropoulos, S. S.; Riahi, A.; Muzart, J. **2006**, *250*, 70–74.

(32) Hydroperoxide, Δ. U.; Li, Y.; Wu, X.; Lee, T. B.; Isbell, E. K.; Parish, E. J.; Gorden, A. E. V. **2010**, No. 24, 1807–1810.

(33) Silva, F. P.; Jacinto, M. J.; Landers, R.; Rossi, L. M. *Catal. Letters* **2011**, *141* (3), 432–437.

(34) Catino, A. J.; Forslund, R. E.; Doyle, M. P. *J. Am. Chem. Soc.* **2004**, *126* (42), 13622–13623.

(35) Li, Z.; Leed, N. a.; Dickson-Karn, N. M.; Dunbar, K. R.; Turro, C. *Chem. Sci.* **2014**, *5* (2), 727.

(36) Angeles-Boza, A. M.; Chifotides, H. T.; Aguirre, J. D.; Chouai, A.; Fu, P. K. L.; Dunbar, K. R.; Turro, C. *J. Med. Chem.* **2006**, *49* (23), 6841–6847.

(37) Cotton, F.; Murillo, C.; Walton, R. *Multiple bonds between metal atoms*; 2005.

(38) Zhu, T. P.; Ahsan, M. Q.; Malinski, T.; Radish, K. M.; Bear, J. L. *Inorg. Chem.* **1984**, *23* (1), 2–3.

(39) Choi, H.; Doyle, M. P. *Org. Lett.* **2007**, *9* (26), 5349–5352.

(40) Ratnikov, M. O.; Doyle, M. P. *Mendeleev Commun.* **2014**, *24* (4), 187–196.

(41) Mclaughlin, E. C.; Choi, H.; Wang, K.; Chiou, G.; Doyle, M. P. *J. Org. Chem.* **2009**, *74*, 730–738.

(42) Bear, J. L.; Yao, C. L.; Lifsey, R. S.; Korp, J. D.; Kadish, K. M. *Inorg. Chem.* **1991**, *30* (2), 336–340.

(43) Bear, J. L.; Han, B.; Li, Y.; Ngubane, S.; Van Caemelbecke, E.; Kadish, K. M. *Polyhedron* **2009**, *28* (8), 1551–1555.

(44) Bear, J. L.; Van Caemelbecke, E.; Ngubane, S.; Da-Riz, V.; Kadish, K. M. *Dalton Trans.* **2011**, *40* (11), 2486–2490.

(45) Das, K.; Kadish, K. M.; Bear, J. L. *Inorg. Chem.* **1978**, *17* (4), 930–934.

Chapter 2

Synthesis and characterization of dirhodium (II) complexes

2.1 Introduction

The chemistry of metal-metal bonded dirhodium(II) complexes has been extensively studied as a result of the fascinating properties of these compounds.[1] The stabilization of these complexes can be attributed to the presence of the bond between each Rh(II) metal centre whereby the overall oxidation state of the complex is characterized as Rh_2^{4+}. The applications of these compounds encompass medicinal chemistry,[2] photochemistry, material chemistry,[3,4] design of supramolecular structures[5] but above all, the use dirhodium as catalysts for organic reactions transformations.[6–8] This versatility is due to the possibility of preparing a large variety of complexes with different properties by modifying, even slightly, the structure of the ligands which surround the dimetal core.

Paddlewheel dirhodium complexes may have axial (*ax*) and equatorial (*eq*) ligands (see *Figure 1.2*, Chapter 1). The presence of the former, is not necessary for catalytic purposes which is the aim of this work. The focus is on the latter which is, instead, crucial to tune the catalytic properties of the complexes. These bridging ligands are generally uninegative, bent, trinuclear anions in which the distance between the donor atoms is similar to the Rh-Rh distance.[1]

After the synthesis of $Rh_2(OCCH_3)_4$, complexes with different donor atoms have been prepared. It has been observed that the substitution of the acetate ligands in $Rh_2(OCCH_3)_4$ with ligands containing nitrogen donor atoms, not only dramatically favours the electrochemical access to the Rh(II)-Rh(III) species but, in some cases, also makes accessible the Rh(III)-Rh(III) species.[9] The enhanced electron density within the Rh_2^{4+} core due to better σ-donor ligands causes dramatic effects on the redox properties of the complexes.

It has been proposed that the mechanism for allylic oxidation catalyzed by $Rh_2(cap)_4$ involves the oxidation of the dimetal core and coordination of OH in the axial position.[6] *N,N'*-formamidine type ligands serve to introduce the amidinate group which makes the dirhodium core more electron rich. This should favour the catalysis of allylic oxidation by easier oxidation of the dimetal core to Rh(II)- Rh(III).

In this chapter the synthesis and characterization of *N,N'*-type ligands and of the complex with either carboxylates or formamidinate ligands will be discussed.

2.2 Synthesis and characterization of *N,N'*-type ligands (L1, L2, L3)

The ligands **L1**, **L2** and **L3** were prepared using a modified literature[10] method (*Scheme 2.1*).

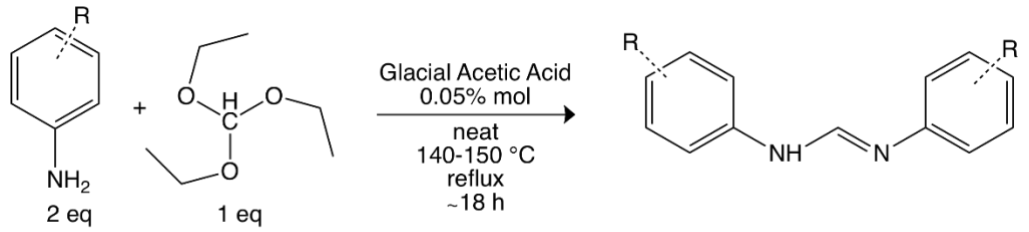

R= 4-methyl **(L1)**; 2-Fluoro **(L2)**; 4-Fluoro **(L3)**

Scheme 2. 1: *Synthesis of the ligands **L1**, **L2** and **L3***

The synthesis involved stirring one equivalent of triethylorthoformate and glacial acetic acid in catalytic amounts, before the addition of the respective anilines. Refluxing this reaction mixture overnight without any additional solvent, led to the formation of the desired ligands **L1**, **L2** and **L3** as solids. The reaction follows the general mechanism described in *Scheme 2.2*.

The formation of the ligands is favoured by the production of EtOH as by-product and the stabilization is due to the resonance of the lone pair on the nitrogen atom.

The ligands were purified by recrystallization from warm DCM resulting in white or yellowish solids with good yields. These were characterized using ^{1}H NMR, ^{13}C{H} NMR, HSQC, FT-IR spectroscopy, elemental analysis and X-ray diffraction.

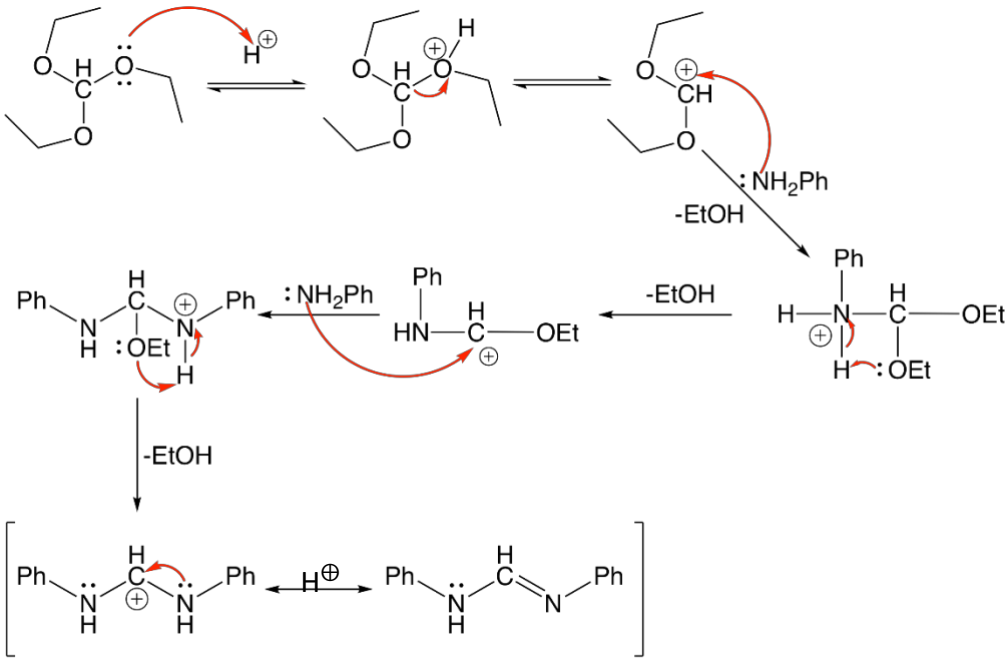

Scheme 2. 2.: *General mechanism for the synthesis of **L1**, **L2** and **L3***

The ^{1}H NMR spectra (*Figure 2.1*) for all the ligands (**L1**, **L2** and **L3**) show the presence of the imine proton at 8.11 ppm, 8.05 ppm and 8.02 ppm respectively, as well as aromatic signals different for each ligand at 6.95-7.12 ppm, 7.10 ppm and 7.00 ppm.

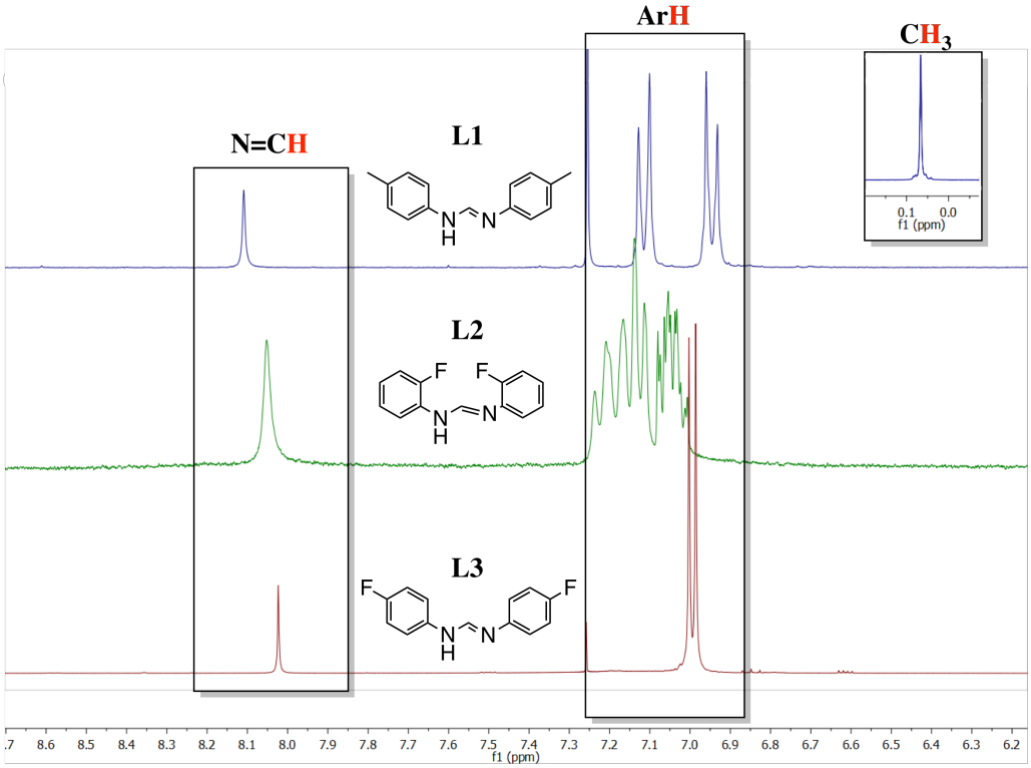

Figure 2. 1: *^{1}H NMR spectra of the ligands **L1** in ($CDCl_3$), (**L2** (in DMSO-d_6) and **L3** (in $CDCl_3$)*

The ^{1}H NMR of the ligand **L2** was collected in DMSO-d_6 to not cover the aromatic signals with the $CHCl_3$ residue, and it shows the presence of a broad signal in the aromatic region. This is attributed to a prototropic tautomerism which has been previously reported in literature.[11–13] The possible isomers for a generic amidinate ligand are shown in *Figure 2.2*. Isomerization can lead to geometric isomers (*Figure 2.2* a), C-N rotation gives *syn* or *anti* isomers (*Figure 2.2* b) while prototropic tautomerism gives the isomers shown in *Figure 2.2* c. This phenomenon is especially visible in the ^{1}H NMR spectrum of the ligand **L2** because it was collected in DMSO-d_6 with strong hydrogen-bonding acceptor properties which favours the tautomerism giving broad signals. This dynamics can also be attributed to the acidity of the proton involved in the tautomerism which is higher for the ligands **L2** and **L3** compared to **L1**. This hypothesis is confirmed by the further reported crystallographic data (reported in section 2.4). All the three ligands (**L1** – **L3**) are therefore, assumed to be tautomeric in solution. Due to the fact that the ^{1}H NMR implies slow relaxation times compared to the molecular motions, if the proton is rapidly delocalized between two positions, the NMR signal will be mediated between the two signals for the undelocalized protons.

In the $^{13}C\{H\}$ NMR (see Appendix A) the imine carbon is observed at 148.06 ppm (**L1**), 148.4 ppm (**L2**) and 158.42 ppm (**L3**). The downfield shift of both the imine proton and imine carbon in the series, is due to the different electronic properties of the aromatic ring substituents. For ligands **L2** and **L3** which contain the electron withdrawing fluorine as substituent in *para*- and *ortho*-position of the phenyl ring, it is possible to observe the downfield shift of the signals. The HSQC NMR spectra (see Appendix B) of the ligands **L1**, **L2** and **L3** were used to validate the assignment in the $^{13}C\{H\}$ NMR spectra.

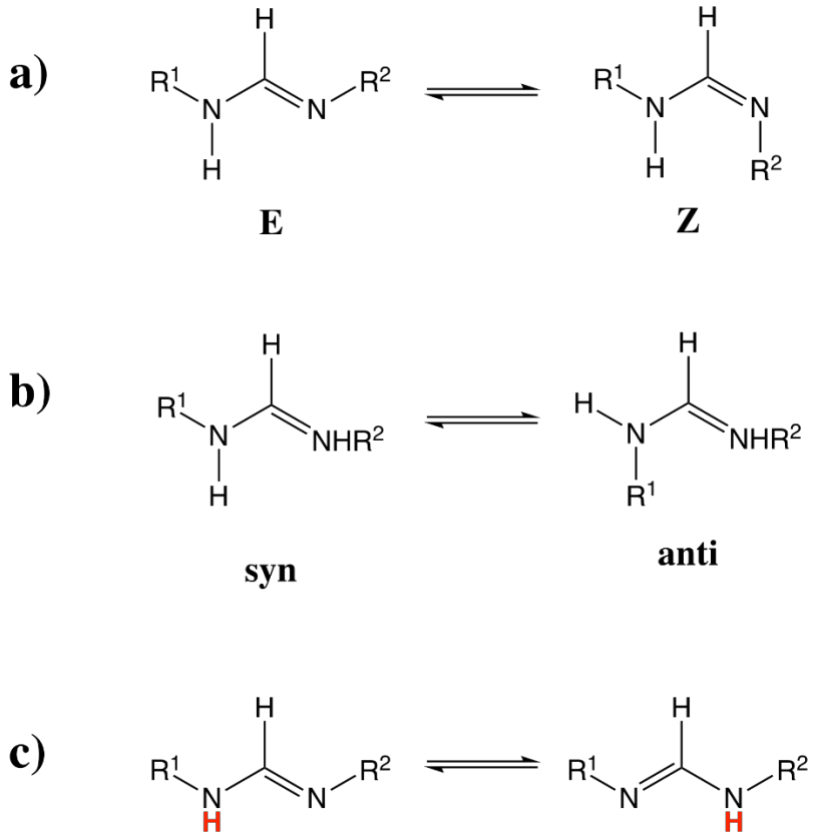

Figure 2. 2: *Possible isomers of the amidine-type ligand*

In the infrared spectrum (*Figure 2.3*) of **L1**, it is possible to observe the characteristic intense imine band at ν(C=N) 1670 cm^{-1}. For **L2** and **L3** the same band is observed at ν(C=N) 1668 cm^{-1} and ν(C=N) 1667 cm^{-1} respectively, and the C-F absorption band at ν(C-F) 1227 cm^{-1} (**L2**) and ν(C-F) 1199 cm^{-1} (**L3**). This last band is obviously absent for the ligand **L1**. For all three ligands is possible to observe a weak broad band between 2800 and 3200 cm^{-1} which is assigned to the N-H stretching. The calculated results for elemental analysis are in agreement with the results obtained experimentally.

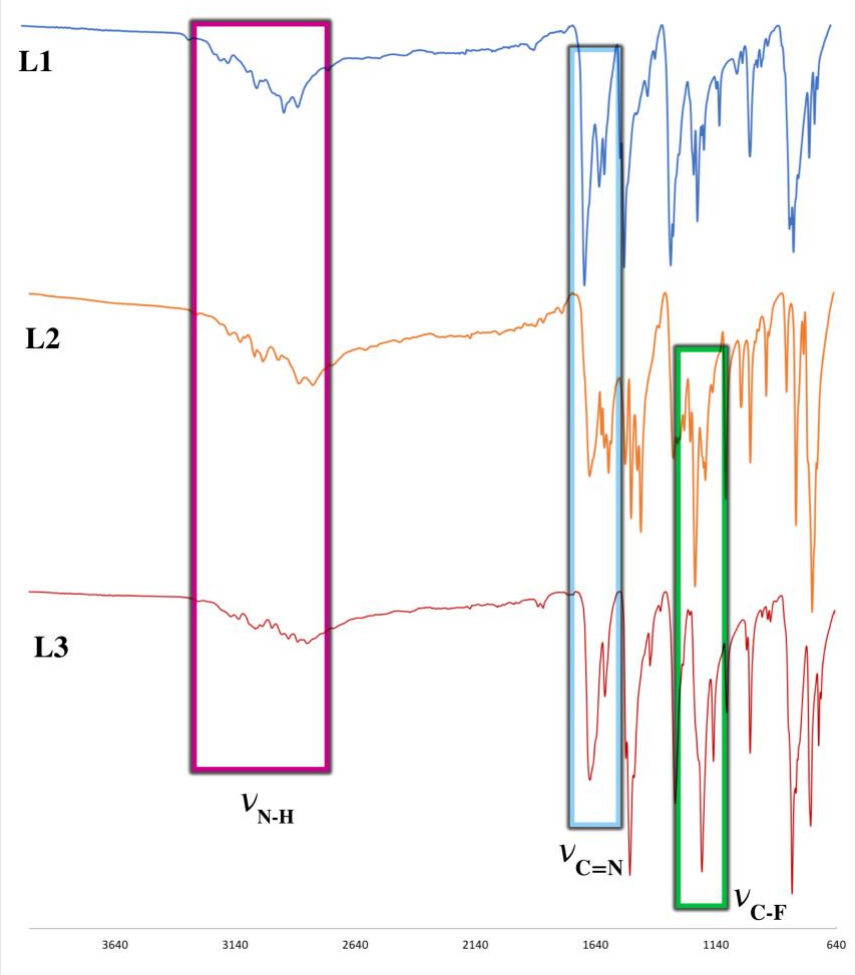

Figure 2. 3: *FT-IR spectra of the ligands* ***L1****,* ***L2*** *and* ***L3***

2.3 Synthesis and characterization of dirhodium(II) complexes

2.3.1 Synthesis of $Rh_2(O_2CCH_3)_4$ (C1)

To prepare the known complex **C1** a literature procedure was followed.[14] The reaction involved refluxing rhodium trichloride trihydrate and sodium acetate trihydrate in glacial acetic acid and absolute ethanol, for 3 h in absence of air (*Scheme 2.3*).

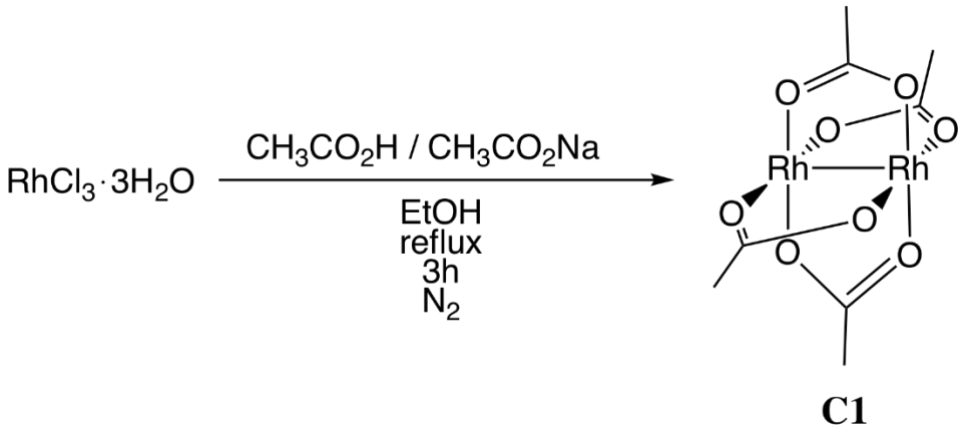

C1

Scheme 2. 3: *Synthesis of the complex* ***C1***

The desired product is obtained when there is a colour change in the reaction mixture from dark red to emerald green due to the formation of the metal-metal bond. Coordination of the acetate ligands to the dirhodium (II) metal centre occurs *via* the carboxylic oxygens of the chelating acetate groups. The crude product was dissolved in boiling methanol to remove the unreacted, but the solvent coordinates to the axial position of the complex causing a colour change of the product from emerald green to blue. Methanol was removed from the axial position by heating the compound under vacuum at 45 °C for 22 h. This process was monitored through FT-IR. The complex was obtained with a moderate yield (67%) probably because the reaction needs to be carried out for longer times**. C1** was characterized using ^{1}H NMR, FT-IR spectroscopy, elemental analysis, mass spectrometry and UV-Vis spectroscopy.

Mononuclear Rh(II) has a d^7 electron configuration and thus contain unpaired electron resulting in paramagnetic complex making the NMR characterization impossible. The formation of the metal-metal bond leads to an electron configuration with 14 paired electrons. This is the reason why it is possible to characterize all the complexes prepared with NMR spectroscopy. The ^{1}H NMR spectrum of **C1** (*Figure 2.4*) shows the methyl signal at 1.81 ppm. Compared to the ^{1}H NMR spectrum of acetic acid in DMSO-d_6 in which the methyl signal occurs at 1.91 ppm,[15] the singlet of the **C1** complex is shifted upfield due to the coordination with the dimetal centre.

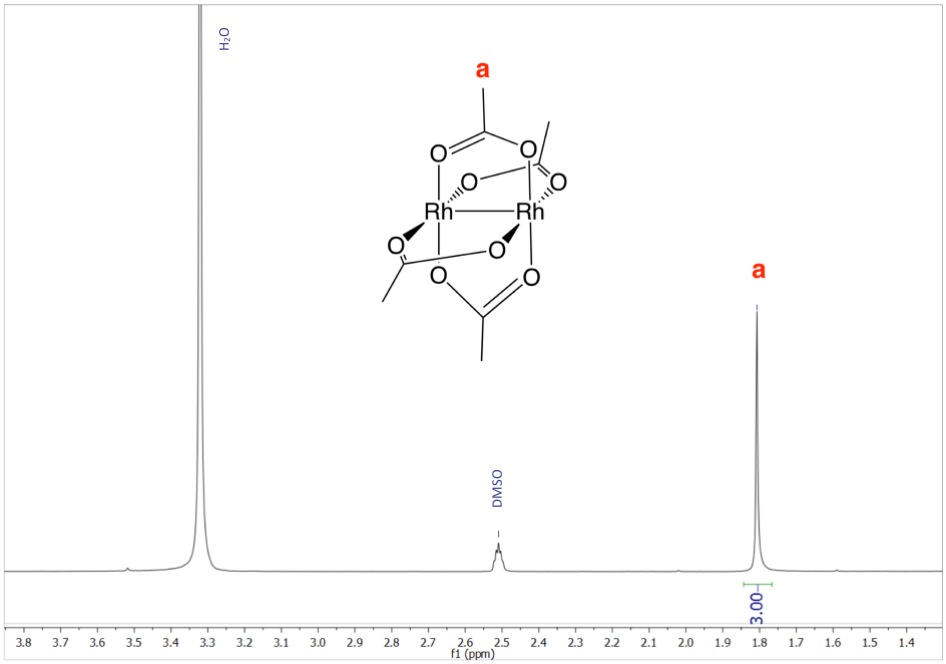

Figure 2. 4: *^{1}H NMR spectrum of the complex **C1** in DMSO-d_6*

In the FT-IR spectrum (*Figure 2.5*) of **C1** ν(C=O) is observed at 1572 cm^{-1}. Above 3000 cm^{-1} is shown the O-H broad band of the coordinated MeOH which gradually disappears after heating the solid under vacuum. This result is in agreement with the one reported in literature.[16]

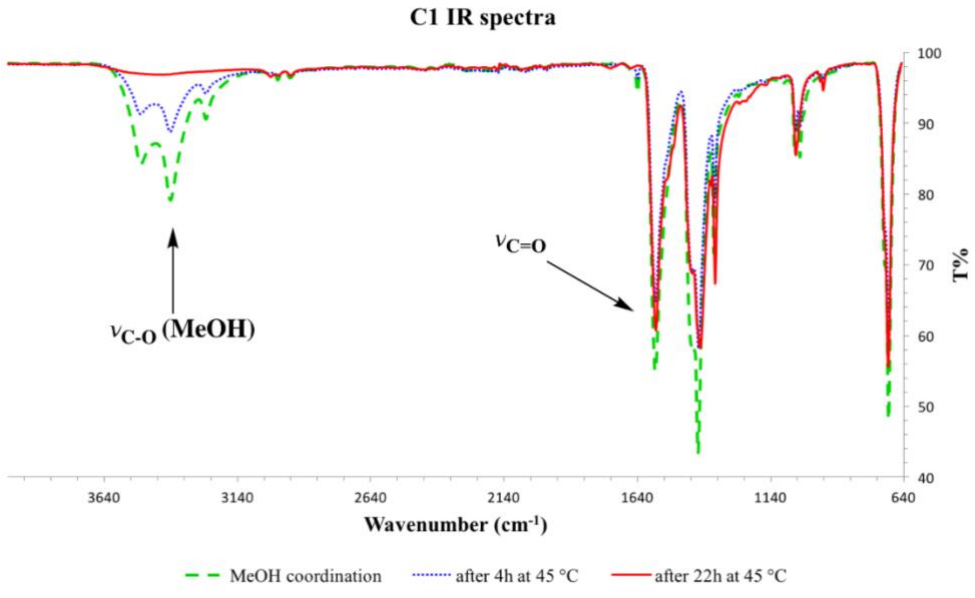

Figure 2. 5: *FT-IR spectra of the complex **C1***

The calculated results for elemental analysis are in agreement with the one obtained experimentally. The ESI mass spectrum shows a base peak for [M–H]$^+$ ion at m/z =442.87, corresponding to the molecular weight of the cationic complex **C1**.

The compound **C1** is only slightly soluble in DCM, DMSO, MeOH and ACN. Interestingly, even the partial dissolution of the emerald green solid in the above-mentioned solvents, gives different coloration (*Figure 2.6*).

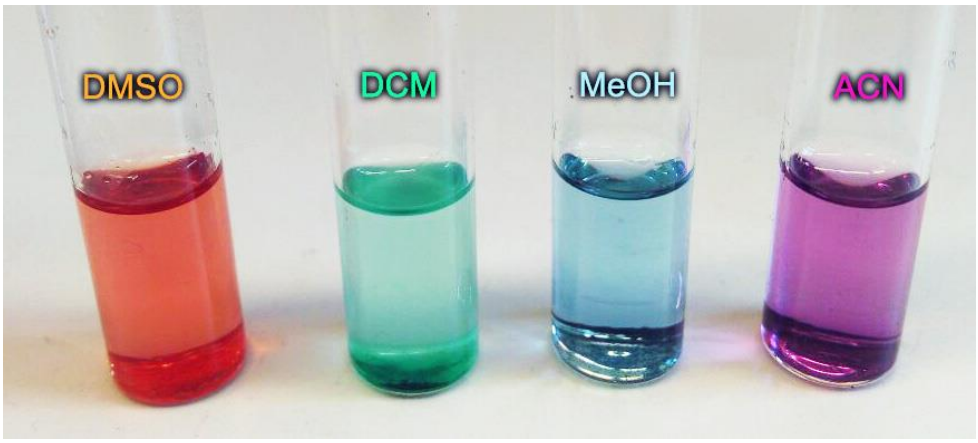

Figure 2. 6: *Complex **C1** in different solvents*

In the non-coordinating DCM, the colour of the mixture is not different from the solid. Instead, in coordinating solvents the change in colour of the complex is due to the coordination of the solvent in axial position and is directly related to the coordinating donor atom. This is strongly linked to the energy of the LUMO (σ^*) orbital.[17] As literature reported,[18] when **C1** is dissolved in DMSO coordination of the DMSO occurs via the sulfur atom due to the soft character of the Rh metal centre and the mixture is orange. In MeOH the coordination takes place through the lone pair of oxygen and the colour is blue. In ACN the donor atom is the nitrogen, so the colour is violet.

2.3.2 Synthesis of $Rh_2(OCCF_3)_4$ (C2)

The complex **C2** was prepared following a previously described procedure (*Scheme 2.4*).[18]

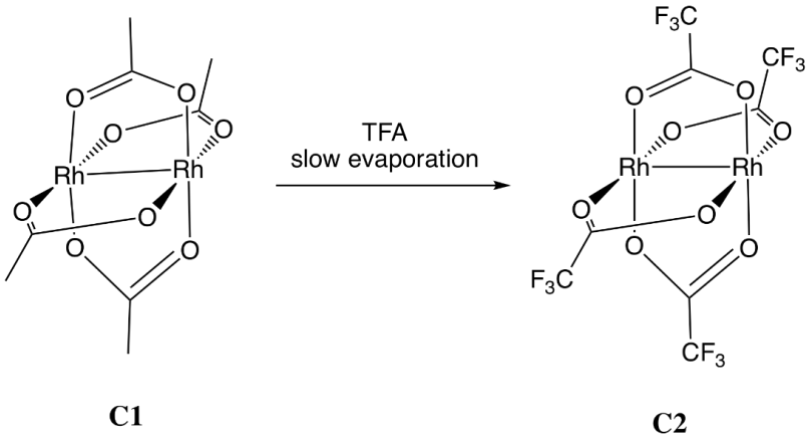

Scheme 2. 4: *Synthesis of the complex **C2***

The compound **C1** was dissolved in trifluoroacetic acid which was then gently evaporated on a steam bath. The exchange reaction follows the mechanism showed in *Scheme 2.5*[19] in which there is the formation of intermediate species that contain both acetate and trifluoroacetate ligands.

The blue coloration of the obtained solid is due to the axial coordination of acetic acid or trifluoroacetic acid. For this reason, the product was dried at 110 °C under vacuum for 5h during which the formation of an emerald green powder was observed which then resulted to be light sensitive.

The complex **C2** was characterized with ^{1}H NMR, FT-IR spectroscopy, elemental analysis, mass spectrometry and UV-Vis spectroscopy.

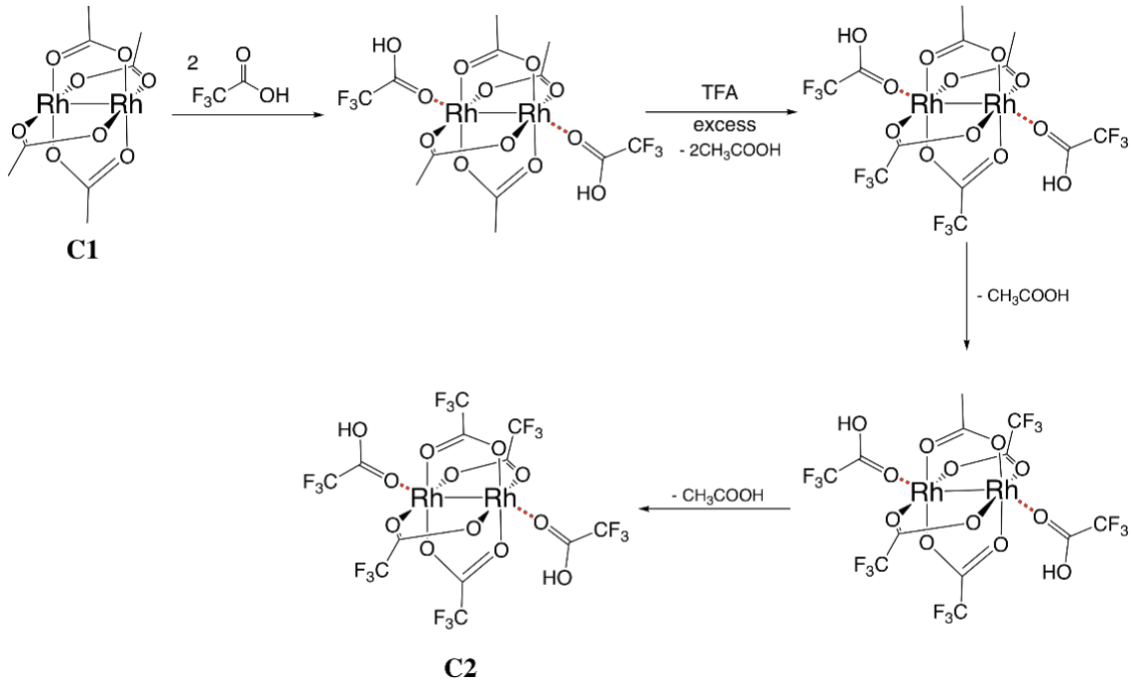

Scheme 2. 5: *General mechanism for the synthesis of* ***C2***

The ^{1}H NMR spectrum (*Figure 2.7*) showed a sharp singlet at 1.73 ppm which was attributed to residual acetic acid axially coordinated to the dimetal centre. Indeed, is upfield shifted compared to the ^{1}H NMR spectrum of the free acid.

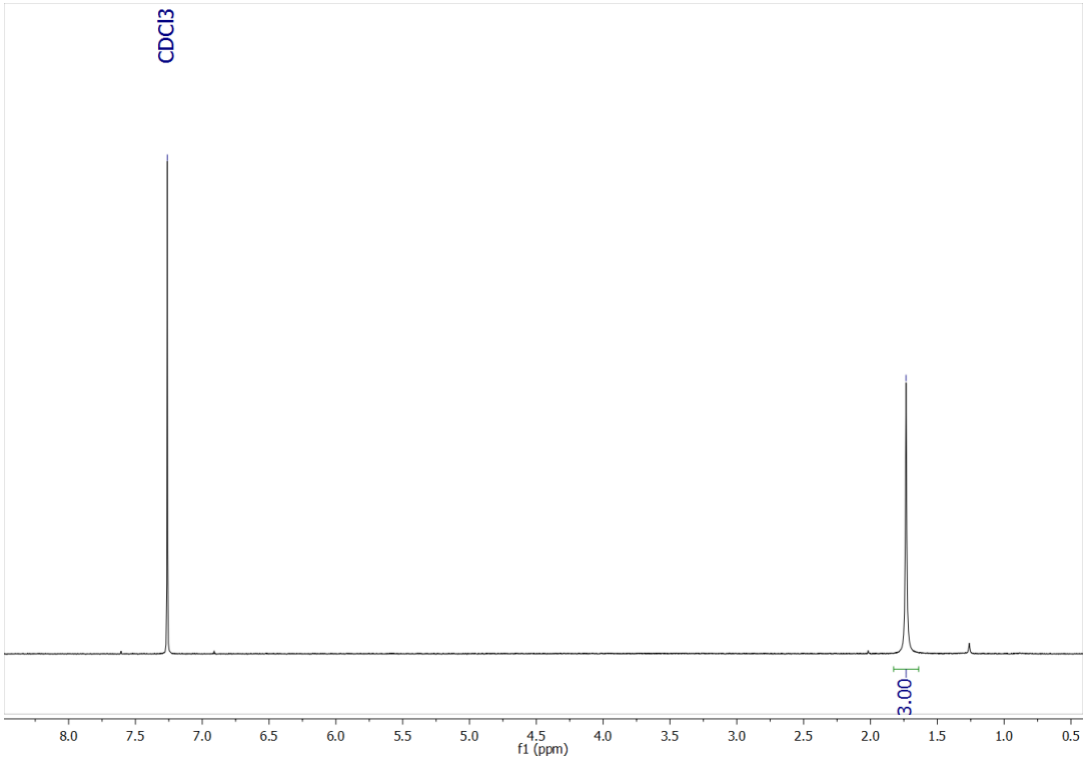

Figure 2. 7: *^1H NMR of the complex **C2** in $CDCl_3$*

The FT-IR spectrum (*Figure 2.8*) shows the C=O stretching band at ν(C=O) 1650 cm^{-1} and the C-F stretching frequency appears at ν(C-F) 1161 cm^{-1} as an intense, sharp band. After the collection of the spectrum using the ATR-IR technique, it has been noticed that the emerald

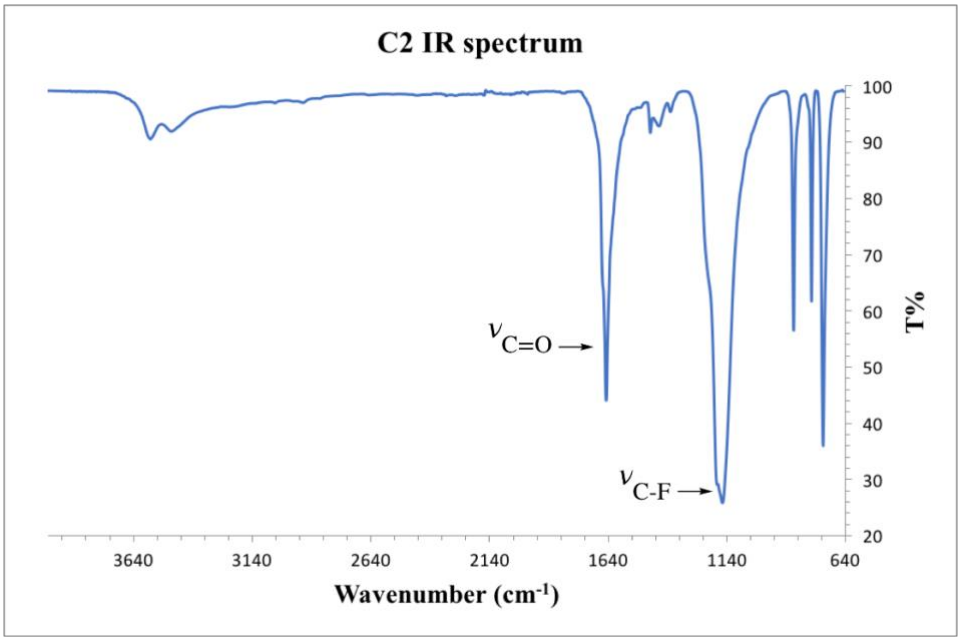

Figure 2. 8: *FT-IR spectrum of the complex **C2***

green solid sample became grey indicating the light sensitiveness of **C2**. This is the same result obtained keeping a sample of the complex **C2** under natural light for few minutes.

The calculated results for elemental analysis are in agreement with the one obtained experimentally.

The mass spectrum shows a very complicated pattern. The signal relative to the molecule **C2**, which should be at 657.87 m/z, is absent. There is instead, the presence of many more signals which cannot be attributed to a precise structure. This is due to the formation of polymeric structures like the one in the *Figure 2.9* in which two adjacent molecules of complex are connected through two oxygen atoms occupying axial positions of neighbouring molecules.[20]

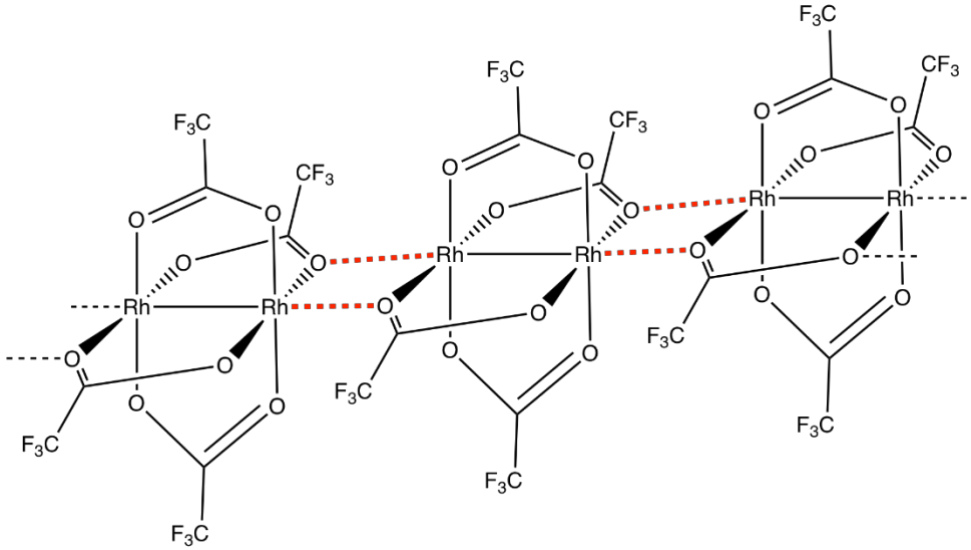

Figure 2. 9: *Polymeric structure of the complex* ***C2***

The complex **C2** resulted to be more soluble than **C1** in DMSO, ACN, MeOH and DCM. It is interesting to note that while dissolving **C1** in the ambidentate solvent DMSO, an orange mixture was obtained, using the same solvent for **C2** gave a blue solution (*Figure 2.10*). This is due to the different donor atoms involved in the axial bond with the complex which are able

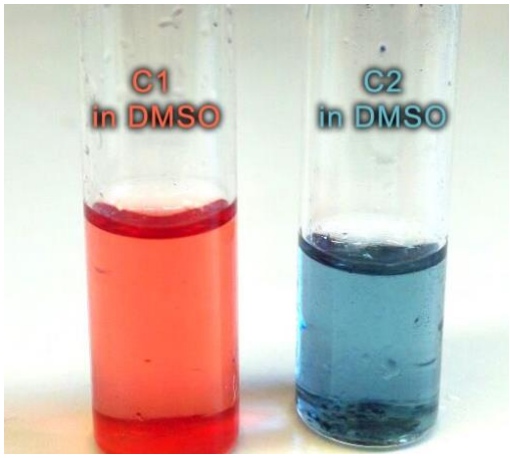

Figure 2. 10: *Complexes* ***C1*** *and* ***C2*** *in DMSO*

to modify the energy of the orbital involved in the electronic transition. In **C2** the presence of the trifluoroacetate bridging ligands leads to an electronic change in the character of rhodium which become a harder acid (HSAB) compared to the situation with **C1**. So, while in the complex **C1** the softer metal centre coordinates DMSO through the sulfur atom, in **C2** the coordination takes place *via* the oxygen atom of the solvent.[21] This causes the different colours of the two compounds in the same solvent.

2.3.3 Synthesis of $Rh_2(dpf)_4$ (C3)

The known compound **C3** was prepared following a literature reported procedure[22] which was then adapted for all the Rh_2^{4+} complexes with a *N,N'*-type bridging ligand using a new developed method (*Scheme 2.6*).[23]

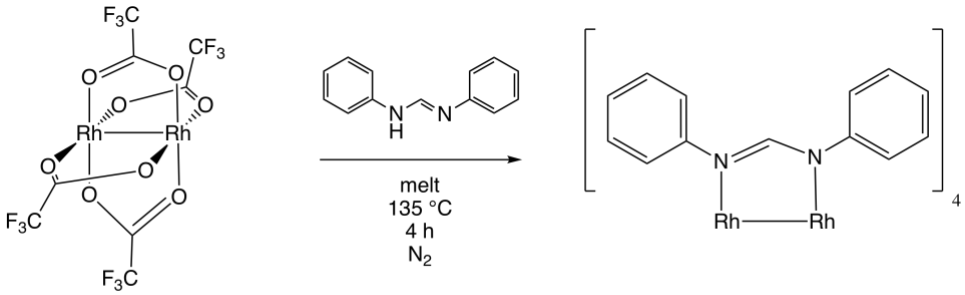

C2 **C3**

Scheme 2. 6: *Synthesis of the complex* ***C3***

N,N'-diphenylformamidine (dpf) was heated to melting (135 °C) in the absence of air before the addition of the complex **C2**. The exchange reaction between the trifluoroacetate ligands and the dpf ligands was immediate evident from the instantaneous colour change of the reaction mixture. The reaction was carried out for 4 h after which the formation of a dark solid was observed. To allow the removal of TFA, the system was heated at 100 °C for 2h, under vacuum. The solid product was washed with MeOH to remove the unreacted ligand and was then purified through recrystallization from DCM/MeOH giving a dark green solid with a moderate yield (52%). The complex **C3** was characterized with ^{1}H NMR, ^{13}C{^{1}H} NMR, FT-IR spectroscopy, elemental analysis, mass spectrometry and UV-Vis spectroscopy.

The ^{1}H NMR spectrum (*Figure 2.11*) shows the presence of the imine signal at 7.80 ppm. The same signal for the ligand occurs at 8.30 ppm.[24] This upfield shift of the imine proton is

attributed to the metal coordination. More precisely, to the back-donation of electrons from the

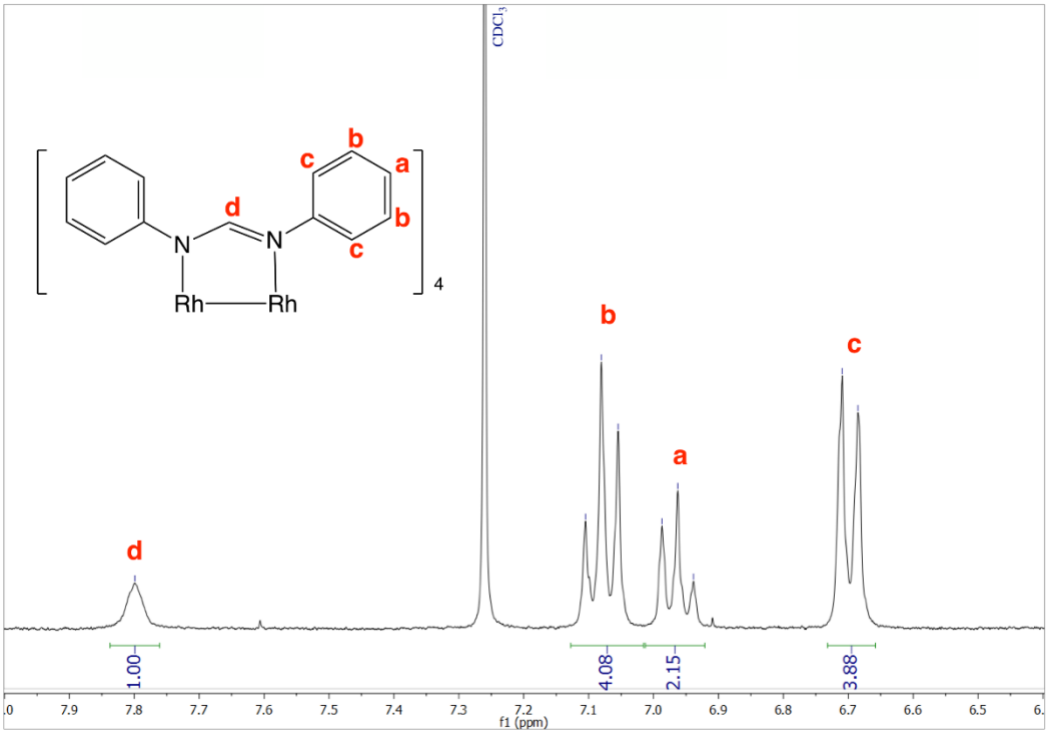

Figure 2. 11: *^{1}H NMR of the complex **C3** in $CDCl_3$*

dirhodium core to the imine nitrogens which increases the electron density.

Due to the limited solubility of the complex, it was not possible to solve the $^{13}C\{^{1}H\}$ NMR spectrum (see Appendix A).

The FT-IR spectrum (Figure 2.*12*) shows the presence of the characteristic imine stretching band at ν(C=N) 1571 cm^{-1}. In the FT-IR spectrum of the free dpf ligand this absorption band occurs at ν(C=N) 1658 cm^{-1}. The shift to lower stretching frequencies of the C=N band for the complex **C3**, confirms the dpf ligand has been coordinated to the dirhodium centre. The formation of the bond between the metal and nitrogen lowers the energy of the C-H imine bond leading to a reduction of the stretching frequency of the latter.

The calculated results for elemental analysis are in agreement with the one obtained experimentally. The ESI mass spectrum shows a base peak for $[M]^{+}$ ion at m/z =986.18 corresponding to the molecular weight of the cationic complex **C3**.

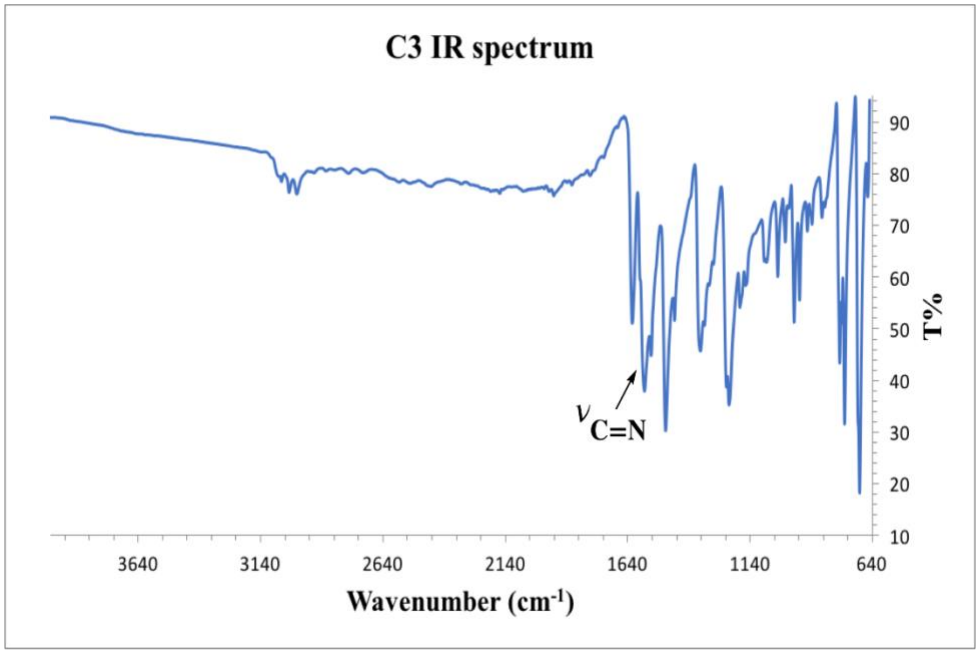

Figure 2. 12: *FT-IR spectrum of the complex* ***C3***

2.3.4 Synthesis of Rh_2(di-p-Tolf)$_4$ (C4)

The known compound **C4** was prepared following the procedure previously described (*Scheme2.7*).

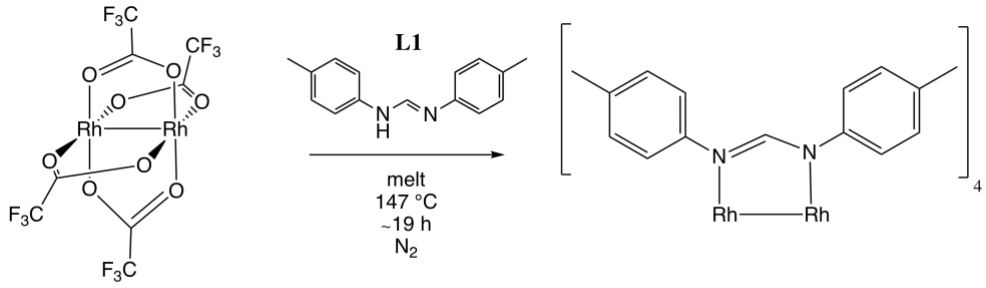

C2 **C4**

Scheme 2. 7: *Synthesis of the complex* ***C4***

The ligand **L1** was heated to melting (147 °C) in absence of air before the addition of the complex **C2**. The formation of a dark solid was immediately observed and the reaction was carried out for 19 h. The solid product was then dried under vacuum at 100 °C for 2 h to allow the evaporation of TFA. It was then washed several times with MeOH to remove the unreacted ligand **L1**. The solid powder obtained was purified through recrystallization from DCM/MeOH giving dark green crystals with a moderate yield (33%). The complex **C4** was characterized with ^{1}H NMR, ^{13}C{^{1}H} NMR, FT-IR spectroscopy, elemental analysis, mass spectrometry, X-

ray diffraction and UV-Vis spectroscopy.

In the ^{1}H NMR spectrum (*Figure 2. 13*) of **C4** the characteristic imine signal is reported at 7.68 ppm. Compared to the ^{1}H NMR spectrum of **L1** in which the same signal occurred at 8.11 ppm, the imine proton of the complex is shifted upfield. This is due to the metal coordination confirming the formation of the complex **C4**. The spectrum shows also the presence of a singlet at 2.23 ppm which is assigned to the methyl protons.

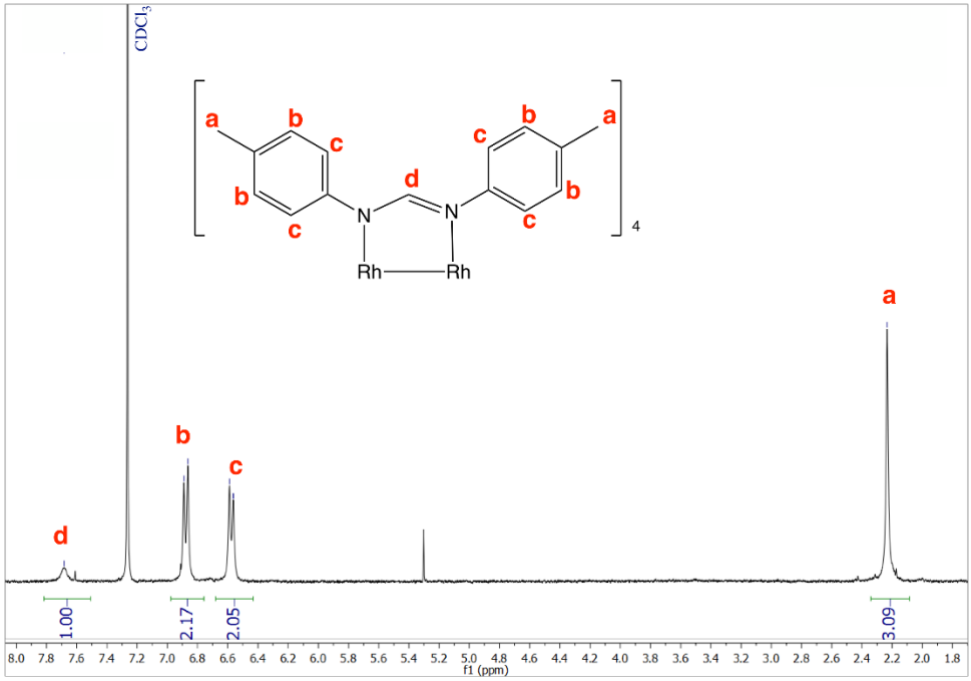

Figure 2. 13: *^{1}H NMR of the complex **C4** in $CDCl_3$*

The ^{13}C{^{1}H} NMR experiment (see Appendix A) shows resonances that correspond to the number of C atoms in complex **C4** with the characteristic imine carbon at 162.28 ppm.

The FT-IR spectrum (*Figure 2.14*) shows the C=N absorption band at ν(C=N) 1585 cm^{-1}. In the free ligand **L1** this absorption band appears at ν(C=N) 1670 cm^{-1} confirming the formation of the complex **C4**.

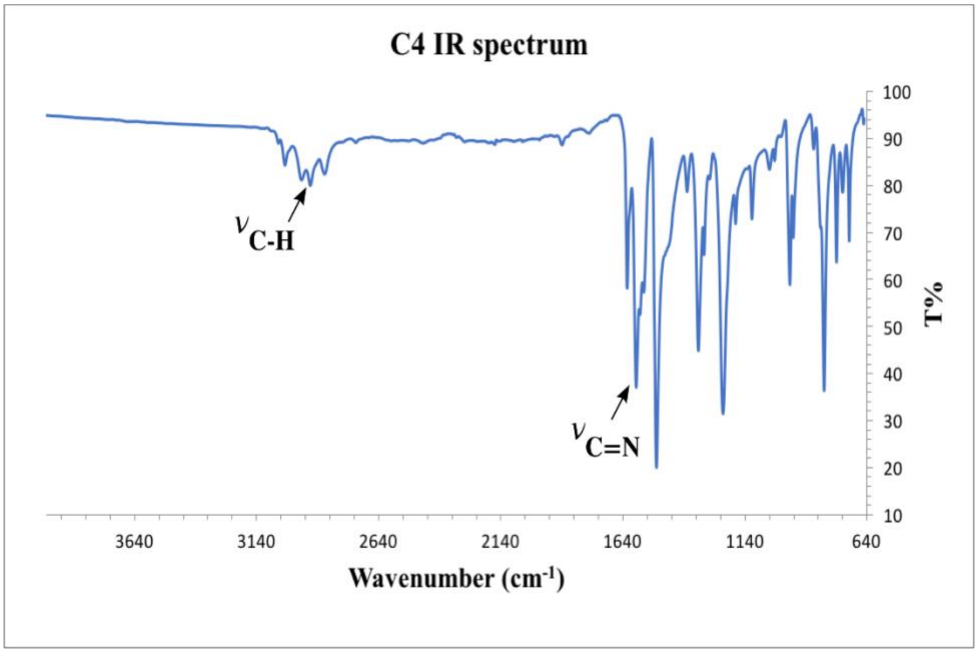

Figure 2. 14: *FT-IR spectrum of the complex* ***C4***

Additionally, in the region between 2863 cm^{-1} and 3051 cm^{-1} it is possible to observe the presence of the C-H absorption bands due to the methyl group. This same region for the ligand **L1** includes a weak broad band which indicates the presence of the N-H bond. The absence of the latter in the FT-IR spectrum of **C4** is proof of the coordination of ligand to the dimetal centre.

The calculated results for elemental analysis are in agreement with the one obtained experimentally. The ESI mass spectrum shows a base peak for $[M]^+$ ion at m/z =1098.30 corresponding to the molecular weight of the cationic complex **C4**.

2.3.5 Synthesis of Rh_2(di-2F-pf)$_4$ (C5)

The new compound **C5** was prepared following the procedure previously described (*Scheme 2.8*).

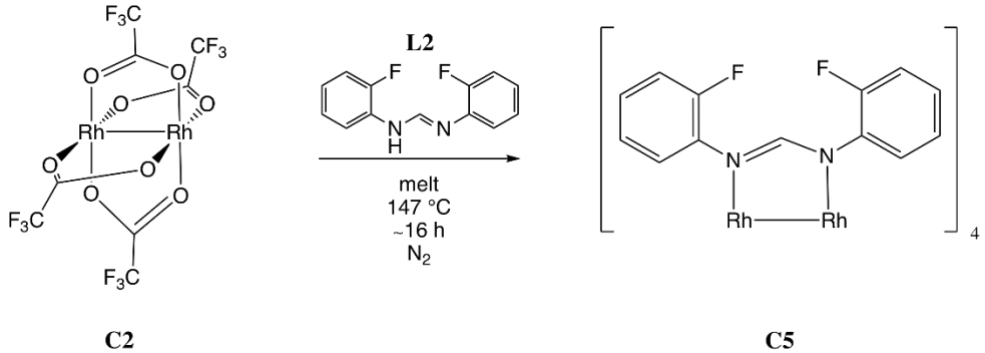

C2 **C5**

Scheme 2. 8: *Synthesis of the complex* ***C5***

The ligand **L2** was heated to melting in absence of air before the addition of the complex **C2**. The exchange reaction was carried out for 16 h and the formation of a dark solid was observed. The latter was heated under vacuum at 100 °C to allow the complete removal of TFA. It was then washed with diethyl ether to remove the unreacted ligand **L2**. The product obtained was purified through recrystallization from DCM/MeOH giving a red powder with a moderate yield (65%). The complex **C5** was characterized with ^{1}H NMR, ^{13}C{^{1}H} NMR, ^{19}F NMR, FT-IR spectroscopy, elemental analysis, mass spectrometry, X-ray diffraction and UV-Vis spectroscopy.

The ^{1}H NMR spectrum (*Figure 2.15*) shows the presence of the imine proton at 7.89 ppm. This signal appears to be shifted upfield when compared to its resonance in the free ligand **L2** (8.05 ppm). This is the evidence of the coordination of the imine nitrogens to the dimetal centre.

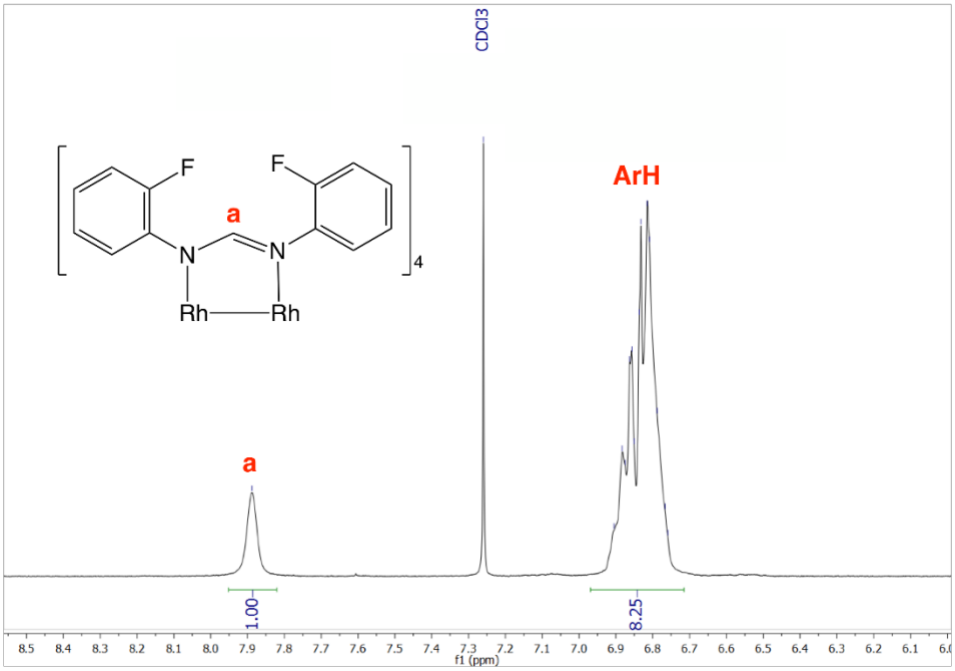

Figure 2. 15: *^{1}H NMR of the complex **C5** in $CDCl_3$*

The complex was not soluble enough to solve the ^{13}C{^{1}H} NMR spectrum (see Appendix A) of the complex **C5**. The ^{19}F NMR spectrum (see Appendix C) shows the presence of a signal at -128.90 ppm.

The infrared spectrum of the complex (*Figure 2.16*) shows a band for the imine functionality at ν(C=N) 1543 cm^{-1}. In the free ligand **L2** this band appears at ν(C=N) 1666 cm^{-1} confirming the formation of the complex **C5**. Even the absence of the weak broad band between 2600 cm^{-1} and 3200 cm^{-1} assigned to the N-H imine stretching, indicates the coordination to the dimetal centre. In the spectrum is possible to observe also the C-F band at ν(C-F) 1238 cm^{-1}.

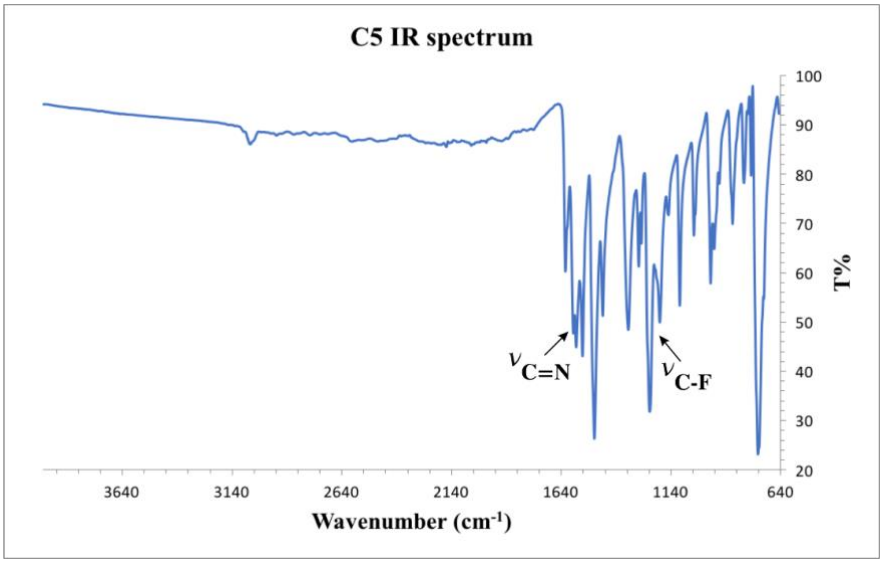

Figure 2. 16: *FT-IR spectrum of the complex* ***C5***

The calculated results for elemental analysis are in agreement with the one obtained experimentally. The ESI mass spectrum shows a base peak for $[M]^+$ ion at m/z =1130.10 corresponding to the molecular weight of the cationic complex **C5**.

2.3.6 Synthesis of Rh_2(di-4F-pf)$_4$ (C6)

The compound **C6** was prepared following the procedure previously described (*Scheme2.9*). The ligand **L3** was heated to melting in absence of air before the addition of the complex **C2**. The reaction was carried out for 19 h and the formation of a dark solid was observed.

The solid was purified through recrystallization from DCM/MeOH giving a green powder with a moderate yield (52%). The complex **C6** was characterized with ^{1}H NMR, ^{13}C{^{1}H} NMR, ^{19}F

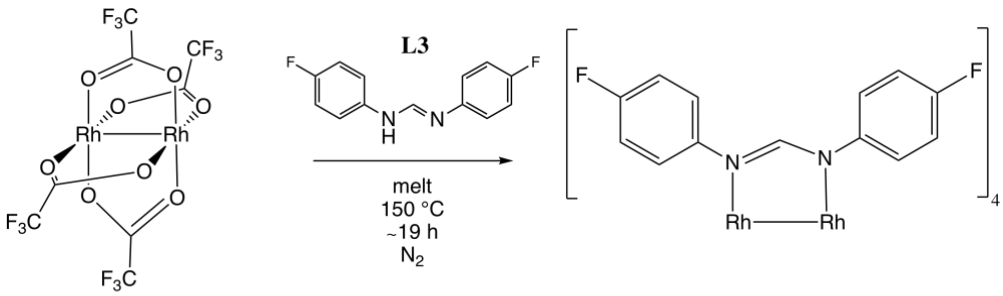

Scheme 2. 9: *Synthesis of the comlex* ***C6***

NMR, FT-IR spectroscopy, elemental analysis, mass spectrometry and UV-Vis spectroscopy.

In the ^{1}H NMR spectrum of the complex **C6** (*Figure 2.17*) it is possible to observe the presence of the imine proton at 7.70 ppm. This signal appears to be shifted upfield when compared to its resonance in the free ligand **L3** (8.02 ppm). This is the evidence of the coordination of the imine nitrogens to the dimetal centre. The signals show a splitting attributable to the long-range coupling with the fluorine atom.

The complex was not soluble enough to solve the $^{13}C\{^{1}H\}$ NMR spectrum (see Appendix A) of the complex **C6**. The ^{19}F NMR spectrum shows (see Appendix C) the presence of a signal at -119.35 ppm.

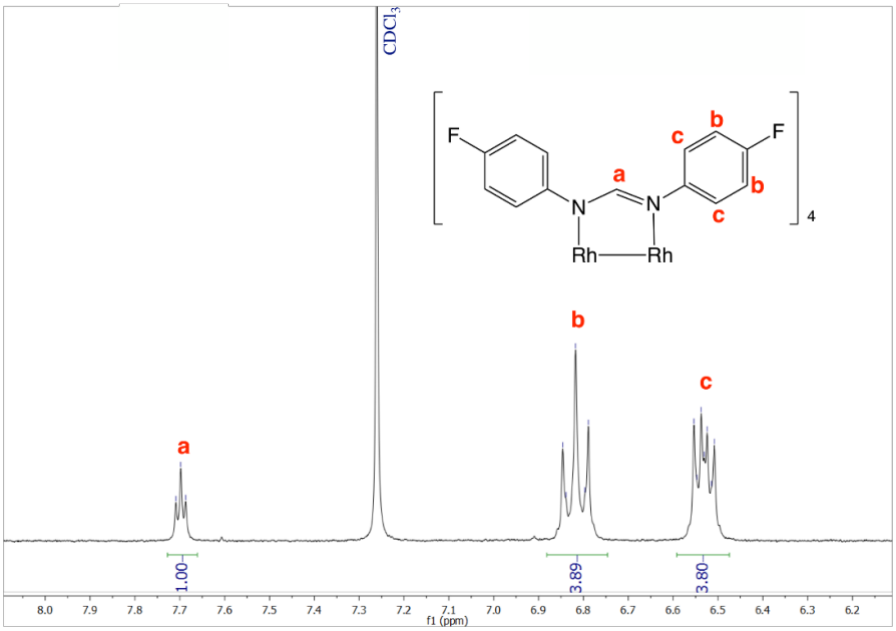

Figure 2. 17: *^{1}H NMR of the complex **C6** in $CDCl_3$*

The infrared spectrum of the complex (*Figure 2.18*) shows a band for the imine functionality at ν(C=N) 1581 cm^{-1}. In the free ligand **L3** this absorption band appears at ν(C=N) 1667 cm^{-1} confirming the formation of the complex **C6**. Even the absence of the weak broad band between 2600 cm^{-1} and 3200 cm^{-1} assigned to the N-H imine stretching, indicates the coordination to the dimetal centre. In the spectrum is possible to observe also the C-F band at ν(C-F) 1207 cm^{-1}.

The calculated results for elemental analysis are in agreement with the one obtained experimentally. The ESI mass spectrum shows a base peak for $[M]^+$ ion at m/z = 1130.11 corresponding to the molecular weight of the cationic complex **C6**.

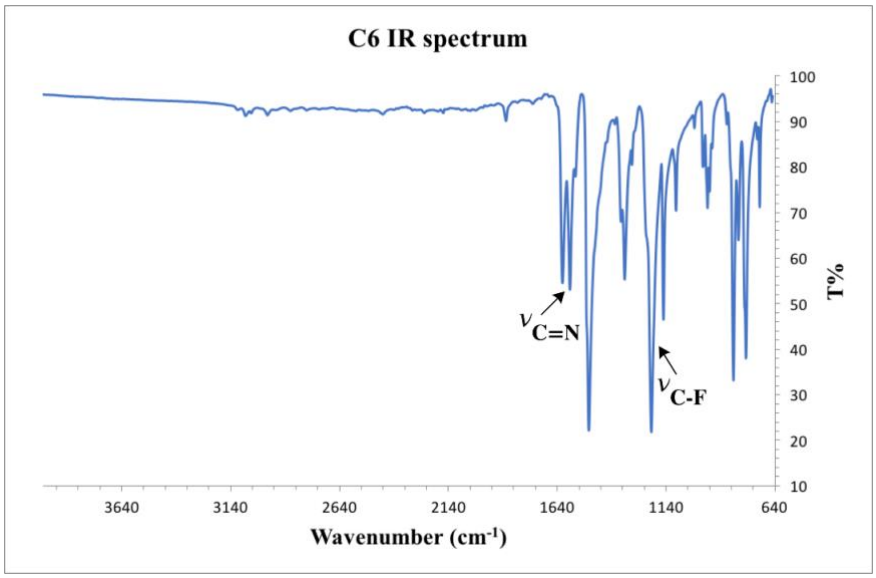

Figure 2. 18: *FT-IR spectrum of the complex* ***C6***

2.4 Solid state analysis

2.4.1 Crystal structure of the ligands L1, L2, L3

Single-crystal x-ray diffraction was also carried out to characterize the ligands. The crystals were grown dissolving the solid in warm DCM and allowing slow cooling. For **L1** (*Figure 2.19*) it was observed that the molecule is not planar, that the bond length between N1-C8 is of 1.218 Å and the one between N2-C8 is of 1.347 Å. These are typical values for an imine bond.[13]

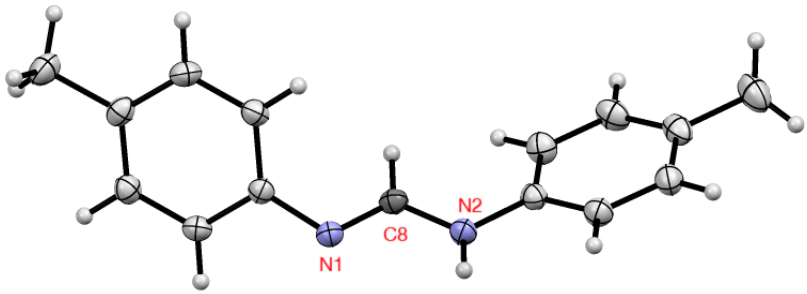

Figure 2. 19: *Crystal structure of the ligand* ***L1***

Even if it is not possible to assign a precise position to the imine double bond, it is possible to observe that the molecule is in a *E* configuration.

In the *Table 2.1* crystal data and structure refinement for **L1** are shown.

The crystal structure of the ligand **L2** (*Figure 2.20*) shows that the bond imine bond length is

respected (d_{N1-C7}= 1.313 Å; d_{N2-C7}= 1.315 Å) and that both of the fluorine atoms are on the same side of the plane. In the crystal structure of **L1** just one of the nitrogen atoms is bound to a proton, for **L2** due to a prototropic tautomerism between the two nitrogens involved in the imine bond. This is probably due to the increase in acidity linked to the presence of fluorine as aromatic substituent. Even if it's not possible to assign a precise position to the imine double bond, it is possible to observe that the molecule is in a *E* configuration.

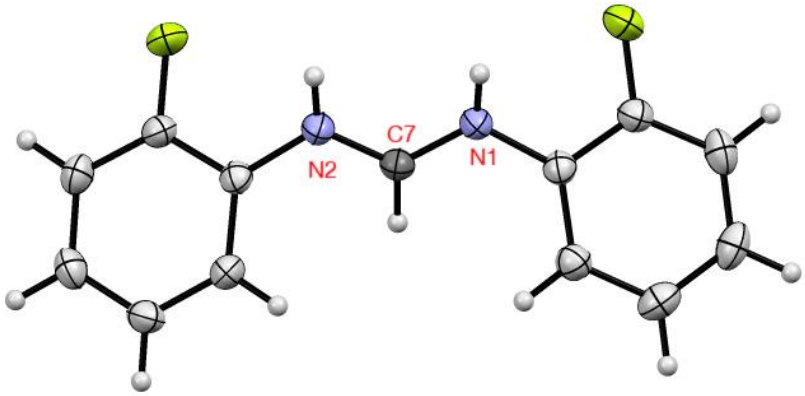

Figure 2. 20: *Crystal structure of* ***L2***

In the *Table 2.1* crystal data and structure refinement for **L2** are shown.

The crystal structure of **L3** (*Figure 2.21*) shows that also in this case the proton is delocalised between the two nitrogens N1 and N2. The bond length is d_{N1-C7}= 1.325 Å and d_{N2-C7}= 1.314 Å. The molecule is bent and it crystalize together with a molecule of solvent (DCM). When there's the total loss of the latter, the crystals become opaque. Even if it's not possible to assign a precise position to the imine double bond, it is possible to observe that the molecule is in a *E* configuration.

In the *Table 2.1* crystal data and structure refinement for **L3** are shown.

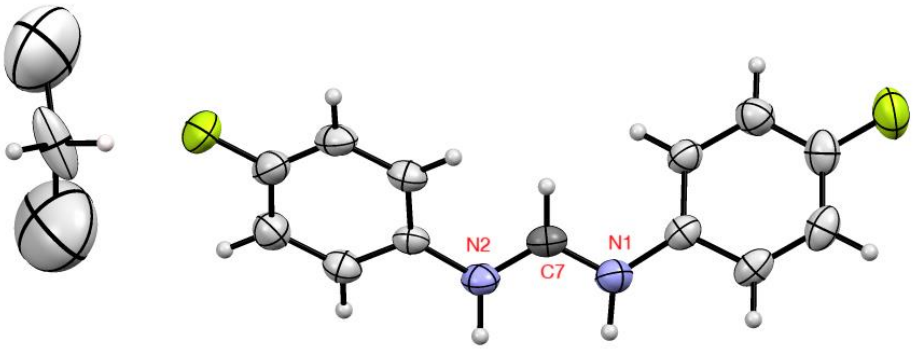

Figure 2. 21: *Crystal structure of* ***L3·CH_2Cl_2***

Table 2. 1: *Crystal data and structure refinement of* ***L1****,* ***L2*** *and* ***L3***

	L1	**L2**	**L3·CH_2Cl_2**
Empirical formula	$C_{15}H_{16}N_2$	$C_{13}H_{10}F_2N_2$	$C_{13.25}H_{10.5}Cl_{0.5}F_2N_2$
Formula weight	224.30	232.23	253.46
Temperature/K	173(2)	173(2)	173(2)
Crystal system	triclinic	monoclinic	tetragonal
Space group	P-1	C2/c	P-42_1c
a/Å	6.0412(12)	11.4578(17)	17.9835(17)
b/Å	10.056(2)	26.829(4)	17.9835(17)
c/Å	10.385(2)	7.3174(10)	7.3899(7)
α/°	86.552(4)	90	90
β/°	81.528(4)	104.226(3)	90
γ/°	83.736(4)	90	90
Volume/$Å^3$	619.6(2)	2180.4(5)	2389.9(5)
Z	2	8	8
ρ_{calc}g/cm^3	1.202	1.415	1.409
μ/mm^{-1}	0.072	0.109	0.214
F(000)	240.0	960.0	1044.0
Crystal size/mm^3	0.400 × 0.270 × 0.220	0.320 × 0.210 × 0.110	0.400 × 0.210 × 0.180
Radiation	MoKα (λ = 0.71073)	MoKα (λ = 0.71073)	MoKα (λ = 0.71073)
2Θ range for data collection/°	3.97 to 56.744	3.97 to 56.758	5.064 to 55.918
Index ranges	-8 ≤ h ≤ 8, -13 ≤ k ≤ 13, -13 ≤ l ≤ 13	-15 ≤ h ≤ 15, -35 ≤ k ≤ 35, -9 ≤ l ≤ 9	-23 ≤ h ≤ 23, -23 ≤ k ≤ 23, -9 ≤ l ≤ 9
Reflections collected	10439	16035	36166
Independent reflections	3074 [R_{int} = 0.0367, R_{sigma} = 0.0320]	2726 [R_{int} = 0.0386, R_{sigma} = 0.0266]	2870 [R_{int} = 0.0548, R_{sigma} = 0.0231]
Data/restraints/parameters	3074/0/161	2726/0/163	2870/28/175
Goodness-of-fit on F^2	1.098	1.038	1.113
Final R indexes [I>=2σ (I)]	R_1 = 0.0452, wR_2 = 0.1224	R_1 = 0.0385, wR_2 = 0.1003	R_1 = 0.0765, wR_2 = 0.2360
Final R indexes [all data]	R_1 = 0.0552, wR_2 = 0.1298	R_1 = 0.0532, wR_2 = 0.1101	R_1 = 0.0887, wR_2 = 0.2555
Largest diff. peak/hole / e $Å^{-3}$	0.28/-0.18	0.20/-0.19	1.09/-0.72
			0.09(10)

2.4.2 Crystal structure of the complex C

The crystal structure of the complex **C5** is showed in *Figure 2.22* (asymmetric unit) and *Figure 2.22*. The compound has an asymmetric unit and that the complete crystal structure is generated through an inversion centre. The distance between the rhodium atoms is of $d_{Rh\text{-}Rh}$=2.452 Å and is coherent with the distances between the two metal atoms when the bridging ligands are two nitrogen atoms.[1] In complexes with carboxylates ligand the distance between the metal atoms is higher.[25,26] This is probably due to the bite of the amidinate ligand which is also bulky and the increase in the bond length is due to its steric hindrance.

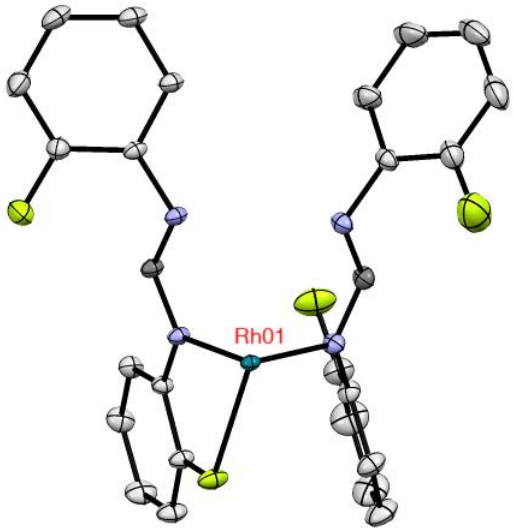

Figure 2. 22: *Asymmetric unit of the complex* ***C5***

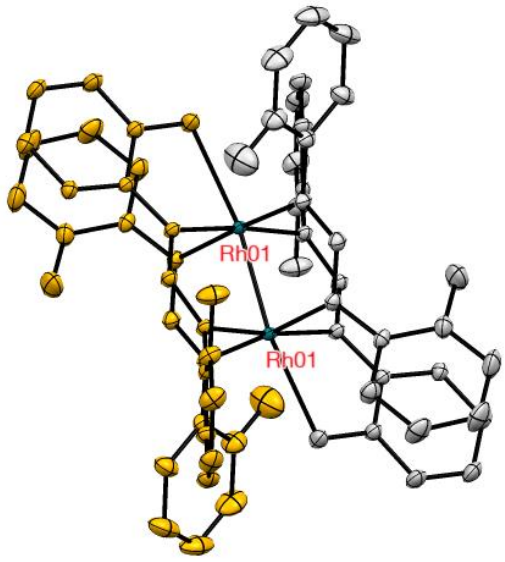

Figure 2. 23*: Crystal structure of the complex* ***C5***

In previous works, Rh-Rh distances have been reported for complexes **C3**[27] and **C4**.[28] In both the cases the distances were comparable with the one found for the complex **C5** confirming the fact that the Rh-Rh distance is almost insensitive to the change of substituent into the phenyl ring of the tetramidinato motif. In the *Table 2.4* crystal data and structure refinement for the asymmetric unit of **C5** are reported.

Table 2. 2: *Crystal data and structure refinement of Rh_2(di-2F-pf)$_4$ (**C5**)*

Empirical formula	$C_{26}H_{18}F_4N_4Rh$
Formula weight	565.36
Temperature/K	173.0
Crystal system	triclinic
Space group	P-1
a/Å	10.2304(11)
b/Å	11.2549(13)
c/Å	11.7659(13)
α/°	117.127(2)
β/°	96.393(2)
γ/°	107.395(3)
Volume/Å^3	1100.6(2)
Z	2
ρ_{calc}g/cm^3	1.7059
μ/mm^{-1}	0.833
F(000)	564.0
Crystal size/mm^3	0.78 × 0.6 × 0.55
Radiation	Mo Kα (λ = 0.71073)
2Θ range for data collection/°	4.2 to 68.88
Index ranges	$-16 \leq h \leq 16$, $-17 \leq k \leq 17$, $-18 \leq l \leq 18$
Reflections collected	54602
Independent reflections	8563 [R_{int} = 0.0285, R_{sigma} = 0.0169]
Data/restraints/parameters	8563/0/315
Goodness-of-fit on F^2	1.037
Final R indexes [I>=2σ (I)]	R_1 = 0.0278, wR_2 = 0.0786
Final R indexes [all data]	R_1 = 0.0294, wR_2 = 0.0800
Largest diff. peak/hole / e Å^{-3}	3.59/-1.18

2.5. UV-Vis study on the complexes C1, C2, C3, C4, C5 and C6

The UV-Vis spectra were recorded using a Shimadzu 1800 UV-Vis series scanning spectrophotometer over a 300 nm to 800 nm range with a medium scan rate. The temperature was kept constant at 25.0 ± 0.2 °C using a water bath. A 0.5 mL quartz cuvette with path length 1 cm was used.

ACN was selected as solvent to record all the spectra because it is able to solubilize all the complexes in the quantity required for the collection.

The UV-Vis spectra of the complexes **C1** and **C2** are reported in *Figure 2. 24*.

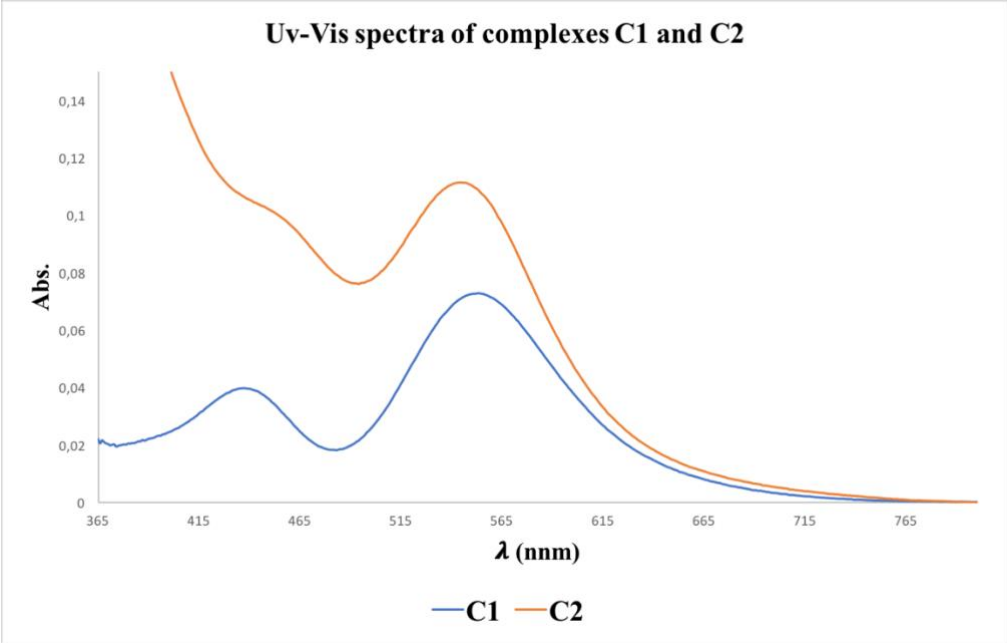

Figure 2. 24: *UV-Vis spectra of the complexes **C1** and **C2** in ACN*

In both the cases is possible to observe two absorption bands which are assigned thanks to works previously reported in literature.[17,21,23,29–31] These are characteristic for the $Rh_2(O_2CCR_3)_4$ moiety in particular for the Rh_2^{4+} oxidation state of the metal centre. The lower energy band (at λ =553 nm for **C1** and λ =544 nm for **C2**) has been assigned to the $\pi^*(Rh_2) \longrightarrow \sigma^*(Rh_2)$ HOMO-LUMO transition. Giving the fact that is a metal based transition and that does not involve any orbital of the ligand, this lower energy band is solvent dependent. Indeed, it has been shown that the energy of the latter is highly sensitive to axial ligand variation.

The higher energy band (λ =437 nm for **C1** and λ =450(sh) for **C2**) has been assigned to the $\pi(Rh\text{-}O) \longrightarrow \sigma^*(Rh\text{-}O)$ transition. In *Table 2.4* the data previously discussed are reported.

Table 2. 3: *Electronic absorption data for the complexes* ***C1*** *and* ***C2***

	λ (nm)	
Compound	π(Rh-O)⟶ σ*(Rh-O)	$\pi^*(Rh_2)\longrightarrow \sigma^*(Rh_2)$
C1	437	553
C2	450 (sh)	544

The UV-Vis spectra of the complexes **C3**, **C4**, **C5** and **C6** are reported in *Figure 2. 25*.

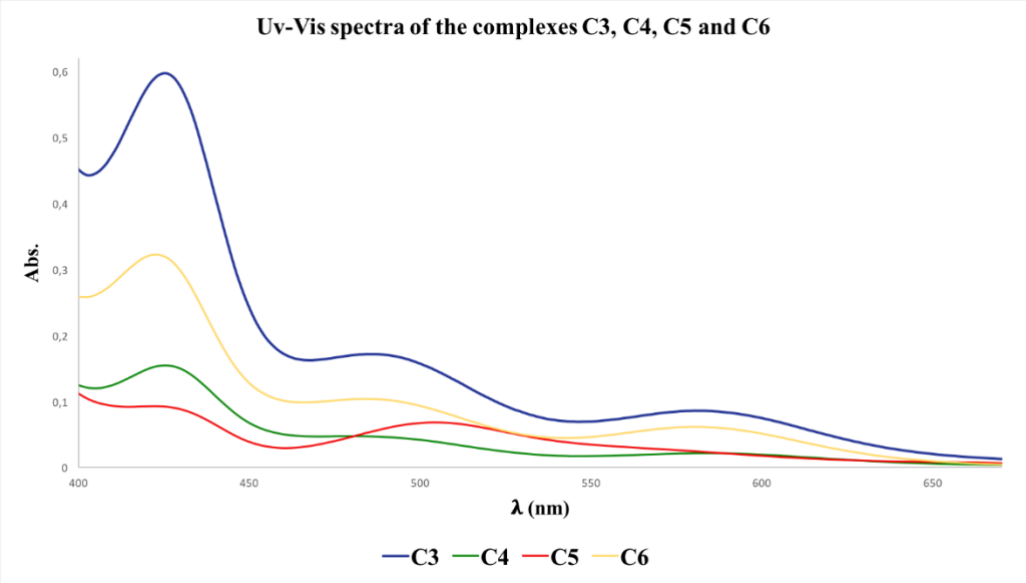

Figure 2. 25: *UV-Vis spectra of the complexes* ***C3, C4, C5*** *and* ***C6***

For each of the complexes the presence of three bands can be observed. The one at higher energies (λ =425 nm for **C**3, λ =426 nm for **C4**, λ =422 nm for **C5** and λ =422 nm for **C6**) have been assigned to the $\pi \longrightarrow \pi^*$ transition occurring within each *N,N'*-type ligand. Compared to other aromatic systems these bands are at lower energies, i.e. are shifted toward longer wavelengths. This is due to the π-conjugation with the imine double bond and with the lone pairs of the nitrogen atoms within the molecule (*Figure 2.26*). It is known indeed, that this conjugation causes a bathochromic shift.

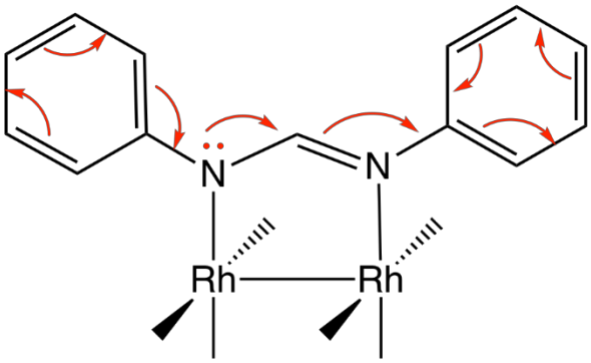

Figure 2. 26: *Conjugation effect in formamidinato-type ligands*

For all of the complexes the presence of the metal in the oxidation state Rh_2^{4+} was confirmed comparing the results with the UV-Vis spectra of Rh_2^{5+} compounds.[32]
In *Table 2.5* the spectral data discussed for the complexes are reported.

Table 2. 4: *Electronic absorption data for the complexes C3, C4, C5 and C6*

	λ (nm)		
Compound	$\pi(L) \longrightarrow \pi^*(L)$	$\pi(Rh\text{-}N) \longrightarrow \sigma^*(Rh\text{-}N)$	$\pi^*(Rh_2) \longrightarrow \sigma^*(Rh_2)$
C3	425	485	583
C4	426	480	584
C5	422	504	570 (sh)
C6	422	484	580

2.6 Summary

After the preparation of *N,N'*-type ligands, a series of dirhodium (II) acetate and formamidinyl complexes were synthetized. These were characterized by various spectroscopic techniques including ^{1}H NMR, ^{13}C {^{1}H} NMR, ^{19}F NMR, HSQC, FT-IR, UV-Vis spectroscopy, elemental analysis, MS spectrometry and X-ray diffraction. The ligands showed a prototropic tautomerism which has been confirmed by the ^{1}H NMR spectra and by the solid-state analysis. The complex **C2** resulted to be light sensitive probably because of the beginning of a

polymerization process in the presence of light. The complexes will be used as catalysts in the allylic oxidation of cyclohexene. These results will be discussed in the following chapter.

2.7 References

(1) Cotton, F.; Murillo, C.; Walton, R. *Multiple bonds between metal atoms*; 2005.

(2) Chifotides, H. T.; Dunbar, K. R. *Acc. Chem. Res.* **2005**, *38* (2), 146–156.

(3) Amo-Ochoa, P.; Jiménez-Aparicio, R.; Torres, M. R.; Urbanos, F. A.; Gallego, A.; Gómez-García, C. J. *Eur. J. Inorg. Chem.* **2010**, *4* (31), 4924–4932.

(4) Lin, C.; Kagan, C. R. *J. Am. Chem. Soc.* **2003**, *125* (2), 336–337.

(5) Petitjean, A.; Puntoriero, F.; Campagna, S.; Juris, A.; Lehn, J. M. *Eur. J. Inorg. Chem.* **2006**, No. 19, 3878–3892.

(6) Catino, A. J.; Forslund, R. E.; Doyle, M. P. *J. Am. Chem. Soc.* **2004**, *126* (42), 13622–13623.

(7) Lebel, H.; Piras, H.; Bartholoméüs, J. *Angew. Chemie - Int. Ed.* **2014**, *53* (28), 7300–7304.

(8) Deng, Y.; Massey, L. A.; Zavalij, P. Y.; Doyle, M. P. *Angew. Chemie - Int. Ed.* **2017**, *56* (26), 7479–7483.

(9) Zhu, T. P.; Ahsan, M. Q.; Malinski, T.; Kadish, K. M.; Bear, J. L. *Inorg. Chem.* **1984**, *2* (8), 2–3.

(10) Kuhn, K. M.; Grubbs, R. H. *Org. Lett.* **2008**, *10* (10), 2075–2077.

(11) Komber, H.; Limbach, H.; Bo, F. *J. Am. Chem. Soc* **2002**, *124*, 11955–11963.

(12) Kalz, K. F.; Hausmann, A.; Dechert, S.; Meyer, S.; John, M.; Meyer, F. *Chem. - A Eur. J.* **2016**, *22* (50), 18190–18196.

(13) Patai, S. *The chemistry of amidines and imidates*; 2010; Vol. 2.

(14) Rempel, G. A.; Legzdins, P.; Smith, H.; Wilkinson, G. *Inorg. Synth.* **1972**, *XIII*, 90–91.

(15) Gottlieb, H. E.; Kotlyar, V.; Nudelman, A. *J. Org. Chem.* **1997**, *62*, 7512–7515.

(16) Rempel, G. A.; Legzdins, P.; Smith, H.; Wilkinson, G. *Inorg. Synth.* **1972**, *103*, 90–91.

(17) Cotton, F. A.; Hillard, E. A.; Murillo, C. A. *J. Am. Chem. Soc.* **2002**, *124* (20), 5658–5660.

(18) Johnson, S. A.; Hunt, H. R.; Neumann, H. M. *Inorg. Chem.* **1963**, *2* (5), 960–962.

(19) Bear, J. L.; Kitchens, J.; Willcott, M. R. *J. Inorg. Nucl. Chem.* **1971**, *33* (10), 3479–3486.

(20) Cotton, F. A.; Dikarev, E. V; Stiriba, S. *Inorg. Chem.* **1999**, *38*, 4877–4881.

(21) Felthouse, T. R. *Prog. Inorg. Chem.* **1982**, *29*, 73–166.

(22) Zhu, T. P.; Ahsan, M. Q.; Malinski, T.; Radish, K. M.; Bear, J. L. *Inorg. Chem.* **1984**, *23* (1), 2–3.

(23) Cooke, M. The Synthesis and Characterization of Rh2(II,II) Templated Phoactive Assemblies, Université de Montréal, 2007.

(24) Hirano, K.; Urban, S.; Wang, C.; Glorius, F. *Org. Lett.* **2009**, *11* (4), 1019–1022.

(25) Piraino, P.; Bruno, G.; Tresoldi, G.; Schiavo, S. Lo; Zanello, P. *Inorg. Chem.* **1987**, *26*, 91–96.

(26) Boeyens, J. C. A.; Cotton, F. A.; Han, S. *Inorg. Chem.* **1985**, *24* (12), 1750–1753.

(27) Bear, J. L.; Yao, C. L.; Lifsey, R. S.; Korp, J. D.; Kadish, K. M. *Inorg. Chem.* **1991**, *30* (2), 336–340.

(28) Piraino, P.; Bruno, G.; Laschi, F.; Zanello, P. *Inorg. Chem.* **1987**, *26* (14), 2205–2211.

(29) Miskowski, V. M.; Schaefer, W. P.; Sadeghi, B.; Santarsiero, B. D.; Gray, H. B. *Inorg. Chem.* **1984**, *23* (8), 1154–1162.

(30) Norman, J. G.; Kolari, H. J. *J. Am. Chem. Soc.* **1978**, *100* (3), 791–799.

(31) Norman, J. G.; Renzoni, G. E.; Case, D. A. *J. Am. Chem. Soc.* **1979**, *101* (18), 5256–5267.

(32) Bear, J. L.; Van Caemelbecke, E.; Ngubane, S.; Da-Riz, V.; Kadish, K. M. *Dalton Trans.* **2011**, *40* (11), 2486–2490.

Chapter 3

Catalytic evaluation of dirhodium (II) complexes in the allylic oxidation of cyclohexene

3.1 Introduction

The allylic oxidation of olefins is an organic reaction transformation which involves the activation of the C-H bond of hydrocarbon.[1] The substrate can either be a linear or a cyclic olefin. The reaction would then be the oxidation of an olefin by an oxidizing agent in the presence of a catalyst, to give a wide range of synthetically useful products. An example with linear alkenes is shown in *Scheme 3.1*.

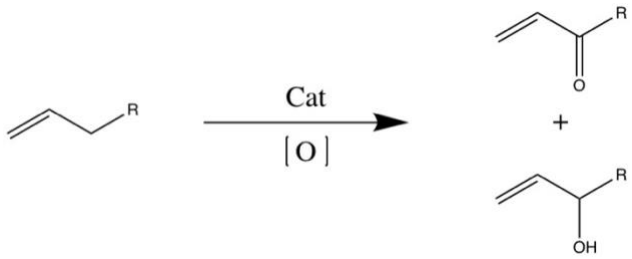

Scheme 3. 1: *General scheme of allylic oxidation of linear olefins*

Particularly important is the direct synthesis of enones and enediones from the oxidation of commercially available and inexpensive alkenes. Indeed, 1,4-enedione moiety is found in a variety of bioactive natural products and can also be useful as a starting material for further synthetic elaboration.[2–4]

One of the first attempts of allylic oxidation was carried out by Riley using selenium dioxide as an oxidizing agent in stoichiometric amount.[5] In the past, this reaction was largely based on the chemistry of Se, Cr, Pd, and Cu species.[2] Associated with his type of reaction however, there were problems of regio- and stereoselectivity, low compatibility with other functional groups or overoxidation issues.[6] Toxicity and cost are the main disadvantages of the oxidizing agents or catalysts previously described, especially when the reagent must be used in stoichiometric amounts.

Kharash and Sosnovsky demonstrated that terminal olefins react with *tert*-butyl peresters in the presence of a Cu or Co salt catalyst yielding only the unarranged secondary allylic esters.[7] As reported, the main obstacle of this reaction is the temperature at which it has to be carried out

(between 80 °C and 125 °C) and the fact that many of the *tert*-butyl peresters are not commercially available.

To find an alternative to these conditions, researchers focused on the carbon-hydrogen activation. It has been demonstrated that this activation involves a free radical chain mechanism that is provided by the metal catalyst in a redox capacity.[8] Metal complexes capable of easily undergoing a l-electron redox reactions ($Fe^{2+} \rightleftarrows Fe^{3+}$, $Cu^{1+} \rightleftarrows Cu^{2+}$, and $Co^{2+} \rightleftarrows Co^{3+}$, etc.) are the most efficient for this catalytic transformation.[8] Bimetallic rhodium complexes such as the Du Bois catalyst, $Rh_2(esp)_4$[9] and the caprolactamate complex, $Rh_2(cap)_4$[10] are able to catalyze conversion of sulfide to sulfoxide[11] and allylic oxidations respectively.[12,13] Using $Rh_2(cap)_4$ as catalyst, most olefins are rapidly converted to the corresponding enones and enediones in 1 h with only 0.1 mol % of catalyst.[14] This could solve the problems linked to the harsh conditions generally necessary to promote this kind of reaction. Furthermore, enhancing the electron density within the dimetal core could be the key to an easier access to the oxidized state of the metal center involved in the catalytic mechanism.

This chapter discusses the evaluation of the dirhodium(II) complexes containing either acetate or formamidinyl bridging ligands, described in Chapter 2, as catalysts in the allylic oxidation of cyclohexene (*Scheme 3.2*).

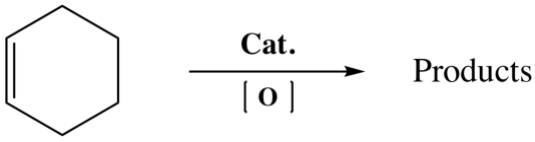

Scheme 3. 2: *Allylic oxidation of cyclohexene*

3.2 Results

The synthetized acetate (**C1** and **C2**) and formamidinate (**C3 – C6**) complexes of Rh(II) (*Figure 3.1*) were evaluated in the allylic oxidation of cyclohexene. The reaction conditions were chosen based on what has been reported in literature[13–16] with slight modifications to promote the activity of the synthetized complexes. In literature, *tert*-butyl hydroperoxide (TBHP) in decane[14] or T-Hydro (70% TBHP in water)[16] were used as oxidizing agents. The catalyst amount employed was between 0.1% mol and 1% mol (0.5% mol added at the beginning plus 0.5% mol added after 1 h). Under these conditions the results obtained were good in terms of yields, selectivity and conversions. Even though the $Rh_2(esp)_4$ catalyst is reported to be less prone to oxidation to the Rh_2^{5+} species compared to $Rh_2(cap)_4$, it has been shown that it successfully catalyses oxidation reactions owing to the stability given by the chelating ligand.[13]

This current work evaluates if the synthetized catalyst, with either *O,O'* or *N,N'* bridging ligands with different electron-donating or electron-withdrawing substituents, were active in the allylic oxidation.

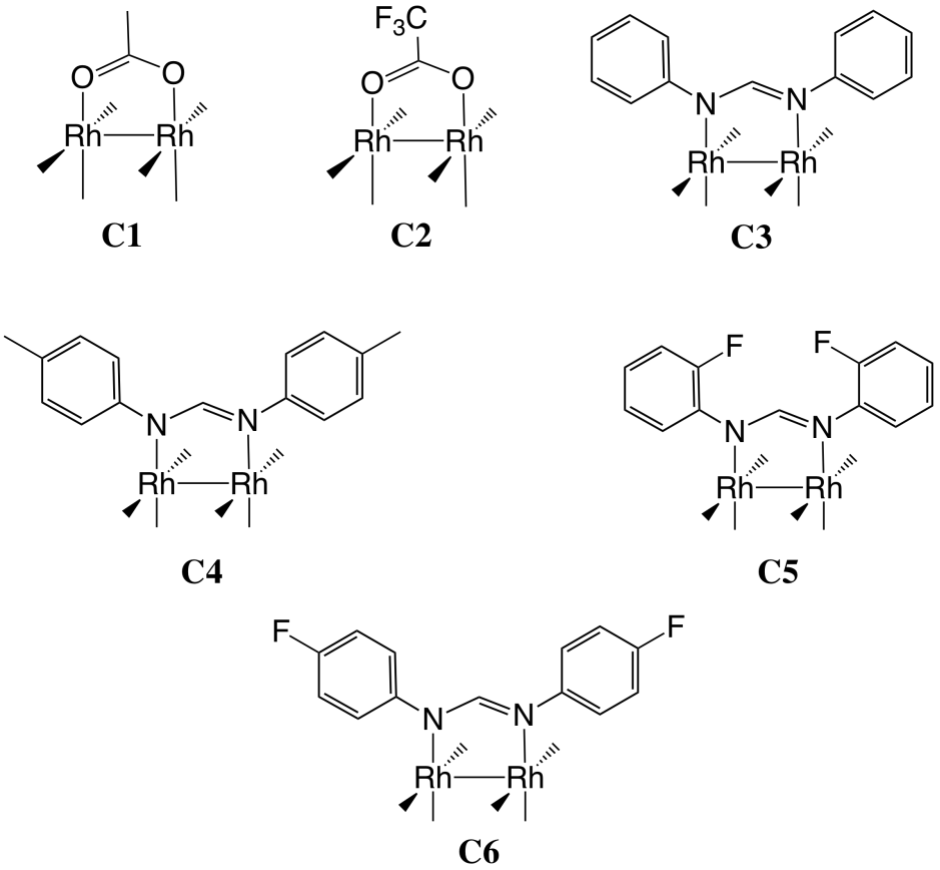

Figure 3. 1: *Catalysts used in allylic oxidation of cyclohexene*

3.2.1 Allylic oxidation using acetate complexes (C1 and C2)

The catalytic activity of the precursor complexes **C1** and **C2** was evaluated on a mmol scale with 2.72 mmol of cyclohexene using 0.5% mol of catalyst. The above-mentioned reagents were added in a round bottom flask with a side arm, together with 10 mL of dichloromethane (DCM). While stirring, T-Hydro (5.0 mol eq, v/v) was added observing a colour change from a colourless to a pink mixture. The formation of oxygen was indicated by inflation of the balloon fitted on top of the condenser as shown in *Figure 3.2*. The reaction mixture was refluxed at 40 °C. After one hour, another portion of T-Hydro (5.0 mol eq, v/v) was added and the reaction was refluxed for a total of 48 h.

Figure 3. 2: *Experimental set-up for the allylic oxidation*

The solvent was removed *via* rotary evaporation. The reaction products were determined by gas chromatography (GC) and as expected,[14] **C1** indicated the presence of traces of 2-cyclohexene-1-one. Unexpectedly the complex **C2** yielded, together with the enone, the allylic alcohol 2-cyclohexene-1-ol. These results are reported in the *Table 3.1* below.

Table 3. 1: *Results for allylic oxidation using **C1** and **C2** as catalysts*

Entry	Catalyst	Solvent	Temperature	Selectivity	
				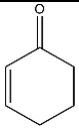	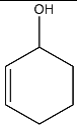
Blank	-	DCM	40 °C	0	0
1	**C1**	DCM	40 °C	100	0[a]
2	**C2**	DCM	40 °C	60	40

Reaction conditions: 2.72 mmol of cyclohexene, 0.5% mol of catalyst, 10 eq of T-Hydro (5 eq at the beginning plus 5 after 1 h), 10 mL of solvent, reflux for 48 h. a) in the presence of K_2CO_3, traces of the allyl alcohol were present in the reaction mixture

3.2.2 Allylic oxidation using formamidinyl complexes (C3 - C6)

The parent *N,N'*-type complex (**C3 - C6**), prepared from the precursor trifluoroacetate complex **C2**, were also evaluated for their catalytic activity. The expectation is that the increased electron density within the dimetal core should favour the oxidation to the Rh_2^{5+} state, having a Rh(II)-Rh(III) dimetal core, which has previously been reported as the key intermediate in the allylic oxidation catalyzed by dirhodium complexes.[14]

Similar reaction conditions were followed in the catalysis of cyclohexene using complexes **C1** and **C2**, with the exception of the solvent in which case DCM, tetrahydrofuran (THF) and acetonitrile (ACN) were used. This allowed us to evaluate the effect of the coordinating solvents as well as their effect on the electron density in the dimetal core. This should influence the catalytic activity of the complexes. In all the cases, the reaction was refluxed at the solvent boiling point for 48 h. The obtained results are reported in *Table 3.2*.

Table 3. 2: *Results for allylic oxidation using **C3 – C6** as catalysts*

Entry	Catalyst	Solvent	Temperature	Selectivity	
				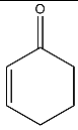	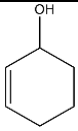
1	**C3**	DCM	40 °C	59	41
2	**C3**	THF	66 °C	62	38
3	**C3**	ACN	82 °C	73	27
4	**C4**	ACN	82 °C	100	0
5	**C5**	ACN	82 °C	100	0
6	**C6**	ACN	82 °C	100	0

Reaction conditions: 2.72 mmol of cyclohexene, 0.5% mol of catalyst, 10 eq of T-Hydro (5 eq at the beginning plus 5 after 1 h), 10 mL of solvent, reflux for 48 h

For **C3** the two products, 2-cyclohexene-1-one and 2-cyclohexene-1-ol, were obtained in traces with slightly different selectivities. The best result was achieved by using ACN as solvent in both selectivity and yield of the products, albeit in traces. This can be attributed to the fact that

it is known that the complexation with ACN as axial ligand, stabilizes the higher oxidation states of the dirhodium species (Rh_2^{5+}),[17] an intermediate produced during the allylic oxidation. The axial binding, indeed, causes a destabilization of the HOMO level in the complex.[18] The Rh-Rh bond length is almost insensitive to this ligation but the oxidation from Rh_2^{4+} to Rh_2^{5+} become easier namely giving $[Rh_2(dpf)_4(CH_3CN)]^+$. Similar but different results are obtained with THF probably due to the softer character of the Rh(II) centre which prefers nitrogen atoms as donor ligands instead of oxygen ones. For this reason, it was decided to carry out the following catalytic reactions with the complexes **C4**, **C5** and **C6** using ACN as solvent. In this case the reactions were conducted at 82 °C in 10 mL of ACN, using the same amount of catalyst as for **C3**. The products were evaluated through GC. The results are reported in *Table 3.2*. The reactions yielded the enone product in traces amount. The substantial difference, compared to the previous reactions, is found in the selectivity of the experiments. For all of the complexes, the only product for the allylic oxidation was 2-cychlohexene-1-one.

3.3 Discussion

The complexes **C1** - **C6** demonstrated activity in the allylic oxidation of cyclohexene. In all cases, the formation of O_2 after the addition of the oxidizing agent T-Hydro, was observed. This supports the formation of the oxidized species Rh_2^{5+} in which, one of the metal atoms is a Rh(III). The catalytic mechanism in which the bridging ligand is a caprolactamate with O and N as donor atoms, has previously been proposed for $Rh_2(cap)_4$.[14,16,19] The reaction involves a 1-electron oxidation of the dimetal core forming the species $Rh_2(cap)_4(OH)$ in the reaction of

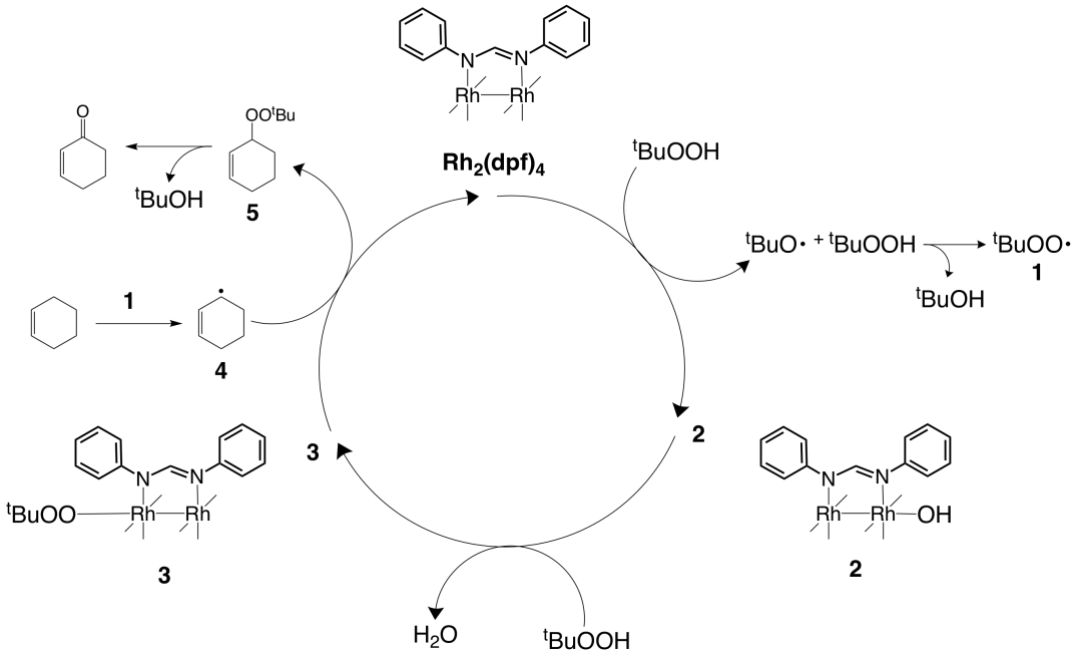

Scheme 3. 3: *Mechanism proposal for the allylic oxidation of cyclohexene with the catalyst* ***C3***

the catalyst with TBHP. The latter is in turn converted into *tert*-butyl peroxy radical which is able to abstract an allylic hydrogen to produce the olefinic radical.[20,21] In this work, based on the results obtained, an assumption that the catalytic reaction follows the same mechanism is valid. This is shown in *Scheme 3.3* using complex **C3** as an example.

Based on the reports from previous literature, it was decided to employ T-Hydro instead of TBHP because it is safer and less expensive. Following its addition, the catalyst is oxidized from Rh_2^{4+} to Rh_2^{5+}. This transformation is indicated by a dramatic colour change giving red, orange or brown mixtures. The system appears homogeneous, further corroborating the formation of the Rh_2^{5+} species which is more soluble than the corresponding Rh_2^{4+} form.

The reduction of T-Hydro gives the *tert*-butoxy radical which reacts rapidly giving the more stable *tert*-butyl peroxy radical. The proposed mechanism probably involves the formation of the species of the type **2**. The *tert*-butyl peroxy radical **1** is able to abstract the allylic hydrogen giving the allylic radical **4**. It is also believed that the formation of the *tert*-butyl peroxyether complex **3** occurs and that this species is involved in the transfer of the axial ligand to the radical **4** giving the mixed peroxide **5**. Therefore, the rapid decomposition of **5** gives the 2-cyclohexene-1-one.

The radical chain mechanism of TBHP disproponation is shown in *Scheme3.4*.[14,16,19] After the formation of the *tert*-butyl peroxy radical **1** it is possible that, if the concentration of the latter is sufficiently high, the formation of di-*tert*-butyl peroxide **6** statistically occurs. This reaction is very significant because it produces, together with the species **6**, molecular oxygen observed in the catalytic reactions reported in this work.

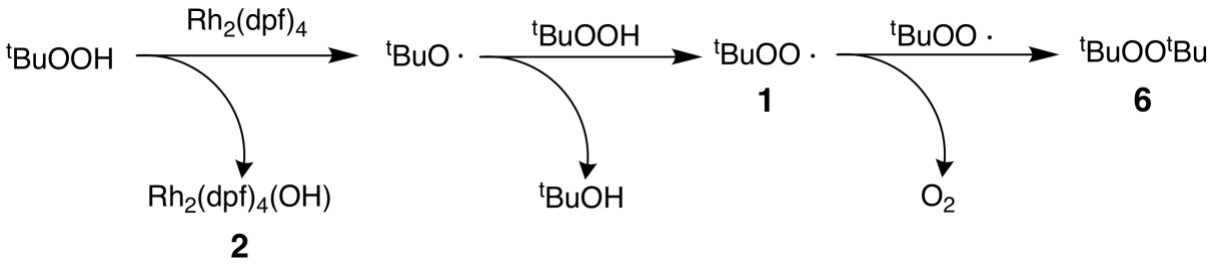

Scheme 3. 4: *Radical chain decomposition of TBHP*

The allylic radical **4** can either react with the species **3** transferring the axial ligand and forming the mixed peroxide **5** as showed in *Scheme 3.3*, or is able to trap the dioxygen formed as by-

product during the formation of di-*tert*-butyl peroxide **6**, as shown in *Scheme 3.5*.[22] This last mechanism gives the cyclohexenyl peroxy radical **7**.

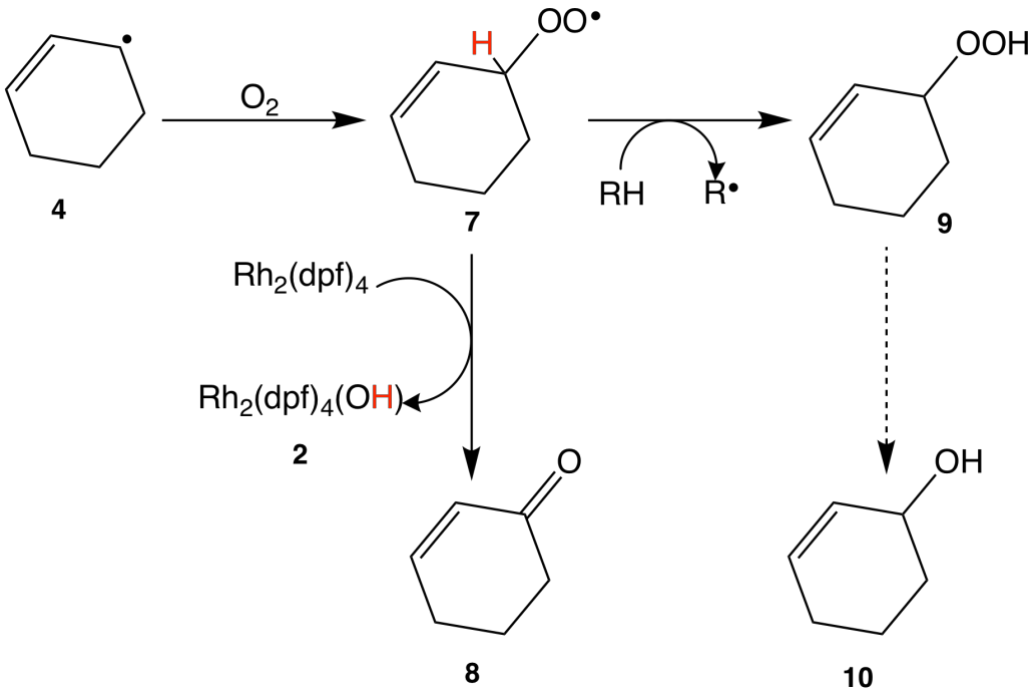

Scheme 3. 5: *Mechanism for the formation of the alcohol and the ketone*

It is known that radicals of the type **7** can go through a Russel's chain termination mechanism[23–26] which gives the enone **8** and the allylic alcohol **10**. The formation of the ketone should be favoured in the presence of the catalyst that could trap the radical **7**. The cleavage of the O-O bond and a hydrogen transfer should lead to the formation of the oxidized catalyst **2** and of the ketone **8**. In this way, the presence of both the ketone and the alcohol as products for the catalysts **C2** and **C3**, is explained.

The allylic oxidation of the cyclohexene reported in this work, yielded just traces of both the 2-cyclohexene-1-one and of 2-cyclohexene-1-ol products for complexes **C4**, **C5** and **C6**. This could be attributed to the bulky nature of the ligands which could hinder the insertion of the OH group in the axial position. In the case of **C5** for example, X-ray crystallography reveals the proximity of the fluorine atoms of the bridging ligand to the Rh atom of the dimetal core to induce a weak Rh-F interaction (as shown in *Figure 2.23* in Chapter 2), preventing access to the axial site of the dimetal core. The steric hindrance of the ligands, the formation of the adducts with ACN which occupies at least one of the axial sites, the formation of unknown products and finally the boiling point of the cyclohexene substrate (~83 °C) and the volatility

of the 2-cyclohexene-1-one and of 2-cyclohexene-1-ol could, in addition, explain the yields of the experiments.

3.4 Summary and conclusions

The dirhodium (II) complexes **C1 - C6** were evaluated as catalysts in the allylic oxidation of cyclohexene. All of the complexes showed limited activity in the formation of the enone or allylic alcohol as products. The selectivities were good for complex **C4 – C6** giving exclusively the enone as product. The scarce yields were explained by many factors like the steric hindrance of the *N,N'*-type ligands and their substituents, the coordination of the solvent as axial ligand and the volatility of both substrate and the products.

A more accurate choice of the reaction conditions could probably give better results. It could be useful to optimize the amount of oxidation agent in order to avoid its radical chain decomposition mechanism. The total amount of catalyst could be added in to two portions at different time due to the known decrease in the concentration of the catalytically active species.[27] Choosing a substrate with higher boiling point which gives products with lower volatility could be the key, together with the other modifications, to obtain a more efficient catalytic system.

3.5 References

(1) Wencel-Delord, J.; Dröge, T.; Liu, F.; Glorius, F. *Chem. Soc. Rev.* **2011**, *40* (9), 4740.

(2) Weidmann, V.; Maison, W. *Synth.* **2013**, *45* (16), 2201–2221.

(3) Hunter, G. L. K.; Brogden, W. B. *J. Food Sci.* **1965**, *30* (5), 876–878.

(4) Smith III, A. B.; Konopelski, J. P. *J. Org. Chem.* **1984**, *49* (21), 4094–4095.

(5) Riley, L.; Frederick, J. *J. Chem. Soc.* **1932**, 1875–1883.

(6) García-Cabeza, A. L.; Marín-Barrios, R.; Moreno-Dorado, F. J.; Ortega, M. J.; Massanet, G. M.; Guerra, F. M. *Org. Lett.* **2014**, *16* (6), 1598–1601.

(7) Kharasch, M. S.; Sosnovsky, G.; Yang, N. C. *J. Am. Chem. Soc.* **1959**, *81* (21), 5819–5824.

(8) Srinivasan, K.; Perrier, S.; Kochi, J. K. *J. Mol. Catal.* **1986**, *36* (3), 297–317.

(9) Espino, C. G.; Fiori, K. W.; Kim, M.; Du Bois, J. *J. Am. Chem. Soc.* **2004**, *126* (47), 15378–15379.

(10) Doyle, M. P.; Westrum, L. J.; Wolthuis, W. N. E.; See, M. M.; Boone, W. P.; Bagheri, V.; Pearson, M. M. *J. Am. Chem. Soc.* **1993**, *115* (3), 958–964.

(11) Zhao, L.; Zhang, H.; Wang, Y. *J. Org. Chem.* **2016**, *81* (1), 129–136.

(12) Wang, Y.; Kuang, Y.; Zhang, H.; Ma, R.; Wang, Y. *J. Org. Chem.* **2017**, *82* (9), 4729–4736.

(13) Wang, Y.; Kuang, Y.; Wang, Y. *Chem. Commun.* **2015**, *51*, 5852–5855.

(14) Catino, A. J.; Forslund, R. E.; Doyle, M. P. *J. Am. Chem. Soc.* **2004**, *126* (42), 13622–13623.

(15) Coelho, J. A. S.; Trindade, A. F.; Wanke, R.; Rocha, B. G. M.; Veiros, L. F.; Gois, P. M. P.; Pombeiro, A. J. L.; Afonso, C. A. M. *Eur. J. Org. Chem.* **2013**, No. 8, 1471–1478.

(16) Choi, H.; Doyle, M. P. *Org. Lett.* **2007**, *9* (26), 5349–5352.

(17) Bear, J. L.; Yao, C. L.; Lifsey, R. S.; Korp, J. D.; Kadish, K. M. *Inorg. Chem.* **1991**, *30* (2), 336–340.

(18) Piraino, P.; Bruno, G.; Laschi, F.; Zanello, P. *Inorg. Chem.* **1987**, *26* (14), 2205–2211.

(19) Mclaughlin, E. C.; Choi, H.; Wang, K.; Chiou, G.; Doyle, M. P. *J. Org. Chem.* **2009**, *74*, 730–738.

(20) Bravo, A.; Bjørsvik, H.-R.; Fontana, F.; Liguori, L.; Mele, A.; Minisci, F. *J. Org. Chem.* **1997**, *62* (21), 7128–7136.

(21) Minisci, F. *Acc. Chem. Res.* **1975**, *8* (5), 165–171.

(22) Chavez, F. a; Mascharak, P. K. *Acc. Chem. Res.* **2000**, *33* (8), 539–545.

(23) Miyamoto, S.; Martinez, G. R.; Medeiros, M. H. G.; Di Mascio, P. *J. Am. Chem. Soc.*

2003, *125* (20), 6172–6179.

(24) Howard, J. A.; Ingold, K. U. *J. Am. Chem. Soc.* **1968**, *90* (4), 1056–1058.

(25) Russell, G. A. *J. Am. Chem. Soc.* **1957**, *79* (1), 3871–3877.

(26) Miyamoto, S.; Martinez, G. R.; Medeiros, M. H. G.; Di Mascio, P. *J. Am. Chem. Soc.* **2003**, *125* (20), 6172–6179.

(27) Mclaughlin, E. C.; Choi, H.; Wang, K.; Chiou, G.; Doyle, M. P.; Mclaughlin, E. C.; Choi, H.; Wang, K.; Chiou, G.; Doyle, M. P. *J. Org. Chem.* **2009**, *74*, 730–738.

Chapter 4

Experimental section

4.1. Materials and methods

All reactions were carried out in air unless otherwise stated. All solvents were reagent grade and used as received from Sigma Aldrich or Kimix. $RhCl_3.3H_2O$ was purchased from SA precious metals. All other chemicals were purchased from Sigma Aldrich and used as received. Nuclear magnetic resonance (NMR) spectra were recorded on a Varian Unity XR400 spectrometer (^1H: 399.95 MHz, $^{13}C\{^1H\}$: 100.58 MHz), Varian Mercury XR300 spectrometer (^1H: 300.08 MHz, $^{13}C\{^1H\}$: 75.46 MHz) or Bruker Ultrashield 400 Plus spectrometer (^1H: 400.20 MHz, $^{13}C\{^1H\}$: 100.60 MHz). Chemical shifts were reported in parts per million (ppm) relative to the internal standard tetramethylsilane (δ 0.00). FT-IR spectra were recorded using Attenuated Total Reflectance Infrared spectroscopy (ATR-IR). Melting points were determined using a Büchi melting point apparatus B-540. Hot Stage Microscopy (HSM) was performed with a Nikon SMZ-10 stereoscopic microscope fitted with a Linkam THMS600 hot stage and a Linkam TP92 temperature control unit. Sony Digital Hyper HAD colour video camera was used to record the images. When needed, samples were covered by silicone oil. Samples were mostly heated at a rate of 10°C/min till evident decomposition. Elemental analysis was performed by the Central Analytical Facility (CAF) at the University of Stellenbosch by using an Elementar Vario EL Cube Elemental Analyser. Mass spectrometry was carried out with a Bruker compact ultimate 3000 HR-MS at the University of Witwatersrand. Single-crystal X-ray diffraction data were collected on a Bruker KAPPA APEX II DUO diffractometer using graphite-monochromated Mo-Kα radiation (χ = 0.71073 Å). Data collection was carried out at 173(2) K. Temperature was controlled by an Oxford Cryostream cooling system (Oxford Cryostat). A Shimadzu 1800 UV-Vis series scanning spectrophotometer was used to record UV-Vis spectra over a 300 nm to 800 nm range with a medium scan rate. The temperature was kept constant at 25.0 ± 0.2 °C using a water bath. A 0.5 mL quartz cuvette with path length 1 cm was used. A Perkin Elmer Clarus 580 GC instrument equipped with a flame ionisation detector and a 30 m capillary column was used for analysing and quantifying the catalytic products.

4.2. Ligands synthesis

4.2.1. Synthesis of *N*,*N*'-Di(p-Tolyl)formamidine (L1)

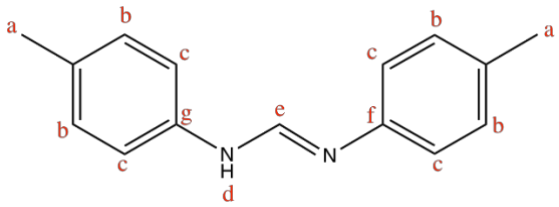

The ligand **L1** was prepared using a known procedure.[1]

Triethylorthoformate (3.10 mL, 18.64 mmol), glacial acetic acid (56 µL, 0.93 mmol) and *p*-toluidine (4 g, 37.33 mmol) were added together in a round bottom flask. The mixture was heated up at 140 °C observing the formation of an orange/brown liquid. The reaction was carried out overnight (18 h), under reflux. The mixture was allowed to cool to room temperature observing the formation of a grey solid. The crude product was purified by recrystallization from warm DCM. The precipitate was filtered through a Buchner funnel obtaining a yellowish solid which was dried under vacuum. Yield: (2.27 g, 54%). M.P. 130-135 °C. ^{1}H NMR ($CDCl_3$, 300 MHz): δ (ppm) = 2.32 (s, 6 H, H_a), 3.75 (br s, 1 H, H_d), 6.95 (d, ^{3}J= 8.4 Hz, 4 H, H_c), 7,12 (d, ^{3}J= 8.1 Hz, 4 H, H_b), 8.11 (s, 1 H, H_e). $^{13}C\{^{1}H\}$ NMR ($CDCl_3$, 400 MHz): δ (ppm) = 20.86 (C_a), 119.06 (C_c), 130.07 (C_b), 132.94 (C_f), 142.82 (C_g), 148.66 (C_e). FT-IR (ν_{max}/cm^{-1}): 1670 (C=N). Elemental analysis (%): Calcd. For $C_{15}H_{16}N_2$: C, 80.32; H, 7.19; N, 12.79. Found: C, 80.22; H, 7.11; N, 12.59.

4.2.2. Synthesis of *N*,*N*'-Bis(2-Fluorophenyl)formamidine (L2)

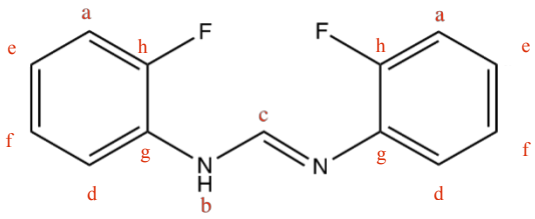

The new compound **L2** was prepare using a known procedure.[1]

Triethylorthoformate (2.15 mL, 12.91 mmol) was added to glacial acetic acid (38 µL, 0.65 mmol) and allowed to stir before the addition of *2*-Fluoroaniline (2.49 mL, 25.83 mmol). The mixture was heated up at 150 °C under reflux. After 1 h, the formation of a white solid was observed. The temperature was raised to 155 °C observing the melting of the solid. The system was allowed to react overnight (17 h). The mixture was cooled down to room temperature. The crude product was purified by recrystallization from warm DCM. The formation of a yellowish solution was observed. While the system was cooling down, the precipitation of a white solid was observed. The precipitate was filtered through a Buchner funnel obtaining a white powder which was dried under vacuum. Yield: (1.89 g, 64%). M.P. 152-154 °C. ^{1}H NMR (DMSO-d_6, 300 MHz): δ (ppm) = 7.10 (m, 8 H, H_a), 8.05 (s, 1 H, H_c), 9.59 (s, 1 H, H_b). $^{13}C\{^{1}H\}$ NMR ($CDCl_3$, 400 MHz): δ (ppm) = 116.0 (C_a), 120.3 (C_d), 123.9 (C_e), 124.7 (C_f), 148.4 (C_c), 152.5 (C_g), 154.9 (C_h). FT-IR (ν_{max}/cm^{-1}): 1227 (C-F), 1666 (C=N). Elemental analysis (%): Calcd. For $C_{13}H_{10}N_2F_2$: C, 67.24; H, 4.32; N, 12.06. Found: C, 67.65; H, 4.20; N, 12.26.

4.2.3. Synthesis of *N,N'*-Bis(4-Fluorophenyl)formamidine (L3)

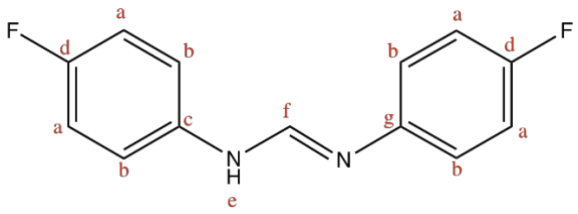

The ligand **L3** was prepared using a known procedure.[1]

Triethylorthoformate (1.87 mL, 11.25 mmol) was added to glacial acetic acid (34 µL, 0.56 mmol) and allowed to stir before the addition of 4-Fluoroaniline (2.13 mL, 22.50 mmol). The mixture was heated up at 150 °C under reflux overnight (18 h). The system was cooled to room temperature. The crude product was purified by recrystallization from warm DCM. The formation of a purple solution was observed. While the system was cooling down, the precipitation of a grey, flaky solid was observed. The precipitate was filtered through a Buchner funnel. The purified product was dried under vacuum. Yield: (1.24 g, 48%). M.P. 145-146 °C. ^{1}H NMR ($CDCl_3$, 300 MHz): δ (ppm) = 7.00 (d, 8 H, H_{Ar}), 8.02 (s, 1 H, H_f). $^{13}C\{^{1}H\}$ NMR ($CDCl_3$, 400 MHz): δ (ppm) = 116.19 (C_a), 120.59 (C_b), 141.34 (C_g), 149.22 (C_c), 158.42 (C_f), 160.82 (C_d). FT-IR (ν_{max}/cm^{-1}): 1199 (C-F), 1667 (C=N). Elemental analysis (%): Calcd. For $C_{13}H_{10}N_2F_2$: C, 67.24; H, 4.32; N, 12.06. Found: C, 67.49; H, 4.18; N, 12.27.

4.3. Synthesis of the complexes

4.3.1. Synthesis of $Rh_2(O_2CCH_3)_4$ (C1)

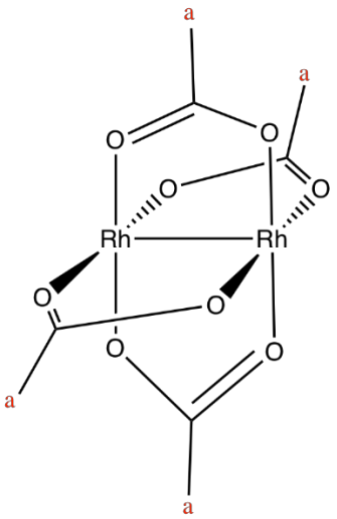

The synthesis of the complex **C1** was carried out using a modified procedure from literature.[2] In a round bottom flask with a side arm, rhodium trichloride trihydrate (1.51 g, 7.62 mmol) and sodium acetate trihydrate (3.11 g, 22.86 mmol) were added. The flask was evacuated and filled with N_2 to create an inert atmosphere. This was carried out in three cycles. Glacial acetic acid (60 mL) and absolute ethanol (60 mL) were added, observing the formation of a red/brown heterogeneous mixture. The system was refluxed under N_2 for 3 hours during which the mixture changed colour from red to emerald green. The system was allowed to cool to room temperature. The formation of the product as an emerald green precipitate was observed. This solid was filtered through Buchner funnel before washing with cold methanol. The crude product was dissolved in boiling methanol (400 mL) giving a bluish solution. This was filtered via gravity filtration. The volume of the solution was reduced by rotary evaporation to about half of the volume of the initial solution. The mixture was cooled overnight in the fridge giving the precipitation of the product. This pure solid was filtered through a Buchner funnel and washed with cold methanol. A blue-green solid was obtained. The mother liquor was further concentrated by rotary evaporation and kept in the fridge overnight giving the precipitation of more product. The resultant green powder obtained as pure product, was dried under vacuum at 45 °C for 22 hours giving emerald green crystals. Yield: (1.06 g, 67%). M. P. 312-322 °C decomposition without melting. ^{1}H NMR (DMSO-d_6, 300 MHz): δ (ppm) = 1.81 (s, 3 H, H_a).

FT-IR (ν_{max}/cm^{-1}): 1572 (C=O). UV-Vis (λ/nm): 437, 553. Elemental analysis (%): Calcd. For $C_8H_{12}O_8Rh_2$: C, 21.74; H, 2.74. Found: C, 20.48; H, 3.228. MS(m/z): 442.87 $[M-H]^+$.

4.3.2. Synthesis of $Rh_2(O_2CCF_3)_4$ (C2)

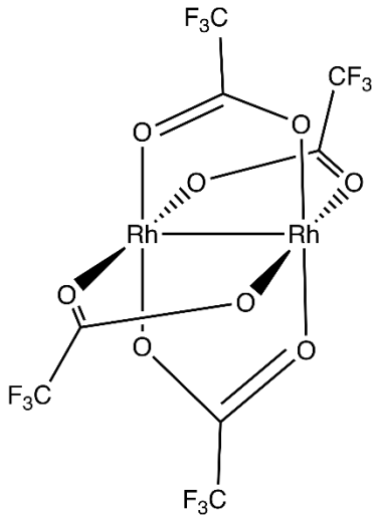

The synthesis of the known complex **C2** was carried out using a literature reported procedure.[3] Rhodium(II) acetate dimer (313 mg, 0.71 mmol) was dissolved in trifluoroacetic acid (100 mL) in a round bottom flask. The excess trifluoroacetic acid was gently evaporated on a steam bath. The mixture was further subject for rotary evaporation. The bluish solid product was dried under vacuum for 2 hours at 110 °C. The product was dissolved in acetone (20 mL) forming a dark violet solution. This was filtered through Buchner filtration. The filtrate was evaporated to dryness leaving a blue solid product. This was dried under vacuum for 5 hours at 110 °C. The formation of an emerald green solid was observed. Yield: (0.42 g, 90%). M. P. 322-348 °C decomposition without melting. ^{1}H NMR ($CDCl_3$, 300 MHz): δ (ppm) = 1.73 (s). FT-IR (ν_{max}/cm^{-1}): 1161 (C-F), 1650 (C=O). UV-Vis (λ/nm): 450 (sh), 544. Elemental analysis (%): Calcd. For $C_8F_{12}O_8Rh_2$: C, 14.61. Found: C, 15.31.

4.3.3. Synthesis of $Rh_2(dpf)_4$ (C3)

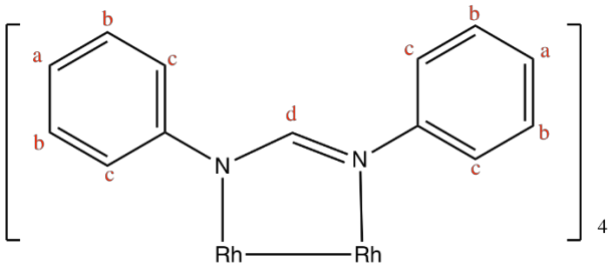

The synthesis of the complex **C3** was carried out using a modified procedure from literature.[4] In a round bottom flask with a side arm, *N,N'*-diphenylformamidine (2.81 g, 14.31 mmol) was added. The flask was evacuated and filled with N_2 to create an inert atmosphere. This was carried out in three cycles. The ligand was heated to melting at 135 °C. Rhodium(II) trifluoroacetate dimer (0.26 mg, 0.56 mmol) was then added into the flask giving an immediate colour change from yellow to dark red. The mixture was allowed to react for 4 hours under magnetic stirring at the same temperature. The product was cooled to room temperature and dried under vacuum for 2 hours at 100 °C. The solid was washed several times with methanol (3x100 mL). Then it was filtrated through a Buchner funnel and then the crude product was recrystallized from DCM/MeOH. The precipitate was collected by filtration with a Buchner funnel and washed with methanol. The dark green product was dried under vacuum. Yield: (0.29 g, 52%). M. P. melting at 362-365 °C. ^{1}H NMR ($CDCl_3$, 300 MHz): δ (ppm) = 6.70 (d, ^3J=6.9, 4 H, H_c), 6.97 (t, ^3J=7.2, 2 H, H_a), 7.08 (t, ^3J=7.2, 4 H, H_b), 7.8 (s, 1 H, H_d). $^{13}C\{^1H\}$ NMR ($CDCl_3$, 400 MHz): δ (ppm)= 124.44, 128.94. FT-IR (ν_{max}/cm^{-1}): 1571(C=N). UV-Vis (λ/nm): 425, 485, 583. Elemental analysis (%): Calcd. For $C_{52}H_{44}N_8Rh_2$: C, 63.33; H, 4.50; N, 11.36. Found: C, 63.11; H, 4.201; N, 11.54. MS(m/z): 986.18 ([M]$^+$).

4.3.4. Synthesis of Rh_2(di-p-Tolf)$_4$ (C4)

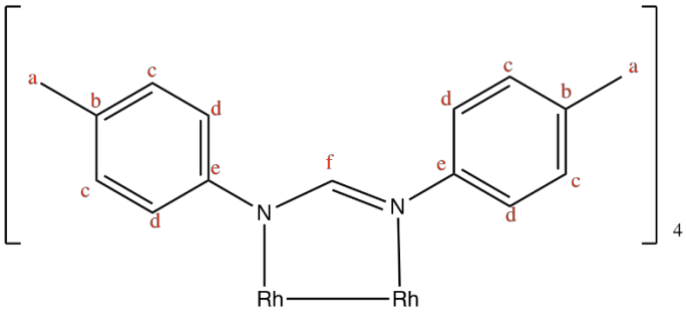

The synthesis of the complex **C4** was carried out using a modified procedure from literature.[4] In a round bottom flask with a side arm *N,N'*-Di(p-Tolyl)formamidine (2.21 g, 9.85 mmol) was added and three cycles N_2/vacuum were done. The ligand was heated to melting at 147 °C, under N_2. Rhodium(II) trifluoroacetate dimer (244 mg, 0.37 mmol) was added observing an immediate colour change from yellow liquid to a darker colour. The reaction was carried out overnight (19 h) under N_2. The product was cooled to room temperature and dried under vacuum for 2 hours at 100 °C. The dark green solid was washed several times with methanol (3x100 mL). Then it was filtrated through a Buchner funnel and then the crude product was recrystallized from DCM/MeOH.. The precipitate was collected by filtration with a Buchner funnel and washed with methanol. The dark green solid was dried under vacuum. Yield: (135 mg, 33%). M. P. >400 °C. ^{1}H NMR ($CDCl_3$, 300 MHz): δ (ppm) = 2.23 (s, 3 H, H_a), 6.57 (d, ^3J=8.1, 2 H, H_d), 6.87 (d, ^3J=7.8, 2 H, H_c), 7.68 (s, 1 H, H_f). ^{13}C{^{1}H} NMR ($CDCl_3$, 400 MHz): δ (ppm) = 20.89 (C_a), 124.30 (C_d), 129.40 (C_c), 132.51 (C_b), 148.81 (C_e), 162.28 (C_f). FT-IR (ν_{max}/cm^{-1}): 1585 (C=N). UV-Vis (λ/nm): 426, 480, 584. Elemental analysis (%): Calcd. For $C_{60}H_{60}N_8Rh_2$: C, 65.57; H, 5.50; N, 10.20. Found: C, 65.34; H, 5.296; N, 10.27. MS(m/z): 1098.30 ([M]$^+$).

4.3.5. Synthesis of Rh_2(di-2F-pf)$_4$ (C5)

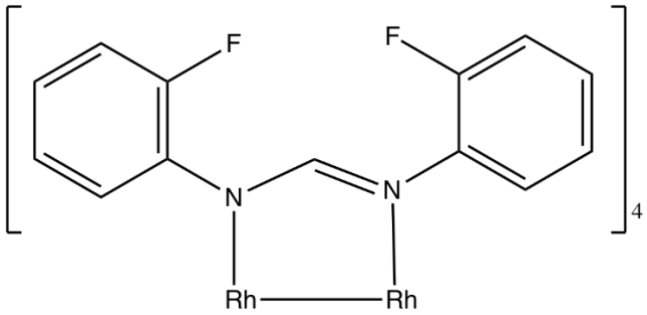

The synthesis of the complex **C5** was carried out using a modified procedure from literature.[4] In a round bottom flask with a side arm, *N,N'*–bis(2-fluorophenyl)formamidine (1.68 g, 7.22 mmol) was added. The flask was evacuated and filled with N_2 to create an inert atmosphere. This was carried out in three cycles.. The ligand was heated to melting at 150 °C, under N_2. Rhodium (II) trifluoroacetate dimer (317 mg, 0.48 mmol) was added observing the formation of a darker melt. The reaction was carried out overnight under N_2 for 16 h at the same temperature. The product was cooled to room temperature and dried under vacuum for 2 hours at 100 °C. The dark red solid was washed several times with diethyl ether. The product was filtrated through a Buchner funnel obtaining a brown/red solid which was recrystallized from DCM/MeOH. The precipitate was collected by filtration with a Buchner funnel and washed with methanol. The red powder obtained, was dried under vacuum. Yield: (355 mg, 65%). M. P. >400 °C. ^{1}H NMR ($CDCl_3$, 300 MHz): δ (ppm) = 6.84 (m, 8 H, H_{Ar}), 7.89 (s, 1 H, H_{immine}). $^{13}C\{^1H\}$ NMR ($CDCl_3$, 400 MHz): δ (ppm) = 115.71, 123.91, 124.04, 126.36. ^{19}F NMR ($CDCl_3$, 400 MHz): δ (ppm)= -128.91. FT-IR (ν_{max}/cm^{-1}): 1238 (C-F), 1543 (C=N). UV-Vis (λ/nm): 422, 504, 570 (sh). Elemental analysis (%): Calcd. For $C_{52}H_{36}F_8N_8Rh_2$: C, 55.24; H, 3.21; N, 9.91. Found: C, 55.11; H, 3.025; N, 10.01. MS(m/z): 1130.10 ([M]$^+$).

4.3.6. Synthesis of Rh_2(di-4F-pf)$_4$ (C6)

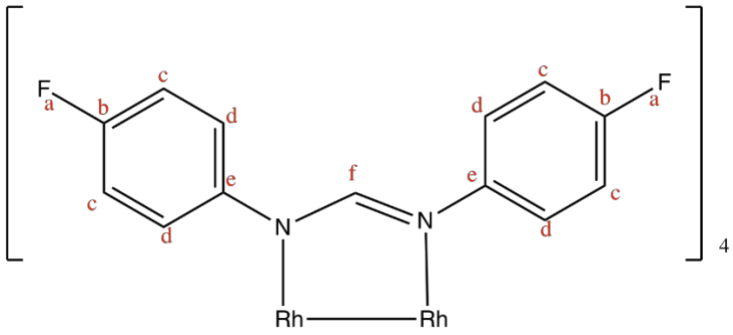

The synthesis of the complex **C6** was carried out using a modified procedure from literature.[4] In a round bottom flask with a side arm *N,N'*–bis(4-fluorophenyl)formamidine (727 mg, 3.13 mmol) was added. The flask was evacuated and filled with N_2 to create an inert atmosphere. This was carried out in three cycles. The ligand was heated to melting at 150 °C, under N_2. Rhodium(II) trifluoroacetate dimer (137 mg, 0.21 mmol) was added observing the formation of a darker melt. The reaction was carried out overnight (19 h) under N_2. The crude product was cooled to room temperature and dried under vacuum for 2 hours at 100 °C. The solid was washed several times with diethyl ether. Then it was filtrated through a Buchner funnel obtaining a brown/red solid which was recrystallized from DCM/MeOH. The precipitate was collected by filtration with a Buchner funnel and washed with methanol. The green powder obtained, was dried under vacuum. Yield: (122 mg, 52%). M.P. >450 °C. ^{1}H NMR ($CDCl_3$, 300 MHz): δ (ppm) = 6.53 (m, 4 H, H_d), 6.82 (m, 4 H, H_c), 7.70 (m, 1 H, H_f). $^{13}C\{^1H\}$ NMR ($CDCl_3$, 400 MHz): δ (ppm) = 115.83, 116.05, 125.28. ^{19}F NMR ($CDCl_3$, 400 MHz): δ (ppm)= -119.36. FT-IR (ν_{max}/cm^{-1}): 1207 (C-F), 1581 (C=N). UV-Vis (λ/nm): 422, 484, 580. Elemental analysis (%): Calcd. For $C_{52}H_{36}F_8N_8Rh_2$: C, 55.24; H, 3.21; N, 9.91. Found: C, 55.99; H, 3.082; N, 9.95. MS(m/z): 1130.11 ([M]$^+$).

4.4. General allylic oxidation procedure

A flask with a side arm equipped with a stirrer bar, was charged with the substrate cyclohexene (2.72 mmol, 100 mol%), 10 mL of the chosen solvent (DCM, ACN, THF) and Rh(II) catalyst (0.5 mol%). The flask was equipped with a condenser and a deflated balloon was attached to indicate the formation of oxygen during the reaction. The system was heated to the boiling point of the chosen solvent. T-Hydro (13.60 mmol, 5 eq) was added to the mixture giving an immediate colour change. After 1h, a second portion of T-Hydro (13.60 mmol, 5 eq) was added to the mixture. After 48h the system was allowed to cool at room temperature. When using volatile solvents (DCM) the systems were evaporated with a rotary evaporator and then, filtered through a silica plug. When using non-volatile solvents, the system was directly filtered through a silica plug.

4.5. References

(1) Kuhn, K. M.; Grubbs, R. H. *Org. Lett.* **2008**, *10* (10), 2075–2077.

(2) Rempel, G. A.; Legzdins, P.; Smith, H.; Wilkinson, G. *Inorg. Synth.* **1972**, *103*, 90–91.

(3) Johnson, S. A.; Hunt, H. R.; Neumann, H. M. *Inorg. Chem.* **1963**, *2* (5), 960–962.

(4) Cooke, M. The Synthesis and Characterization of Rh_2(II,II) Templated Phoactive Assemblies, Université de Montréal, 2007.

Chapter 5

Summary and Future work

5.1 Summary

A series of symmetrical p-tolyl, 2-fluoro and 4-fluoro substituted formamidine-type ligands, (**L1**, **L2** and **L3**) were synthesized *via* a solvent-free reaction, promoted by the evolution of EtOH as by-product. These were characterized as to their spectroscopic and solid-state properties showing a prototropic tautomerism for **L2** and **L3** in the solid state. The acetate precursor complexes $Rh_2(O_2CR)_4$ where R = CH_3 (**C1**) or CF_3 (**C2**) were synthetized and fully characterized. The solvent-free reaction of **C2** with an excess of formamidine ligands yields the corresponding complexes (**C3**, **C4**, **C5** and **C6**). The 2-fluorophenyl complex $[Rh_2(2\text{-F-pf})_4]$ **C5**, was structurally characterized by XRD techniques revealing a paddle-wheel type structure. These complexes were screened for activity as catalysts in the allylic oxidation of cyclohexene. The catalytic reactions using the binuclear Rh complexes, showed that these are active in cyclohexene conversion giving 2-cyclohexene-1-one and 2-cyclohexene-1-ol as products, both in traces amount. Solvent coordination was shown to have an effect on the catalytic behavior of the complexes, with acetonitrile (ACN) being the best solvent due to the solubility properties of complexes. ACN could favor the reaction also by its insertion as axial ligand in the complex which may favor the stabilization of the catalyst's oxidized form (Rh_2^{5+}). The yields in traces of the catalytic processes can be attributed to the bulkiness of the formamidinate ligands which could interfere in the formation of the catalyst active form Rh_2^{5+} by the steric hindrance of the phenyl groups. The volatility of both substrate and products can also explain the overall yields of the processes. In terms of selectivity, the best results were obtained with **C1**, **C4**, **C5** and **C6** which yielded just the enone as product. This can be attributed to the slow concentration of the species *tert*-butyl peroxy radical due to the low activity of **C1** and the steric hindrance of the ligands and their substituents for **C4**, **C5** and **C6**.

5.2 Future work

This work contributes to the novel approaches in allylic oxidation catalysis and in the design of dirhodium(II) catalysts to obtain an efficient and green method to the preparation of synthetically useful products from cheap and readily available substrates. The activity of the catalyst can be increased by the design of less bulky *N,N'*-type ligands favoring the access to the axial site, in order to increase the formation of the catalytically active species. A chelating ligand similar to the Du Bois's esp[1] can be prepared, paying attention in the inclusion of

nitrogens as donor atoms in the complex to increase the electron density within the dimetal core. The preparation of dendrimers containing more than two metal centers may also improve the activity of the catalyst due to the higher quantity of active sites. An accurate screening of the reaction conditions could have an influence on the effectiveness of the system. The amount of oxidant, for example, can be choose in such a way that its radical chain decomposition mechanism can be avoided. The total amount of catalyst could be added in to two portions at different time due to the decrease in the concentration of the catalytically active species. The choice of the substrate could be done considering its volatility and the one of the products probably obtained, in the overall process. The study of a possible way in which the catalyst could be recovered might be carried out, even considering the paramagnetism of its catalytically active form. To better understand the mechanism of the catalysis, this should be studied extensively by cyclic voltammetry (CV), Uv-Vis and EPR spectroscopy. This can be helpful in a more conscious design of the catalyst and choice of the reaction conditions.

5.3 References

(1) Espino, C. G.; Fiori, K. W.; Kim, M.; Du Bois, J. *J. Am. Chem. Soc.* **2004**, *126* (47), 15378–15379.

Appendices

Appendix A

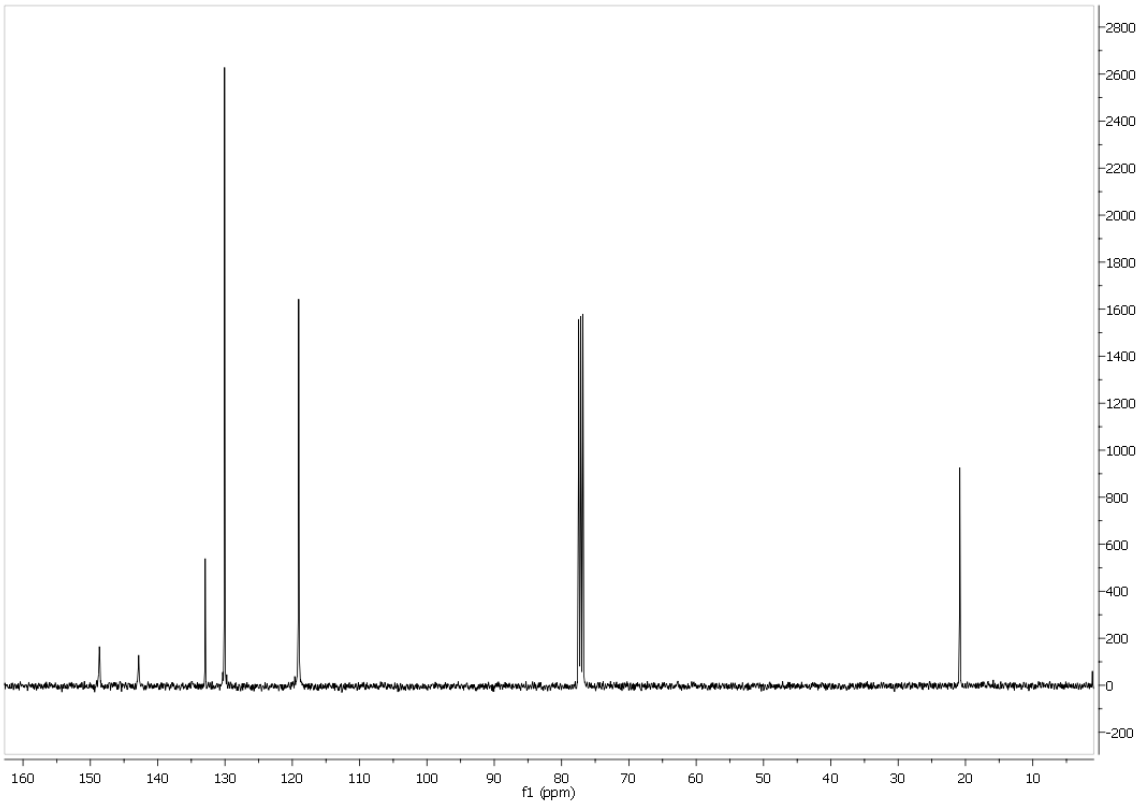

Figure 1: *^{13}C {H} NMR spectrum of* ***L1***

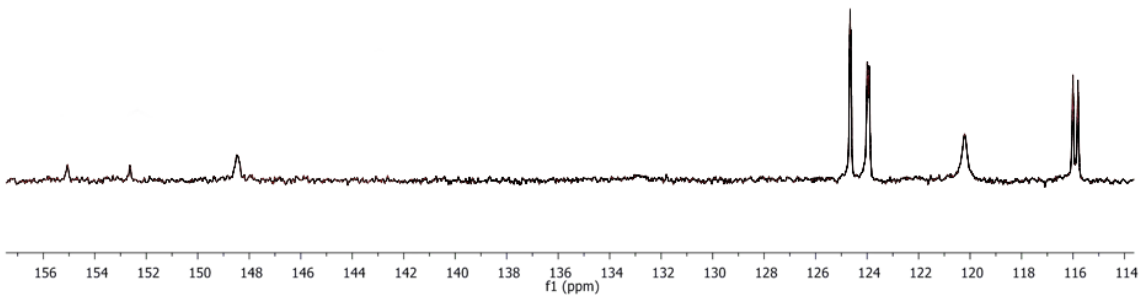

Figure 2: *^{13}C {H} NMR spectrum of* ***L2***

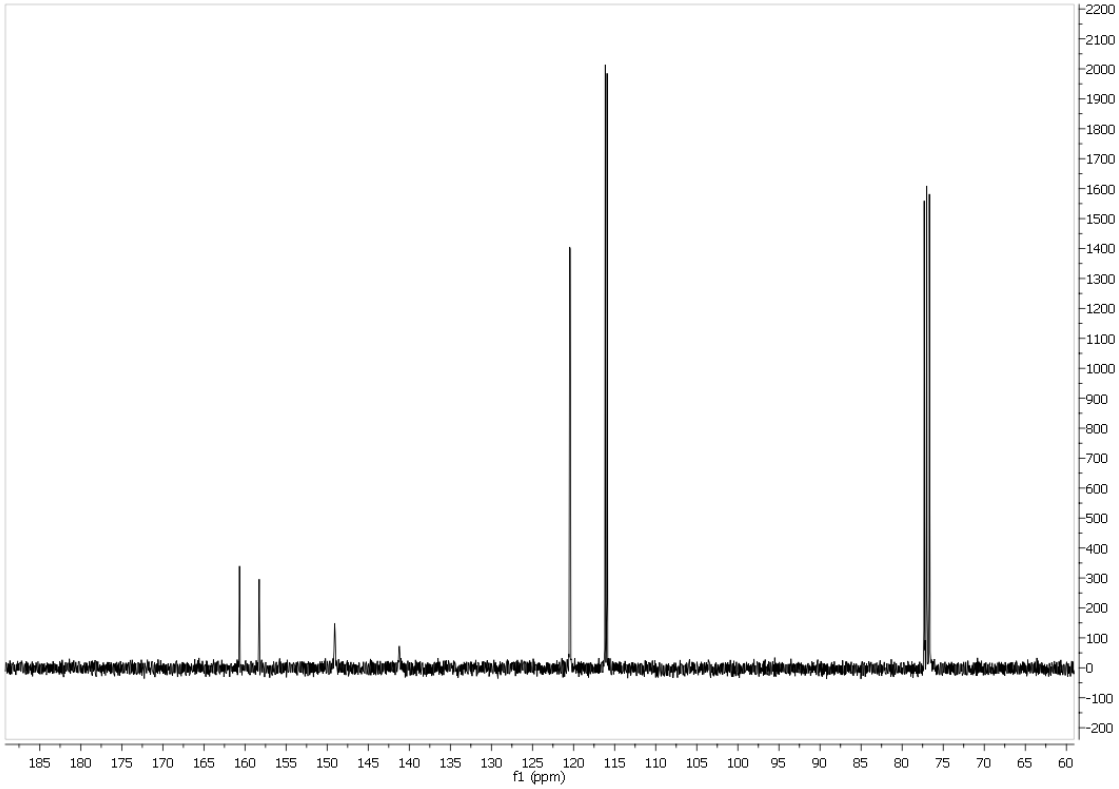

Figure 3: *^{13}C {H} NMR spectrum of* ***L3***

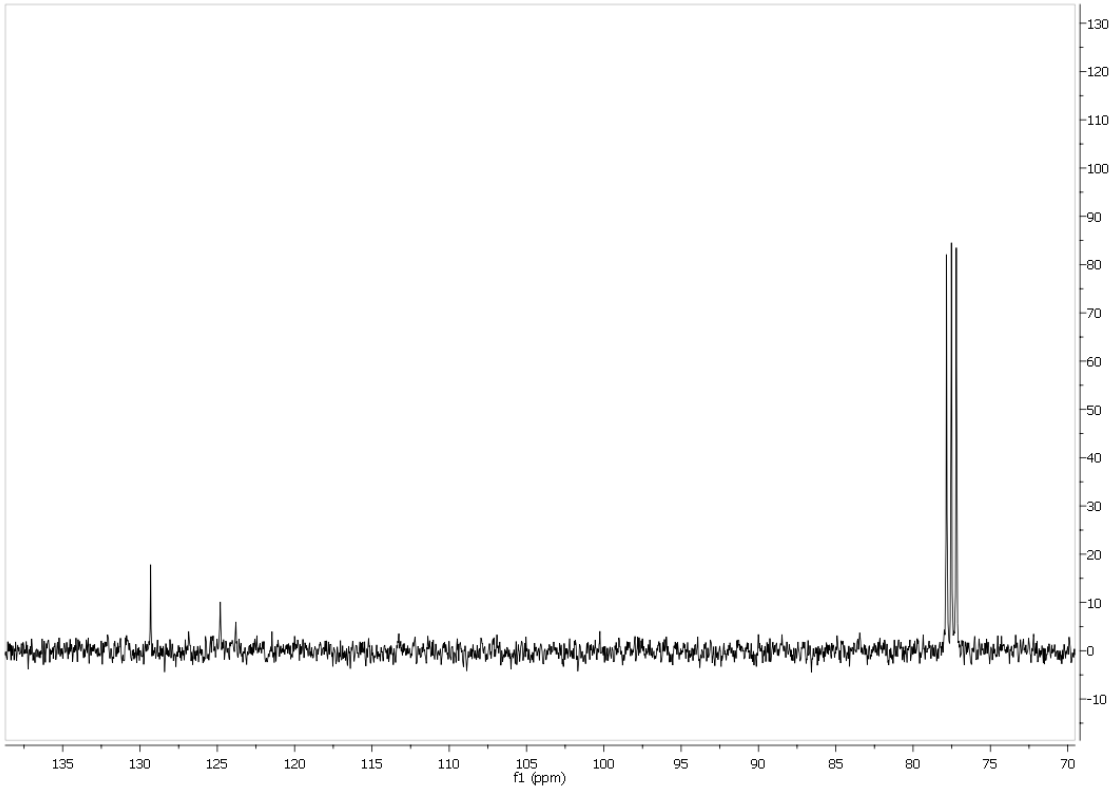

Figure 4: *^{13}C {H} NMR spectrum of* ***C3***

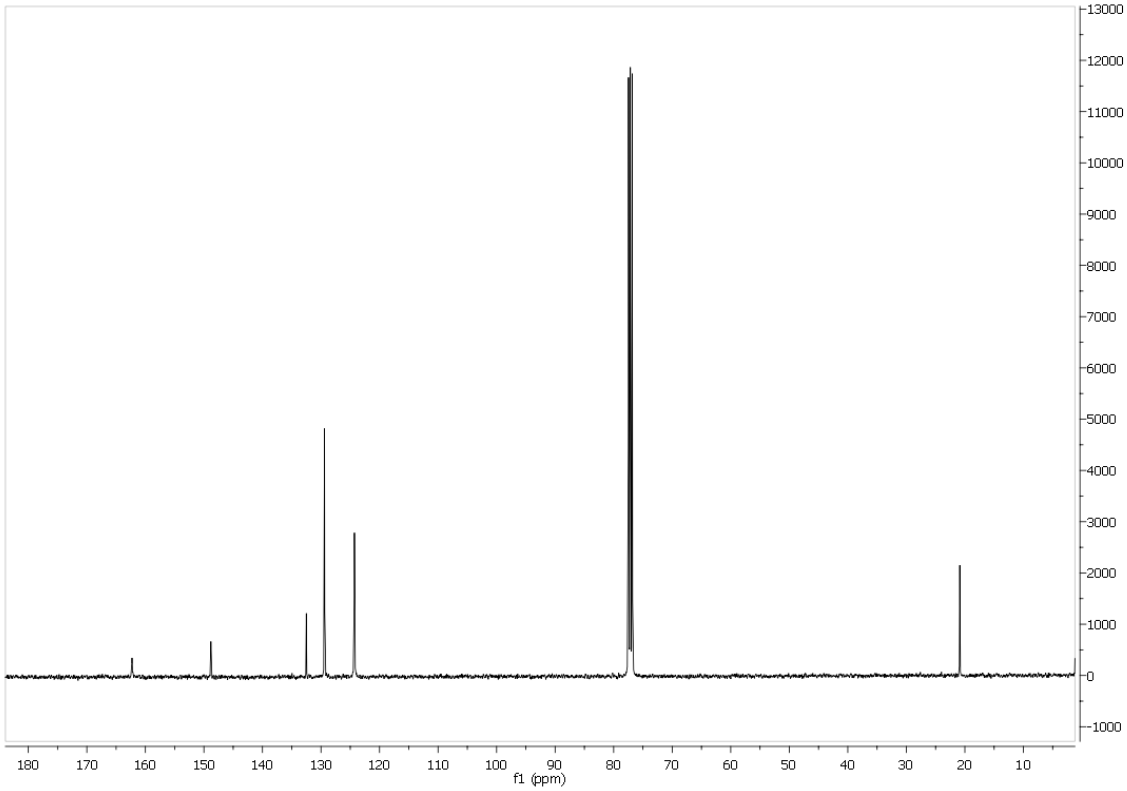

Figure 5: *^{13}C {H} spectrum of* ***C4***

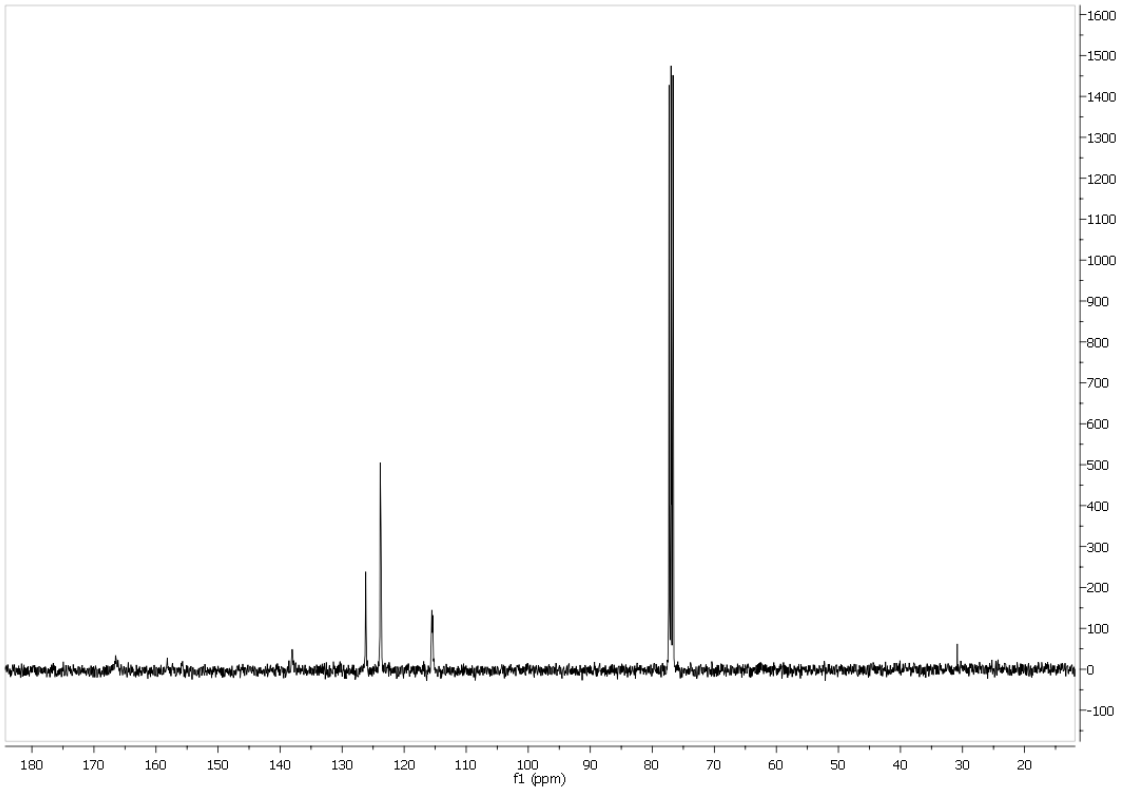

Figure 6: *^{13}C {H} spectrum of* ***C5***

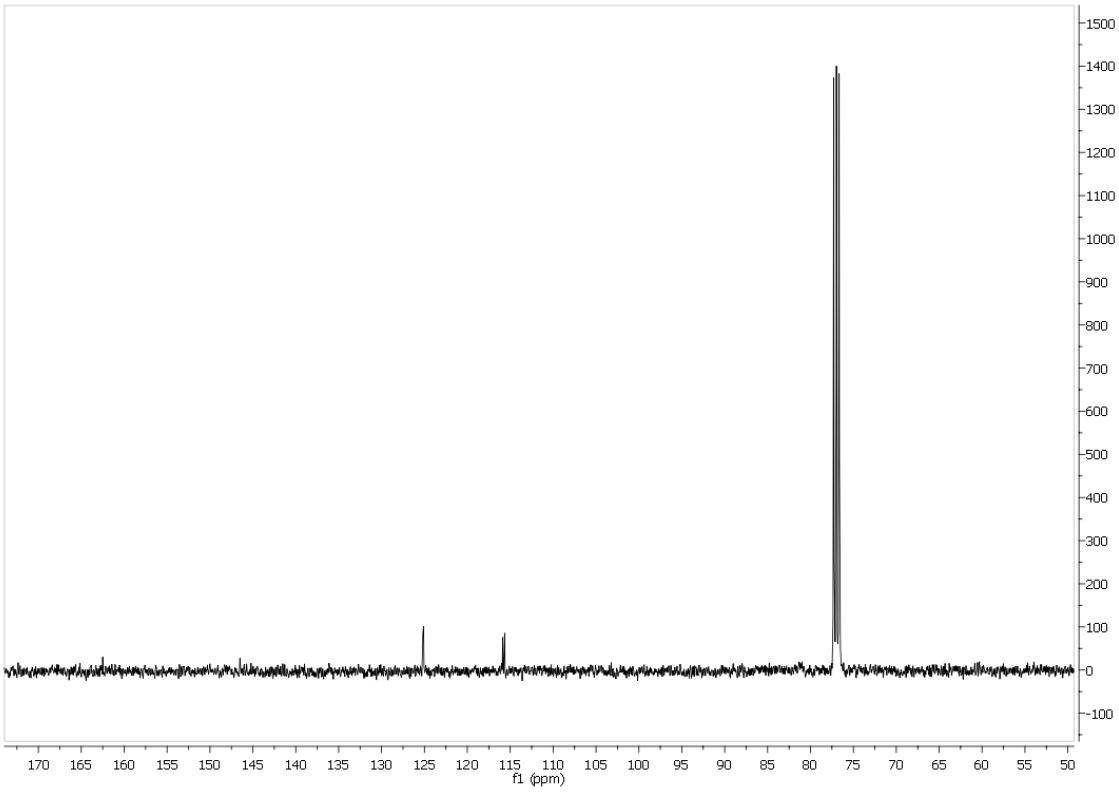

Figure 7: ^{13}C {H} spectrum of C6

Appendix B

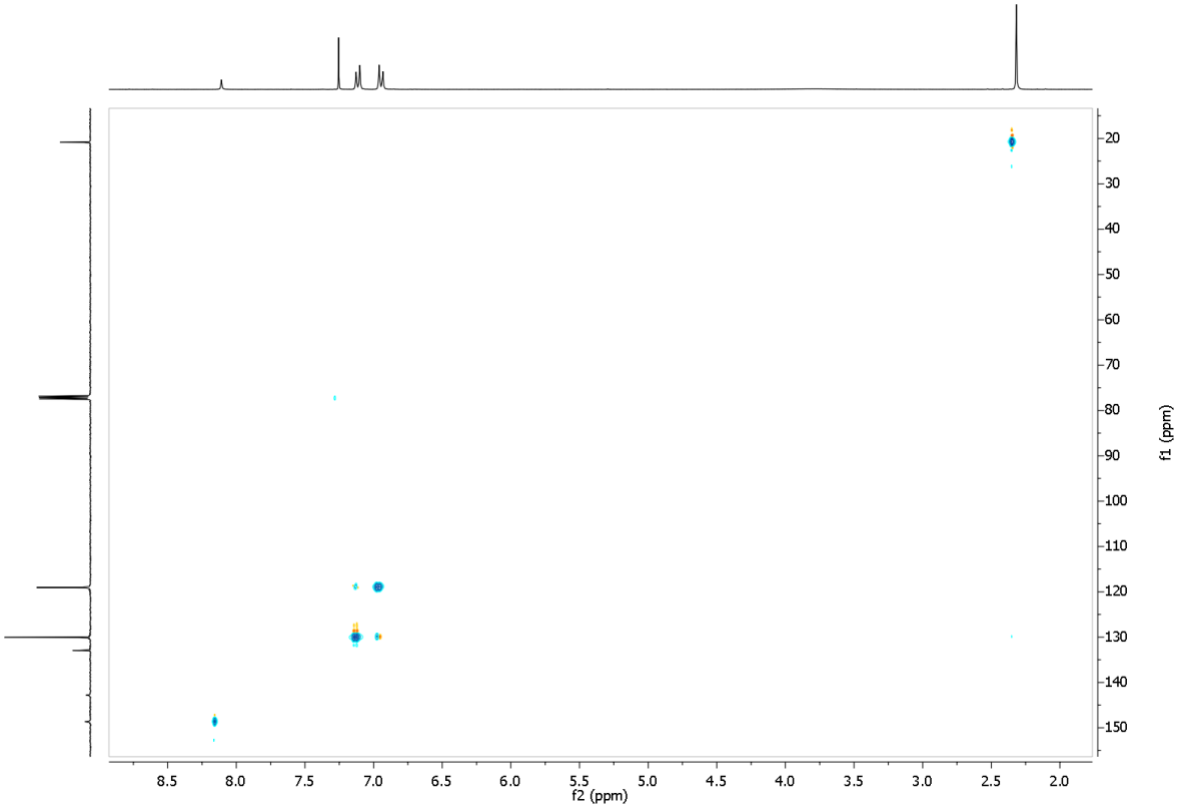

Figure 1: *HSQC NMR spectrum of* ***L1***

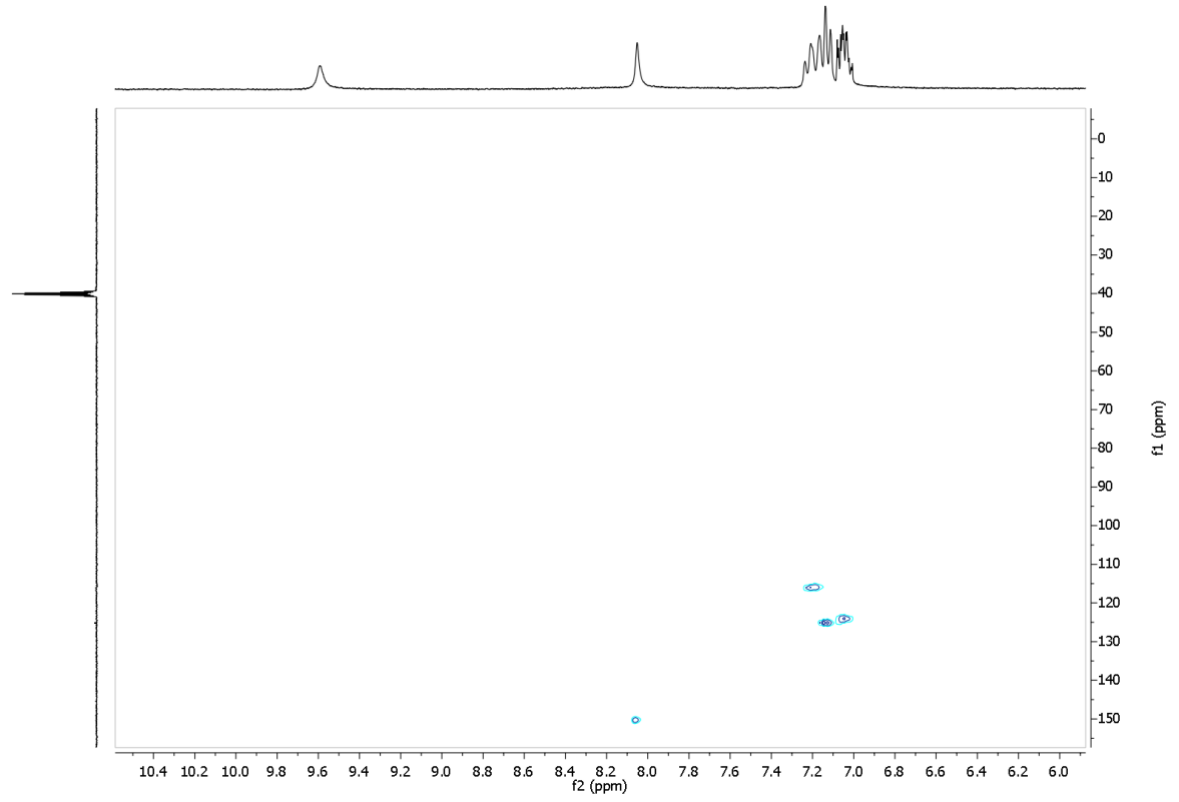

Figure 2: *HSQC NMR spectrum of* ***L2***

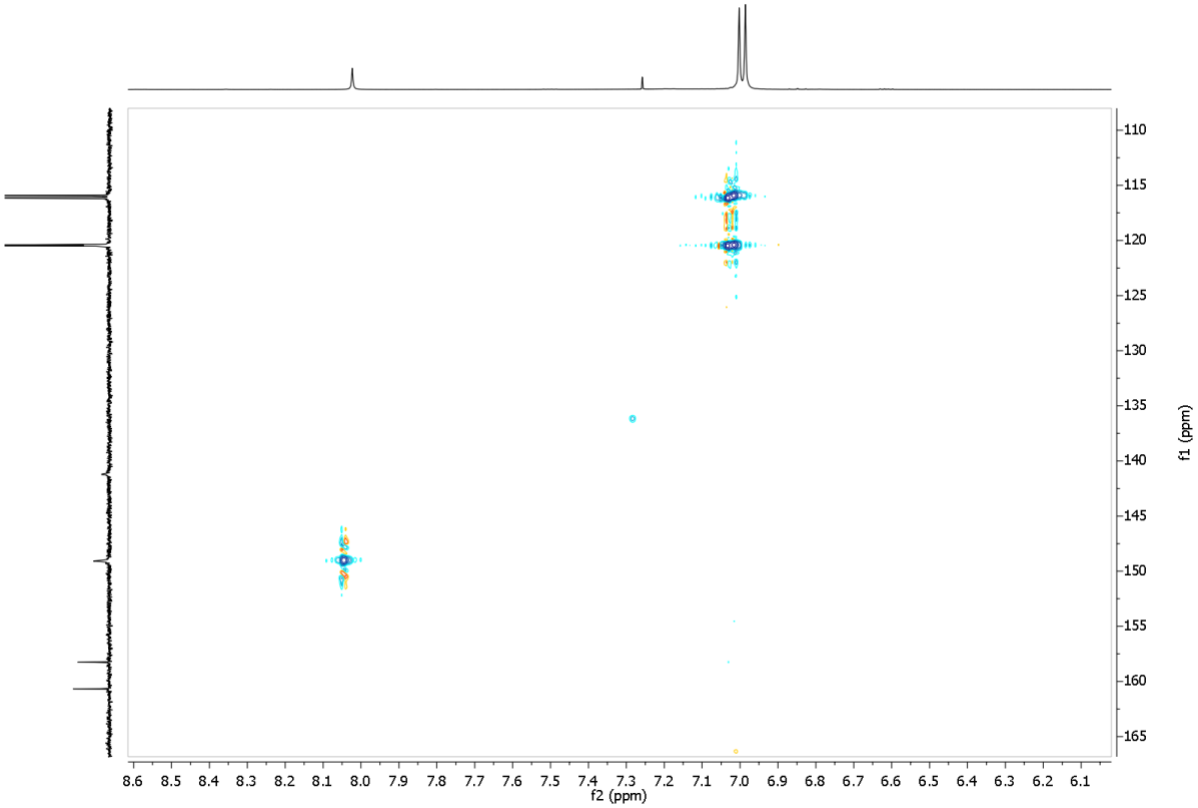

Figure 3: *HSQC NMR spectrum of* ***L3***

Appendix C

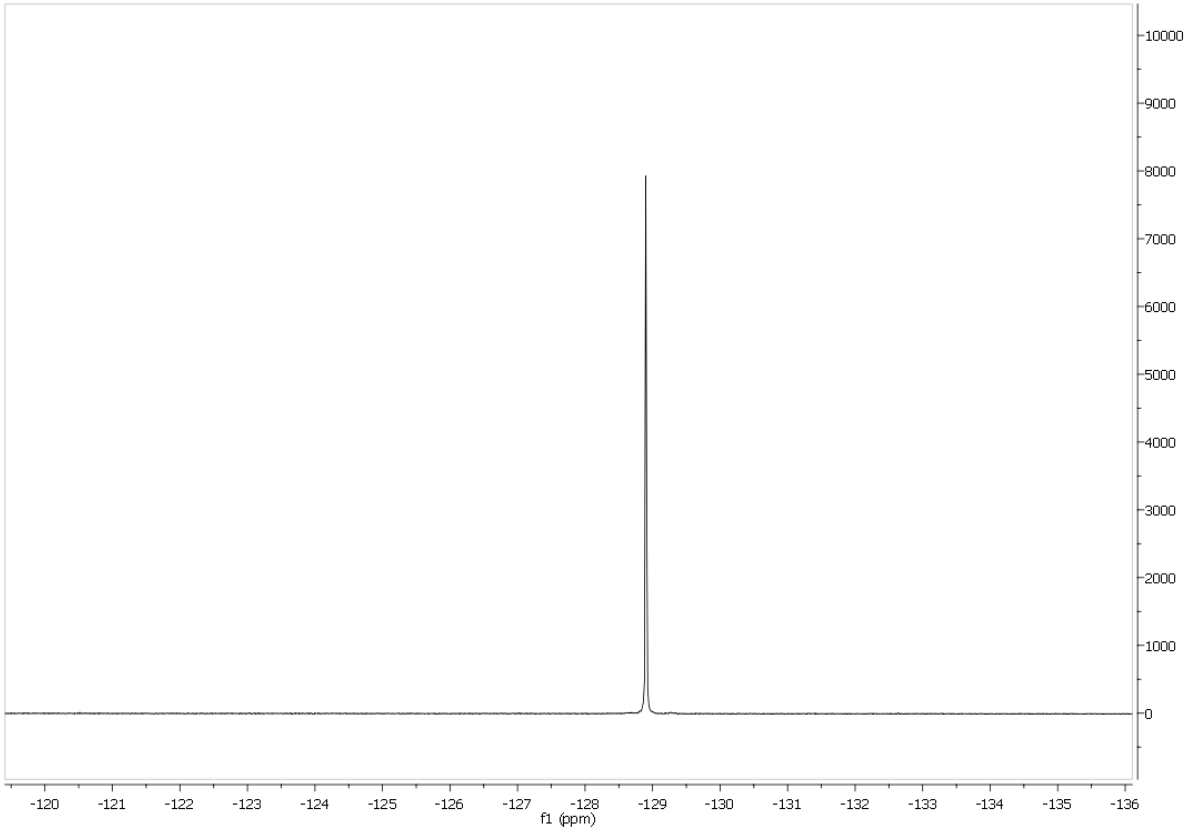

Figure 1: *^{19}F NMR of* ***C5***

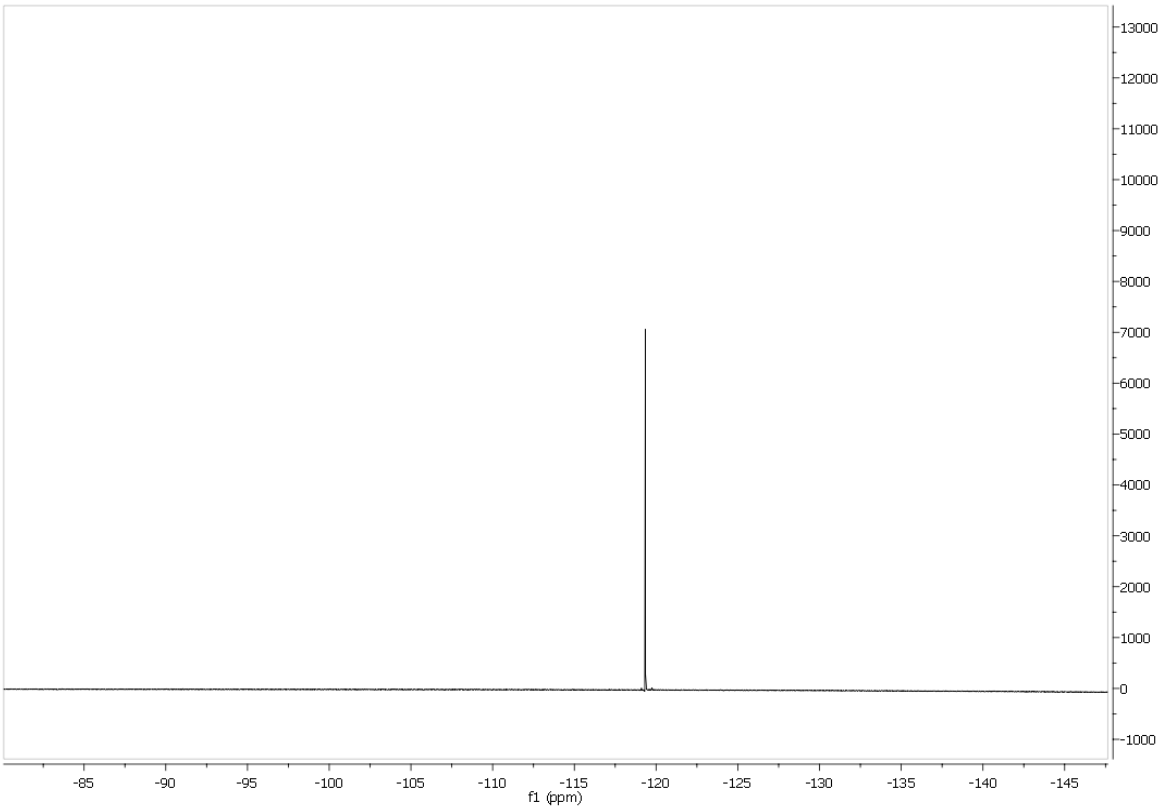

Figure 2: *^{19}F NMR of* ***C6***

Appendix D

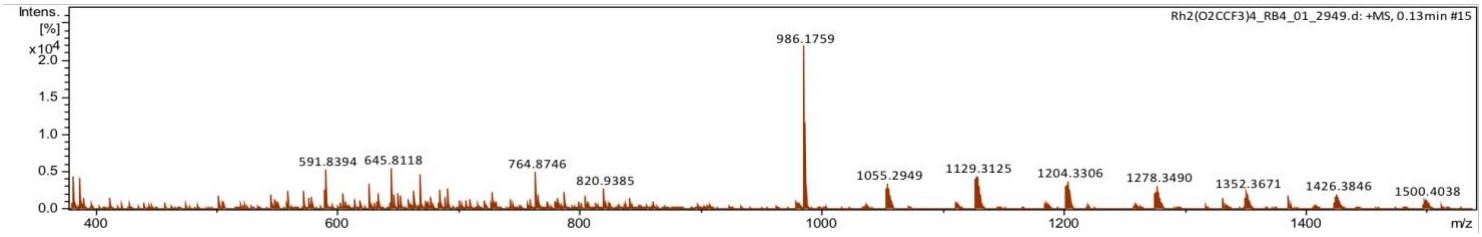

Figure 1**: HPLC/MS spectrum of **C2